HYBRID REGION-BASED IMAGE COMPRESSION SCHEME FOR MAMMOGRAMS AND ULTRASOUND IMAGES

BOSHARA M. ARSHIN

ELECTRICAL AND ELECTRONICS ENGINEERING
UNIVERSITI TEKNOLOGI PETRONAS

JUNE 2007

UNIVERSITI TEKNOLOGI PETRONAS

Approval by Supervisor

The undersigned certify that he has read, and recommends to The Postgraduate Studies Programme for acceptance, a thesis entitled

Hybrid Region-based Image Compression Scheme for Mammograms and Ultrasound Images

submitted by

Boshara Merghani Arshin

for the fulfilment of the requirements for the degree of

Masters of Science in Electrical and Electronics Engineering

Date 23/7/07

Signature :

Main Supervisor : *Prof. Dr. P.A. Venkatachalam*

Date : 23/7/07

Prof. Dr. P.A. Venkatachalam
Professor
Electrical & Electronic Engineering
Academic Block No. 22
Universiti Teknologi PETRONAS
Bandar Seri Iskandar
31750 Tronoh, Perak Darul Ridzuan, MALAYSIA

UNIVERSITI TEKNOLOGI PETRONAS

Hybrid Region-based Image Compression Scheme for Mammograms and Ultrasound Images

By

Boshara Merghani Arshin

A THESIS

SUBMITTED TO THE POSTGRADUATE STUDIES PROGRAMME

AS A REQUIREMENT FOR THE

DEGREE OF MASTERS OF SCIENCE IN ELECTRICAL AND ELECTRONICS ENGINEERING

Electrical and Electronics Engineering

BANDAR SERI ISKANDAR,

PERAK

JUNE, 2007

DECLARATION

I hereby declare that the thesis is based on my original work except for quotations and citations which have been duly acknowledged. I also declare that it has not been previously or concurrently submitted for any other degree at UTP or other institutions.

Signature: Boshara

Name : *Boshara Merghani Arshin*

Date : 23/7/07

ACKNOWLEDGEMENT

This work would never have been done without the help and support that I received from numerous people during my study at Universiti Teknologi PETRONAS (UTP). I would like to take this opportunity to express my sincerest thanks to these individuals.

First of all I would like to thank my supervisor, Prof. Dr. P.A Venkatachalam for his constant encouragement and invaluable guidance throughout the course of this work, for so many fruitful discussions and sharing his ideas. I am still amazed by the diversity and the spectrum of his scientific working knowledge. I cannot emphasize enough how much I benefited from his knowledge, wisdom and personality. It was honor to know and work with him.

I was very fortunate in joining Electrical & Electronic Engineering Programme of UTP as master student. Gratitude is expressed to the staff of the programme for their technical support and advices. Special thanks goes to the programme head Assoc. Prof. Dr. Mohd Noh Karsiti, for providing the facilities and excellent research environment. I wish also to thank the staff of Postgraduate Studies Programme and Research Enterprise Office for assisting and helping me in time of need and support.

I would like to thank department of imaging and diagnostic of Ipoh general hospital for providing me with the medical images used in this work. Special thank is due to Dr. Nazri Bin Ismail. He has given a lot time studying the sample images and marking the diagnostic relevant regions.

I would like to take this opportunity to express my profound gratitude to my father for his tremendous care and spiritual support. It is his never-ending encouragement leading me here.

ABSTRACT

The need for transmission and archive of mammograms and ultrasound images has dramatically increased in tele-healthcare applications. Such images require large amount of storage space which affect transmission speed. Therefore an effective compression scheme is essential. Compression of these images, in general, faces a great challenge to compromise between the higher compression ratio and the relevant diagnostic information. Out of the many studied compression schemes, lossless JPEG-LS and lossy SPIHT are found to be the most efficient ones. JPEG-LS and SPIHT are chosen based on a comprehensive experimental study carried on a large number of mammograms and ultrasound images of different sizes and texture. The lossless schemes are evaluated based on the compression ratio and compression speed. The distortion in the image quality which is introduced by lossy methods evaluated based on objective criteria using Mean Square Error (MSE) and Peak signal to Noise Ratio (PSNR). It is found that lossless compression can achieve a modest compression ratio 2:1 – 4:1. Lossy compression schemes can achieve higher compression ratios than lossless ones but at the price of the image quality which may impede diagnostic conclusions.

In this work, a new compression approach called Hybrid Region-based Image Compression Scheme (HYRICS) has been proposed for the mammograms and ultrasound images to achieve higher compression ratios without compromising the diagnostic quality. In HYRICS, a modification for JPEG-LS is introduced to encode the arbitrary shaped disease affected regions. Then Shape adaptive SPIHT is applied on the remaining non region of interest. The results clearly show that this hybrid strategy can yield high compression ratios with perfect reconstruction of diagnostic relevant regions, achieving high speed transmission and less storage requirement. For the sample images considered in our experiment, the compression ratio increases approximately ten times. However, this increase depends upon the size of the region of interest chosen. It is also found that the pre-processing (contrast stretching) of region of interest improves compression ratios on mammograms but not on ultrasound images.

ABSTRAK

Keperluan dalam pemindahan mammograms dan imej ultrabunyi telah meningkat secara mendadak di dalam aplikasi tele-kesihatan. Imej-imej tersebut memerlukan ruang simpanan yang besar dan ini mempengaruhi kelajuan pemindahan. Justeru, skema pemampatan yang berkesan adalah penting. Secara amnya, pemampatan imej tersebut mengalami cabaran yang besar dalam mengimbangi nisbah pemampatan yang lebih tinggi dan kerelevanan diagnostik. *Lossless JPEG-LS* dan *lossy SPHIT* telah dikenalpasti antara kaedah-kaedah yang paling berkesan dalam skema pemampatan. *JPEG-LS* dan *SPHIT* dipilih berdasarkan eksperimen terperinci yang dilakukan ke atas sejumlah besar *mammogram* dan imej ultrabunyi. Kaedah *lossless* dinilai berdasarkan nisbah dan kelajuan pemampatan. Kaedah *lossy* pula dinilai berdasarkan kriteria objektif menggunakan *Mean Square Error (MSE)* dan *Peak Signal to Noise Ratio (PSNR).* Walau bagaimanapun, pemampatan *lossless* hanya boleh mencapai nisbah pemampatan sederhana sekitar 2:1 – 4:1. Skema *lossy* boleh mencapai pemampatan yang lebih tinggi berbanding skema *lossless* tetapi menjejaskan kualiti imej yang menjadi penghalang dalam membuat kesimpulan diagnostik.

Dalam penyelidikan ini, '*Hybrid Region-based Image Compression Scheme (HYRICS)*' telah dicadangkan *bagi* mencapai nisbah pemampatan tertinggi tanpa menjejaskan kualiti diagnostik. Dalam *HYRICS*, *JPEG-LS* telah digubah untuk mengekod setiap bahagian berbentuk rawak yang dilanda penyakit. SPIHT yang boleh disesuaikan mengikut bentuk pula diaplikasikan ke atas bahagian selebihnya yang bukan dalam pemerhatian.

Keputusan yang diperolehi menunjukkan hybrid ini boleh menghasilkan kadar nisbah pemampatan tinggi, pembinaan semula bahagian diagnostik yang relevan dengan sempurna, mencapai pemindahan dalam kelajuan yang tinggi dan mengurangkan keperluan storan. Bagi sampel imej yang digunakan dalam eksperimen, kadar pemampatan telah meningkat lebih kurang sepuluh kali ganda. Bagaimanapun, peningkatan ini bergantung kepada saiz bahagian yang dipilih. Ia juga telah didapati bahawa pra-pemprosesan (contrast stretching) pada bahagian yang dipilih telah meningkatkan kadar pemampatan dalam *mammograms* sahaja.

TABLE OF CONTENT

STATUS OF THESIS i
APPROVAL PAGE ii
TITLE PAGE iii
DECLARATION iv
ACKNOWLEDGEMENT v
ABSTRACT vi
ABSTRAK vii
TABLE OF CONTENT viii
LIST OF TABLES xii
LIST OF FIGURES xii
ABBREVIATIONS xiv

CHAPTER 1 INTRODUCTION 1
1.1 General Background 1
1.2 Motivation 2
1.3 Organization of Thesis 3

CHAPTER 2 LITERATURE SURVEY 5
2.1 Introduction 5
2.1.1 Medical Imaging 5
2.1.2 Telemedicine 6
2.2 Medical Imaging Modalities 7
2.2.1 X-ray Radiography 7
2.2.2 Computed Tomography 7
2.2.3 Mammography 8
2.2.4 Magnetic Resonance Imaging 9
2.2.5 Nuclear Medicine 9
2.2.6 Ultrasonography 10
2.3 Images Compression 12
2.3.1 Redundancy 12
2.3.2 Lossless Image Compression 12
2.3.2.1 Predictive with statistical Modeling 13

2.3.2.2 Transform-based Schemes 14
2.3.2.3 Dictionary-based Schemes 15
2.3.2.4 Entropy Coding 15
2.3.3 Lossy Image Compression 16
2.3.3.1 Scalar Quantization 17
2.3.3.2 Vector Quantization 18
2.4 Performance Criteria of Image Compression Methods 18
2.4.1 Compression Efficiency 19
2.4.2 Computational Speed 19
2.4.3 Distortion Measurements 20
2.5 Medical Image Compression 21
2.6 Survey of Medical Image Compression 22
2.6.1 Lossless Medical Image Compression 22
2.6.2 Lossy Medical Image Compression 24
2.7 Region-based Image Compression 25
2.7.1 Shape Adaptive DCT 26
2.7.2 ROI in JPEG2000 26
2.7.3 Shape Adaptive DWT 27
2.8 Summary 28

CHAPTER 3 EVALUATION OF IMAGE COMPRESSION SCHEMES 29
3.1. Introduction 29
3.2. Mammograms and Ultrasound Image Compression 29
3.3. Efficient Lossless Image Compression Schemes 30
3.3.1 LJPEG 30
3.3.2 JPEG-LS 31
3.3.3 CALIC 31
3.3.4 FELICS 32
3.3.5 BTPC 32
3.3.6 JPEG2000 32
3.3.7 S+P 33
3.3.8 PNG 33
3.4. Efficient Lossy Image Compression Schemes 33
3.4.1 JPEG 34

3.4.2 SPIHT 34
3.5. Image compression Software Implementations and Libraries 34
3.6. Experiment 36
3.6.1 Sample Images Database 36
3.6.2 System setup 37
3.6.3 Evaluation Procedure 37
3.6.3.1 Evaluation of lossless Compression schemes 38
3.6.3.2 Evaluation of lossy Compression schemes 39
3.7. Summary 39

CHAPTER 4 EFFICIENT COMPRESSION SCHEMES FOR MAMMOGRAMS AND ULTRASOUND IMAGES 40
4.1 Introduction 40
4.2 Performance of the lossless schemes on mammograms 40
4.2.1 Compression Efficiency 40
4.2.2 Compression Speed 41
4.3 Performance of the lossless schemes on ultrasound images 42
4.3.1 Compression Efficiency 42
4.3.2 Compression Speed 43
4.4 Comparison of lossless schemes on both modalities 43
4.5 Performance of Lossy schemes on mammograms 44
4.5.1 Image Quality 44
4.5.2 Compression Speed 45
4.6 Performance of Lossy schemes on ultrasound images 47
4.6.1 Image Quality 47
4.6.2 Compression Speed 48
4.7 Summary 50

CHAPTER 5 HYBRID REGION-BASED IMAGE COMPRESSION SCHEME51
5.1 Introduction 51
5.2 JPEG-LS 51
5.2.1 Modification on JPEG-LS 54
5.3 Characteristics of Wavelet Decomposition in SPIHT 55
5.3.1 Spatial Orientation Trees 55

5.3.2 SPIHT Algorithm 57
5.3.3 Shape Adaptive SPIHT Encoding 61
5.4 Hybrid Region-based Compression Schemes 63
5.5 HYRICS on pre-processed mammograms and ultrasound images 65
5.6 Summary 66

CHAPTER 6 RESULTS AND DISCUSSION 67
6.1 Introduction 67
6.2 Compression Efficiency 67
6.3 Computational time 72
6.4 HYRICS on preprocessed images 73
6.5 Case studies on sample Mammograms 75
6.5.1 Sample mammogram 1 75
6.5.2 Sample mammogram 2 76
6.5.3 Sample mammogram 3 78
6.6 Case studies on sample ultrasound images 79
6.6.1 Sample ultrasound 1 79
6.6.2 Sample ultrasound 2 81
6.6.3 Sample ultrasound 3 83
6.7 Summary 86

CHAPTER 7 CONCLUSION AND RECOMMENDATIONS 87
7.1 Conclusion 87
7.2 Recommendations 88

REFERENCES 89
PUBLICATIONS 95
APPENDIX A 96
APPENDIX B 99
APPENDIX C 107
APPENDIX D 109

LIST OF TABLES

Table 2.1 : Sizes and brightness levels of various medical images..... 22
Table 3.1: Lossless/Lossy compression schemes with their respective libraries.........36
Table 3.2: System setup for the experiment..37
Table 4.1: Average distortion (PSNR and MSE) vs. CR on mammograms 45
Table 4.2: Average of CT/DT for the 4 lossy methods applied on mammograms......46
Table 4.3: Average distortion (PSNR and MSE) vs. CR on ultrasound images..........48
Table 4.4: Average of CT/DT for the 4 lossy methods applied on US images 49
Table 6.1: Comparison of compression ratios of HYRICS on mammograms 68
Table 6.2: Effect of ROI area on compression ratio for mammograms.......................69
Table 6.3: Comparison of compression ratios of HYRICS on ultrasound images 70
Table 6.4: Effect of ROI area on compression ratio for ultrasound images 71
Table 6.5: CT/DT: modified JPEG-LS, SA-SPIHT , HYRICS on mammograms 72
Table 6.6: CT/DT: modified JPEG-LS, SA-SPIHT and HYRICS on ultrasound 73
Table 6.7: CR of ROI-JPEG-LS after and before contrast stretch on mammograms 74
Table 6.8: CR JPEG-LS after and before contrast stretch on ultrasound 74

LIST OF FIGURES

Figure 2.1: Different electromagnetic spectrum that are used in medical imaging 6
Figure 2.2: Mammograms :(A) Normal (B) Benign (C) cancerous malignant.............9
Figure 2.3: Typical ultrasound image of a normal liver 11
Figure 2.4: Examples of (a) uniform and (b) non-uniform scalar quantization..........18
Figure 2.5: General Scaling and MAXSHIFT ROI method in JPEG2000 27
Figure 2.6: Decomposition of ultrasound image scanned area using SA-DWT.........28
Figure 3.1 A typical data compression system (codec) 35
Figure 3.2: A comparative study of compression schemes.......................................38
Figure 4.1: Compression efficiency on mammograms 40
Figure 4.2: Compression/decompression time in seconds on mammograms 41
Figure 4.3 : Compression/decompression time without CALIC on mammograms....42
Figure 4.4: Compression efficiency on ultrasound images...42
Figure 4.5: Compression/decompression time on ultrasounds images 43
Figure 4.6: Comparison between PSNR and CR on mammograms 44

Figure 4.7: Comparison between MSE and CR on mammograms 45
Figure 4.8: Average CT/DT in seconds for the four lossy methods on mammograms46
Figure 4.9: Comparison between PSNR and CR on ultrasound images 47
Figure 4.10: Comparison between PSNR and CR on ultrasound images 48
Figure 4.11: Average CT/DT in seconds for the four lossy methods on ultrasound ...49
Figure 5.1: JPEG-LS lossless simple coder diagram 52
Figure 5.2: (a)Four neighboring pixels (b) formula to obtain the initial prediction 52
Figure 5.3: Two dimensional subband analysis 56
Figure 5.4: 2-level wavelet decomposition of US image with spatial orientation tree57
Figure 5.5: Initial state of SPIHT algorithm 59
Figure 5.6: Flowchart of SPIHT Algorithm 60
Figure 5.7: Parent-children relationship in SA-DWT subbands 62
Figure 5.8: HYRICS Steps 63
Figure 5.9: Sequences of the Hybrid Compression- mammogram 2 65
Figure 6.1: Plot of ROI area and Compression ratios on mammograms 69
Figure 6.2: Plot of ROI area and Compression ratios on ultrasound images 71
Figure 6.3: sample mammogram 1 75
Figure 6.4: HYRICS on sample mammogram 1 76
Figure 6.5: sample mammogram 2 77
Figure 6.6: HYRICS on sample mammogram 2 77
Figure 6.7: sample mammogram 3 78
Figure 6.8: HYRICS on sample mammogram 3 79
Figure 6.9: sample ultrasound 1 80
Figure 6.10: HYRICS on sample ultrasound 1 81
Figure 6.11: sample ultrasound 2 82
Figure 6.12: HYRICS on sample ultrasound 2 83
Figure 6.13: sample ultrasound 3 84
Figure 6.14: HYRICS on sample ultrasound 3 85

ABBREVIATIONS

BR	Bit Rate
BTPC	Binary Tree Predictive Coding
CALIC	Context-based Adaptive Lossless Image Compressor
CE	Compression Efficiency
CP	Compression Percentage
CR	Compression Ratio
CS	Compression Speed
CT	Compression Time
CT-scan	Computed Tomography
DCT	Discrete Cosine Transform
DDSM	Digital Database for Screening Mammography
DICOM	Digital Imaging and Communications in Medicine
DM	Distortion Measures
DT	Decompression Time
DWT	Discrete Wavelet Transform
EBCOT	Embedded Block Coding with block Truncation
EZW	Embedded Zerotree Wavelet
FELICS	Fast and Efficient Lossless Image Compression
GIF	Graphic Interchange Format
HYRICS	HYBRID Region-based Image Compression Scheme
LIP	List of Insignificant Pixels
LIS	List of Insignificant Sets
LJPEG	Lossless JPEG
LOCO-I	LOw COmplexity lossless compression
JPEG	Joint Photographic Experts Group
LSP	List of Significant Pixels
MRI	Magnetic Resonance Imaging
MSE	Mean Square Error
NM	Nuclear Medicine
Non-ROI	Non Region of Interest
PBM	Portable BitMap
PET	Positron Emission Tomography

PGM	Portable GreyMap
PNG	Portable Network Graphics
PNM	Portable Any Map
PPM	Portable PixMap
PSNR	Peak Signal to Noise Ratio
QccPack	Quantization, Compression, and Coding
RLE	Run Length Encoding
ROI	Region of Interest
SA-DCT	Shape Adaptive Discrete Cosine Transform
SA–DWT	Shape Adaptive Discrete Wavelet Transform
SA-SPIHT	Shape Adaptive Set Partition in Hierarchical Trees
SPECT	Single Photon Emission Tomography
SPIHT	Set Partition in Hierarchical Trees
S+P	Said Pearlman
US	Ultrasound

CHAPTER 1

INTRODUCTION

1.1 General Background

The interior structures and the functions of the living human body can be visualized to diagnose abnormal conditions and guided therapeutic procedures using various medical modalities such as X-ray, Ultrasound (US), Mammography, Magnetic Resonance Imaging (MRI), Nuclear Medicine (NM) and Computed Tomography (CT).

These medical images in general can be categorized according to the interaction of energy with the tissue into either external energy source where the energy is penetrating the target organ from outside such as X-ray, Mammography, US and MRI or internal source of radioactive energy such as NM in which radioactive substances are injected into the body to interact with the selected tissue.

The abdominal and breast related diseases are dominating over other diseases all over the world. Breast cancer which is often detected using periodic screening of mammography is the most serious disease affecting women. About one in 19 women in Malaysia are at risk, compared to one in 8 in Europe and the United States[1]. Ultrasonography is being used to examine abdominal disorders in liver, kidney, gallbladder and spleen that are responsible for a considerable burden of suffering and death in all age groups worldwide. In the United Kingdom, almost 2700 people are diagnosed liver cancer, 6700 are diagnosed with kidney cancer and bladder cancer is affecting more than 10000 individuals each year. Besides, ultrasound is also well-known for its applications in obstetrics, where it is used to examine the different stages of fetus during pregnancy [2].

In view of the increased complexity of the breast and abdominal diseases worldwide there is a necessity to have tele-consultation with medical experts at distance placeless within and outside the country. For this purpose there is a necessity to transmit and store large amount of image data.

In this work the research is concentrated on finding out efficient compression techniques for transmission and archiving of mammograms and ultrasound images.

Mammography is a low-dose x-ray system that provides images of the breast's inner structure and is used as a screening tool to detect breast cancer and other diseases. Studies have shown that early detection of breast cancer using periodical screening by mammography decreases the mortality rate [3].

Ultrasonography is a technique that uses reflected ultrasonic waves to display visual images of structures within the body. The images generated are stored in digital form, and accessed and transmitted as archival records of physical examination for diagnostic and surgical usage in hospitals or health-care centers.

Recently, the need for transmission/archive of mammograms and ultrasound images has dramatically increased due to the growing need to deliver healthcare to patients in remote areas (tele-healthcare), sharing medical knowledge over distance (tele-consultation) and long-term medical image storage (archive) for future interpretation and research.

The massive number of above medical images generated per patient and the high resolution needed to represent an image require large amount of storage. As a result, the transmission of these images over a network to a remote place may be time consuming. For example, a typical mammogram digitized at a resolution of about 5000 x 4000 pixels and 12 bits, results in approximately 40Mb of digital data. Such high resolution is required in order to detect isolated clusters of micro-calcifications that herald an early stage cancer. Similarly, in a single medical ultrasound examination there are on the average 10 to 20 still images of 640x480 pixels generated equaling to approximately 24.6 to 49.2Mb of grayscale image data. Due to the increasing numbers of patients and elongated case histories, ultrasound images require large space and transmission time[4].

1.2 Motivation

It is clear that advances in technologies for transmission or storage are not sufficient to solve transmission/storage problem of medical images. Therefore, an effective compression scheme is essential to reduce the unnecessary data as much as possible for fast transmission and efficient storage.

There are many approaches to image compression which can be used. These can be categorized into two fundamental groups: lossless and lossy. In recent years, there has been a long-standing debate over which compression schemes are appropriate for the medical images. While lossless compression can retain the important information in the image, it can achieve only modest compression ratio (2:1 – 4:1) which is inadequate for the growing need for medical images transmission and archive[5]. On the other hand, lossy compression schemes can achieve very high compression ratios but at the price of image quality. Medical image which holds important diagnostic values (i.e. micro-calcifications in mammograms and speckle texture in ultrasound), cannot afford much degradation which may negatively affect radiological diagnosis[6].

The aim of this work is to design an ideal compression method to encode ultrasound and mammogram images by removing unnecessary data without affecting the sensitive details which give vital diagnostic information. In medical images, normally there are few small selected disease intensive regions that are diagnostically relevant, while the remaining regions are much less important for diagnosis but may be necessary to give some spatial information. The approach is to select the best among the well known lossless and lossy compression scheme. Then combine them in a hybrid manner that allows perfect reconstruction of the diagnostically relevant regions and permits some degradation in non-relevant areas yielding a higher compression ratio while still maintaining the diagnostic values.

1.3 Organization of Thesis

Chapter 2 introduces various medical imaging modalities and their necessity in tele-healthcare application giving special focus on mammography and ultrasonography. The features of telemedicine and significance of medical image compression are introduced. A review of compression categories with some terminology and concepts are also discussed in this chapter. An overview of the literature survey is carried out on the evaluation of some efficient image compression schemes on medical images is presented.

Chapter 3 provides a detailed description of a comparative study to pinpoint efficient and well suited lossless and lossy compression methods for mammograms and ultrasound images. A brief overview of all the compression methods used in this study is presented along with their libraries and software implementation. The methodology of evaluating the compression methods is described in detail.

In Chapter 4, eight frequently used lossless and four lossy compression schemes are applied on set of mammograms and ultrasound images of different sizes and texture. The results obtained are analyzed and thence JPEG-LS and SPIHT are found to be better schemes among lossless and lossy respectively.

In Chapter 5, a new hybrid compression technique called Region-based Image Compression Scheme (HYRICS) that combines modified JPEG-LS for arbitrary shaped regions of interest and shape adaptive SPIHT for non-region of interest yielding a high overall compression ratio while still retaining diagnostic values is presented. The algorithms that are involved in this approach with the proposed modifications are reviewed.

In Chapter 6, the results of compression ratios and compression/decompression time of JPEG-LS applied on whole image, the modified JPEG-LS on the regions of interest, shape adaptive SPIHT on the non-regions of interest and the overall compression ratio of the proposed HYRICS on the selected set of mammograms and ultrasound images for various breast and abdomen diseases are presented. The results of compression efficiency by applying modified JPEG-LS on preprocessed (contrast stretched) mammograms and ultrasound images are also discussed.

Chapter 7 presents the overall conclusion of the research work and the recommendations for further improvements.

CHAPTER 2

LITERATURE SURVEY

2.1 Introduction

In this chapter a brief description of various medical imaging modalities for telemedicine is presented. Basic theory of image compression in general and lossless and lossy compression in particular is discussed. Previous comparative studies on various compression techniques used in medical imaging and evaluation of their performance are given. The background information regarding region-based image compression is also discussed.

2.1.1 Medical Imaging

The interior structures and the functions of the living human body are not generally visible to the human observer. However, by various medical imaging methods, these internal aspects can be visualized through which the medical professional can look into the body to diagnose abnormal conditions and guide therapeutic procedures[7]. Image of human body in general can be derived from the interaction of energy with the tissue. The energy source can be categorized either as external or internal[8]. Different electromagnetic waves that are used in clinical imaging are presented in Figure 2.1[9]. External energy source like ionized radiation is used in some imaging methods such as X-ray radiography and Computed Tomography which are associated with health hazards that require methodology that guarantees high level diagnosis while limiting the possible harm to the patient. Ultrasound (US) and Magnetic Resonance Imaging (MRI) - which use ultrasonic waves and radiofrequency respectively - are other examples of external energy sources using non-ionizing radiations. Therefore there are no risks for long term effects of exposure. However in MRI, there is an identified impact associated with tissue heating from exposure to the radiofrequency field and the presence of implanted devices in the body. Nuclear Medicine (NM) imaging modalities use an internal energy source through an emission process to generate images of the human organs. In emission imaging, radioactive substances are injected into the body to interact with the selected tissue to form an internal source of radioactive energy.

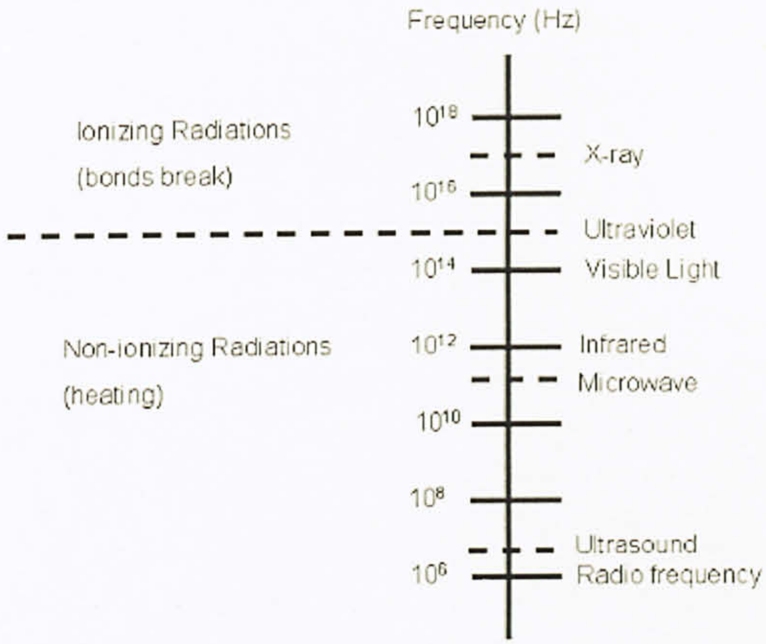

Figure 2.1: Different electromagnetic spectrum that are used in medical imaging

2.1.2 Telemedicine

The reality of geographic and socio-economic barriers to health-care access in rural communities has been recognized for many years. Health-care services in rural areas face professional isolation, and must also deal with additional expenses for transportation when sending patients for referral. These problems outside urban centers increase the cost of health-care to the individual patient, and therefore the entire system. These problems have inspired clinicians, health service researchers and engineers to investigate and develop what's called telemedicine systems to improve the standard of health-care by providing quick medical intervention in a timely manner, instead of sending rural patients to urban hospitals[10]. Therefore, the term telemedicine refers to the use of communications technology and electronic information to provide and support health-care and exchange medical information remotely without regard to the distance that separates the participants[11]. The concept of using communication technology for diagnosis and treatment of patient in other locations is probably as old as the telephone. Telemedicine, however, is more than simple voice communication over telephone lines; since it includes the transmission of still images, video, and other forms of medical data. Telemedicine requires a multidisciplinary approach spanning various sectors like biology, medical science, networks, communications and multimedia processing. The current computer network and communication technologies enable us to create a virtual health-care environment that will cover most areas that conventional health-care can not. Specialized application software and medical devices capable of electronic data collection, storage and transmission are the key components of the telemedicine infrastructure. This infrastructure includes the physical facilities and equipment used to capture, transmit, store, process, and display medical data and images[12].

2.2 Medical Imaging Modalities

2.2.1 X-ray Radiography

Conventional radiography, more commonly known as X-ray, is the oldest and the most widespread technique of medical imaging[13]. In X-ray images are created by passing small, highly controlled amounts of radiation through the body, capturing the resulting shadows and reflections on a photographic films or radiation sensitive plates. Due to their calcium content, bones are the most opaque and thus the most visible tissue on X-ray images. Soft tissues are less opaque than bones, but more opaque than adipose tissues. Air and gas are completely radio-transparent. X-ray radiography is the method of choice for the first line diagnostic of skeletal pathologies. It is also currently used for imaging lungs and breasts (mammography). This most commonly used clinical method has however, some drawbacks. As the depth information is lost, the 2-dimensional X-ray image will be a complex superposition of all the structures of the 3-dimensional body. Furthermore, the size on the image of an object is dependent on its distance to the X-ray source resulting in a distorted scaling factor of the picture. In addition, the contrast of the image suffers from limited dynamic range of the attenuation coefficients that exist in the human body[14]. Besides, there are few serious hazards associated with usage of ionizing radiation.

2.2.2 Computed Tomography

Conventional X-ray imaging has an inherent limitation in resolving overlying structures as everything seen in the images are the result of a projection. However, by using Computed Tomography (CT) scan, it is possible to reconstruct 3D distribution based on a large set of X-ray projections obtained at different angles covering a complete circle around the patient[13]. Once the projected values are collected, they can be digitally filtered and back-projected mathematically onto a matrix which represents fine differentiation of tissue densities[14]. Naturally the 3D information cannot easily be displayed as such; instead it is most often displayed as a series of axial slices. Since the image is digital and represents a slice, multiple slices can be obtained and a volume estimated and displayed as a three-dimensional structure on a video display tube or film. This distinction is enough to discriminate most of the soft tissue organs of the brain, abdomen and lungs. Computed tomography has the advantage of rapid acquisition of images, but employs ionizing x-ray radiation which must be used conservatively to avoid harmful cumulative biologic effect. But the cost involve in this modality will be on the higher side.

2.2.3 Mammography

Breast imaging can be performed using different medical imaging techniques. However the most effective and economical breast imaging modality so far has been mammography because of its simplicity, portability and low cost. A Mammogram is an X-ray picture of the breast acquired by low doses of ionizing radiation to reveal tumor growths that are undetectable in a physical examination[15]. The abnormal growths of tumors or micro-calcification clusters in mammograms are diagnostic signs of breast cancer that may be malignant or benign. Figure 2.2 shown 3 different mammograms: normal, benign and malignant taken from Digital Database for Screening Mammography (DDSM)[16]. Malignant clusters appear as groups of small, bright particles with arbitrary shapes embedded in a non-homogeneous background.

Therefore, early detection of breast cancer using periodical screening program based mammography is currently the most effective way to prevent the fatal stage.

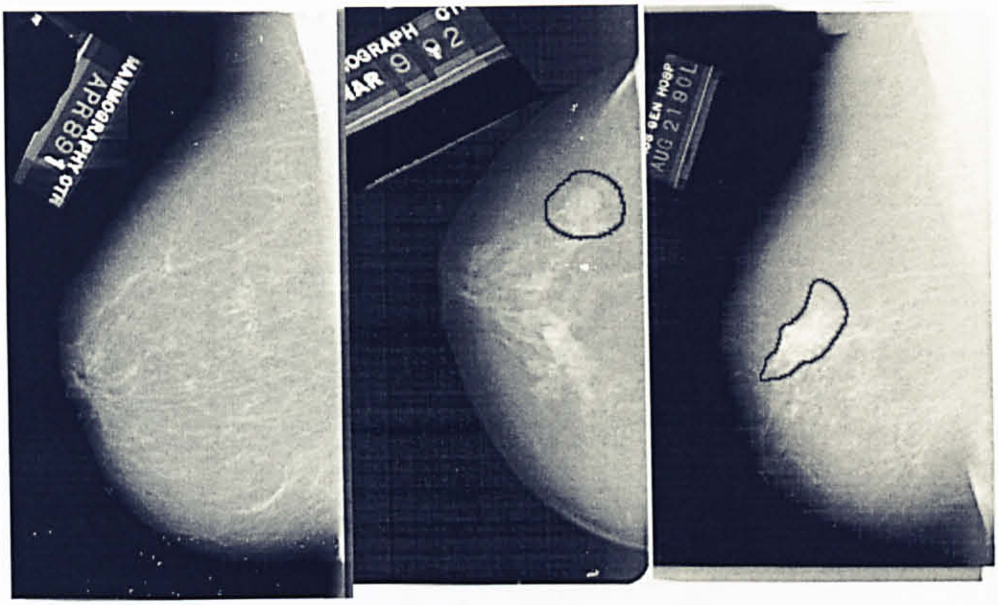

(A) (B) (C)

Figure 2.2: Mammograms :(A) Normal (B) Benign (C) cancerous malignant[16]

2.2.4 Magnetic Resonance Imaging

Magnetic resonance imaging (MRI) is an imaging technique used primarily in medical fields to produce high quality cross-sectional image of the human body. The MRI technology is based on a spectroscopic technique used by scientists to obtain microscopic chemical and physical information about molecules. In MRI, the characteristics of nuclei of atoms of certain elements in the body tissues that can be magnetized when placed in a strong magnetic field. These magnetized nuclei are then energized by a radiofrequency pulse. The stored radio signals emitted by the protons are used by highly specialized equipment to make sectional images of the body. Contrast between the images of different types of tissues made by MRI is the result of variation in their composition and concentration of protons. MRI is non-invasive and does not use radiation, however it is costlier compared to X-ray and ultrasound [17].

2.2.5 Nuclear Medicine

Nuclear Medicine (NM) comprises the medical diagnosis and therapy use of radioactive isotopes for imaging of organs, distribution of metabolism or pathophysiological processes by the use of position sensitive detectors for detection of penetrating ionizing radiation, most often gamma rays[18]. In diagnosis, radioactive substances are administered to patients and the radiation emitted is measured. The majority of these diagnostic tests involve the formation of an image using a gamma camera. In therapy, radionuclide is administered to treat the disease or provide palliative pain relief. The topographic methods used in nuclear medicine are Single Photon Emission Tomography (SPECT) and Positron Emission Tomography (PET). SPECT is able to provide true 3D information by using a gamma camera to acquire 2-D images from multiple angles. This information is typically presented as cross-sectional slices through the patient, but can be freely reformatted or manipulated as required[19]. Because SPECT permits accurate localization in 3D space, it can be used to provide information about localized function in internal organs such as functional cardiac or brain imaging. PET scan is a diagnostic examination that involves the acquisition of physiologic images based on the detection of radiation from the emission of positrons that administered to the patient[20]. The subsequent images of the human body developed with this technique are used to evaluate a variety of diseases such as characterizing biochemical changes in the cancer to examine the effects of cancer therapy, determining blood flow to the heart muscle and help evaluate signs of coronary artery disease and PET scans of the brain are used to evaluate patients who have memory disorders of an suspected or proven brain tumors or seizure disorders. PET can give false results if a patient's chemical balances are not normal. Specifically, test results of diabetic patients or blood sugar or blood insulin levels. The radioactive substance may expose radiation to the fetus in patients who are pregnant or the infants of women who are breast-feeding.

2.2.6 Ultrasonography

Medical ultrasonography refers to the use of echoes from ultrasonic waves to generate visual images of abdominal organs (liver, kidney, and gallbladder)[21]. In Medical profession, ultrasound is considered as the most widespread and versatile medical imaging modality for diagnosis of various major diseases. While it may provide less diagnostic information than more sophisticated techniques such as CT or MRI, it has several advantages which make it ideal as a first line test to estimate the degree of complexity. These advantages include safety, as the patient is not exposed to radiation. The equipment is relatively small, easy to handle, quickly to perform and more economical than other options. Furthermore, ultrasound is also well-known for its applications in obstetrics, where it is used to examine the different stages of fetus during pregnancy.

Ultrasound images have some unique features that make them different from natural images. A simple natural image consists of a few edges against a relatively uniform background, but ultrasound images exhibit speckle texture over the entire ultrasound scanned area. The oriented speckle texture, an ultrasonic scanning artifact caused by scattered reflections, is typically concentrated in certain spectral regions due to the orientation of the speckle pattern[22]. An example of an organ that produces a particularly speckle ultrasound image is the liver, as shown in Figure 2.3.

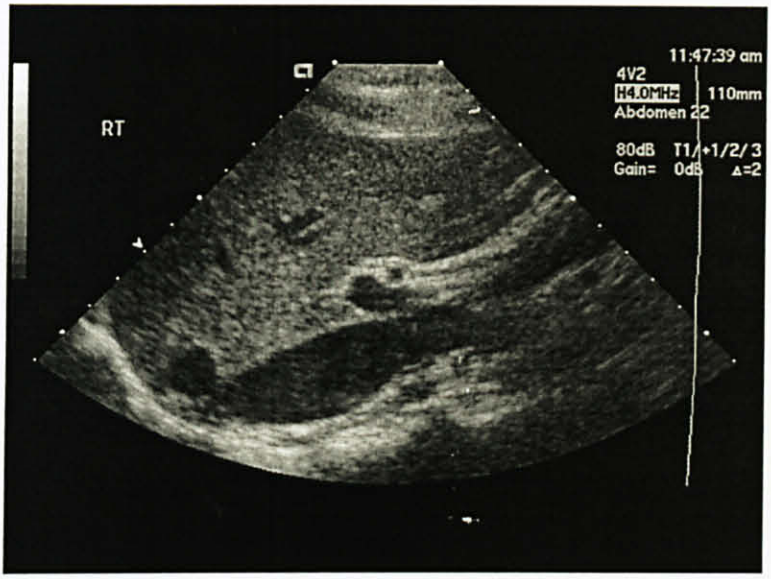

Figure 2.3 :Typical ultrasound image of a normal liver [23]

Depending on the context and application, speckle in medical images can be viewed as signal or noise. For example, speckle can be used to characterize tissue or it can mask diagnostically relevant features [23].

Another characteristic of ultrasound images is the spatial variation in pixel statistics across an individual image. A typical image consists of an ultrasound-scanned area, which is often special conical shape, against a passive background, which may contain text and limited graphics as shown in Figure 2.3.

2.3 Images Compression

The aim is of image compression is to encode images to reduce the size as possible with a decoding mechanism which reconstructs the original image with an acceptable visual quality. Image compression is becoming more crucial and regarded as key technology in the development of multimedia and telecommunication in general and tele-healthcare application in particular.

2.3.1 Redundancy

Image compression takes advantage of the fact that there is a lot of redundant information contained in the original image. Mostly there are three kinds of redundancy: psycho-visual, inter-pixel and coding redundancy. In inter-pixel redundancy, there are statistical dependencies between pixels especially between neighboring pixels. Such dependencies can be suppressed by compression. Psycho-visual redundancy is due to the fact that human eye does not respond with equal sensitivity to all image signals since some are even not perceivable and certain information simply has less relative importance than the other in human visual processing. Therefore eliminating some information may be acceptable. In coding redundancy, the uncompressed image usually has pixel of fixed length code which is convenient for processing the image but uses unnecessary space. By using some variable length coding saves requirement can be reduced. There are different methods for dealing with the different kinds of redundancy. Image compression methods are usually multi-step algorithms which are applied to reduce these redundancies. Image compression schemes can be categorized as lossless and lossy. Application of these schemes depends upon the required quality of the reconstructed image.

2.3.2 Lossless Image Compression

In lossless compression, the image reconstructed after decompression is numerically identical to the original image. This is obviously most desirable since no information is compromised. However, it can achieve only compression ratio of 2:1 – 4:1[5]. Lossless image compression is preferred in sensitive applications such as medical imaging, military and astronomy.

To perfectly reconstruct the original image, lossless compression methods take advantage of the statistical properties of the redundant data (inter-pixel and coding redundancy). The goal of lossless compression is to find and eliminate this statistical redundancy with a guarantee to generate an exact duplication of the input image after a compress/decompress cycle. Modern lossless image compression algorithms employ different techniques. Most of the lossless compression methods can be classified under three fundamental paradigms namely: Predictive with statistical modeling, Transform-based and Dictionary-based.

2.3.2.1 Predictive with statistical Modeling

There are two distinct and independent components for the predictive and statistical modeling: Modeler and Coder [24]. As the modeler is gathering some information about the image data by tracking some context and identifying a probability distribution, the coder, after scanning the current pixel x_i , uses this information to encode the next pixel x_{i+1}. The goal is to find an estimate (prediction) of x_{i+1} that maximizes the conditional probability: $P\ (x_{i+1} \mid x_1, x_2 \ldots x_i)$ while scanning image data sample by sample in raster-scan. Because of the high correlation between neighboring pixels, the prediction value usually is estimated by using a simple function of previous neighboring samples. The difference between the actual pixel value and its predicted value is expected to be relatively small in absolute terms and this is called as differential or the error signal .The value of this error signal is always entropy coded.

After estimating the prediction value, the next step is the determination of context (function of possible different casual template) in which a value x_{i+1} occurs. Then a probabilistic model for prediction error is estimated. Some examples of predictive and statistical modeling are Lossless-JPEG, JPEG-LS, Context-based Adaptive Lossless Image Compressor (CALIC), Fast and Efficient Lossless Image Compression (FELICS) and Binary Tree Predictive Coding BTPC (BTPC). In Lossless-JPEG a simple linear prediction combined with Huffman coding. JPEG-LS is based on LOw COmplexity lossless compression (LOCO-I) method that employs nonlinear simple edge detector prediction [25], in particular with Golomb-Rice coding and Run Length Encoding (RLE). CALIC combines non-linear prediction with advanced statistical error modeling techniques to improve compression efficiency but at the price of the coder complexity. FELICS is able to achieve reasonable compression ratio in optimal time by coding each pixel in the context of two nearest neighbors. BTPC is a multi-resolution technique designed to perform both lossy and lossless compression and working efficiently for different types of images. The main idea behind BTPC is to decompose the image into a binary tree.

2.3.2.2 Transform-based Schemes

In transform-based scheme, the image is transformed to a new domain in which they are better organized and easier to compress than in the normal spatial domain. Natural images have a lot of spatial correlation between pixel intensities, and these correlations can be exploited by the transform. A transform operates on an image's pixel intensities and converts them into a set of transform coefficients. This transformation concentrates the important image information into a more compact form in which the redundancy can be removed. Transforms generally come in pairs of forward and inverse forms. If both the forward and inverse transforms are applied without compression, then the transform is either perfectly reconstructing (lossless), or the image information is quantized and lost after the transform stage (lossy). A lossless transform does not further complicate an image compressor since it makes no decisions about which parts of the image data are useful. However a lossy transform can often produce more compression and allow the transform algorithm to run faster. The transform can either be orthogonal, orthonormal or non-orthogonal. It is common to use orthogonal/orthonormal transforms in image compression, because they are efficient and the transform coefficients are highly de-correlated. The Discrete Cosine Transform (DCT) and the Wavelet Transform are examples of orthonormal transforms that are used in image compression. JPEG2000 and SPIHT are examples of transform-based in wavelet domain[26, 27]. JPEG2000 is the latest standard for still image coding that is based on the discrete wavelet transform (DWT), scalar quantization, context modeling, arithmetic coding and post-compression rate allocation. Lossless mode of JPEG2000 is achieved through the use of a special integer wavelet filter (biorthogonal 3/5 instead of Daubechies biorthogonal 7/9) and a quantization step size of 1. Both lossless and lossy mode of JPEG2000 bitplanes have to be encoded by the Embedded Block Coding with block Truncation EBCOT with no drop of any bitplane [28]. SPIHT is achieving lossless mode by using reversible wavelets (S+P). S+P is a reversible wavelet transform that allows for reversible image recovery by truncating the transform coefficients at some step in the transformation and encoding all of the transform coefficients. The S+P transform allows for either progressive fidelity or progressive resolution implementations and utilizes the information from both the low and high-resolution bands for prediction and then truncates the prediction value to an integer. This transformation reduces the source entropy in the resulting image representation, which is then encoded using either arithmetic or Huffman coding[29, 30].

2.3.2.3 Dictionary-based Schemes

The dictionary based compression algorithms substitute shorter codes for longer patterns of strings within the image data. Pixel patterns (substrings) in the data stream found in the dictionary are replaced with a single code[31]. If a substring is not found in the dictionary, a new code is created and added to the dictionary. Some examples of dictionary-based methods are Graphic Interchange Format (GIF) and Portable Network Graphics (PNG) [32] which are widely used in the Internet. PNG was created to improve upon and replace the GIF. It uses preprocessing to remove data redundancy, that is followed by the deflate algorithm.

2.3.2.4 Entropy Coding

An entropy coding is a coding scheme that assigns codes to symbols so as to match code lengths with the probabilities of the symbols and it usually the last stage in the image compression. Typically, entropy encoders are used to compress data by replacing symbols represented by equal-length codes with symbols represented by codes proportional to the negative logarithm of the probability. Therefore, the most common symbols use the shortest codes. According to Shannon's theorem[33], the optimal code length for a symbol is $\log\frac{1}{bp}$, where b is the number of symbols used to make output codes and p is the probability of the input symbol. Three of the most common entropy encoding techniques are Huffman coding, Golomb -Rice coding and arithmetic encoding.

2.3.3 Lossy Image Compression

Lossy compression permits distortion over original image to obtain much higher compression ratio than lossless methods. Theoretically, it can compress an image to any ratio. However, as the compression ratio goes higher, the degradation of the image will become serious. Lossy compression takes advantage of two factors to achieve this goal: on one hand spatial image is highly correlated (i.e. neighboring pixels tend to have similar value), and the limitation of human eye which cannot perceive small errors in images especially the sensitivity which is lower in the high frequency domain. The degree of degradation of the compressed image usually depends on the compression algorithm and the targeted compression ratio. In most lossy compression the original image is transformed from spatial domain to frequency domain such as DCT and the DWT. The compressor then removes the redundancy in the transformed image and stores it in a compressed format. JPEG is DCT-based standard and has several modes: baseline, lossless, progressive and hierarchical. Baseline mode supports only lossy coding in which the image is divided into 8x8 pixels blocks and each of these is transformed with the DCT. The transformed blocks are quantized with a uniform scalar quantizer, zigzag scanned and entropy coded with Huffman code. Some of the well-known wavelets-based compression schemes are JPEG2000 and SPIHT. JPEG2000 is a wavelet-based image compression standard in which the pixel data is wavelet transformed. The wavelet transform coefficients are then quantized and the indices of each sub-band are divided into code blocks (e.g. 32x32 pixels). Then the bit-plane coding is performed in each code block independently. SPIHT is an image compression algorithm that exploits the inherent similarities across subbands in a wavelet decomposition of an image. It implies uniform quantization and bit allocation applied after wavelet decomposition. In some systems the transformation is combined with predictive stage where previously and/or subsequently decoded data are used to predict the current image sample. The error between the predicted data and the real data, together with any extra information needed to reproduce the prediction, is then quantized and coded. Lossy mode of BTPC is not a transform-based scheme, but uses a binary pyramid, predictive and Huffman coding.

2.3.3.1 Scalar Quantization

Quantization is to reduce set of possible symbols S to much smaller set S` by mapping each element of S to element in S`. An example of quantization is analog-to-digital converter with a fixed number of bits. Another example is to take the set of all 8-bit integers (2^8 = 256 elements) and divide by 4 (*i.e.*, drop the lower two bits). That means, each element is represented by 6-bit (2^6 = 64 elements). Since the mapping used in quantization is many-to-one; it is irreversible (lossy) and therefore the quantization is the main cause of loss in lossy compression. In general, quantization proceeds by taking the interval of variation of the signal and decomposing it into subintervals (quantization bins). The center of the quantization bin (midpoint of the interval) can serve as a symbol representing all elements in this subinterval. In the case that the set S comes from a total order and the total order is broken up into regions that map onto the elements of S', the mapping is called *scalar quantization*. Application of scalar quantization includes reducing the number of color bits or gray-scale levels in images. Figure 3 shows the input-output characteristic (the output with respect to input) of the two types of scalar quantization[34].

The term *uniform scalar quantization* is typically used in special case where the domain of input values partitions into equally spaced intervals (bins of the same length), except the possibly the outer intervals. The length of each interval is referred to as the step size, denoted by the symbol Δ. Uniform scalar quantization has two types as shown in Figure 2.4. Midrise quantizes have even number of output levels and Midtread quantizers have odd number of output levels, including zero as one of them. For special case where Δ =1, the output values for these quantizers can be computed as:

$$Q_{\text{midrise}}(x) = \lceil x \rceil - 0.5 \tag{2.1}$$

$$Q_{\text{midtread}}(x) = \lfloor x + 0.5 \rfloor \tag{2.2}$$

A non-uniform quantizer uses bins of different sizes. In practice it is often better to use a *nonuniform scalar quantization*.

The result of quantization is serves as an input to entropy coding.

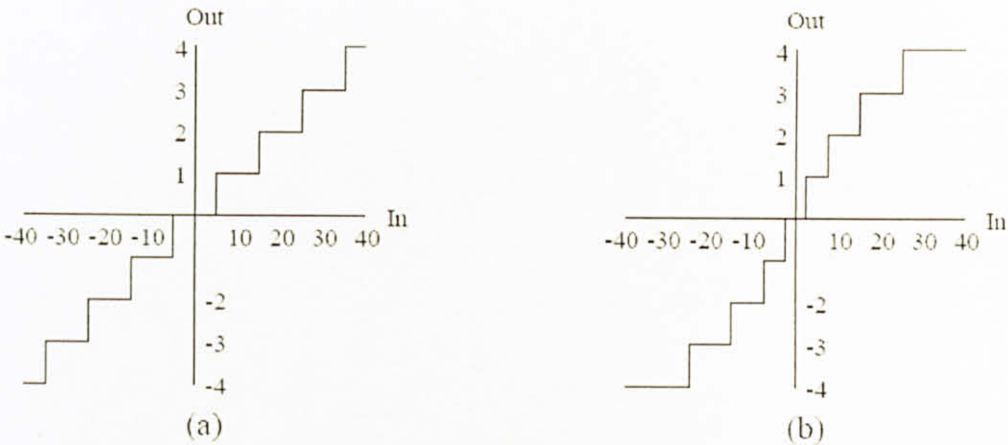

Figure 2.4: Examples of (a) uniform and (b) non-uniform scalar quantization.

2.3.3.2 Vector Quantization

The general idea of mapping a multidimensional space into a smaller set of messages S' called *vector quantization*[35]. Vector quantization is typically implemented by selecting a set of representatives from the input space, and then mapping all other points in the space to the closest representative. The representatives could be fixed for all time and part of the compression protocol, or they could be determined for each file (message sequence) and sent as part of the sequence. If one considers quantization and entropy coding together, it is better to represent the signal with a minimal number of components, and control the dynamic range and significance of these components. The choice of the transformation is critical for the effective overall lossy compression.

2.4 Performance Criteria of Image Compression Methods

Each compression scheme has some merits and demerits that manifest on showing different performance on different types of images. Normally, such algorithms are designed in a way that suite and give better performance. In order to have a comparison between various images compression schemes, different performance criteria should be measured. Three most important characteristics of image compression algorithms are Compression Efficiency (CE), Compression Speed (CS) and Distortion Measures (DM). While the first two are algorithm-dependant, the later criterion is used to measure the distortion made by lossy compression.

2.4.1 Compression Efficiency

Compression efficiency gives the measure of reduction in data volume achieved by a given compression algorithm. The most common used unit to quantify compression efficiency is Compression Ratio (CR). CR is simply the size of the original image divided by the size of the compressed image as shown in Equation (2.3). This measure accurately shows the effect of compression on the original data.

$$CR = \frac{Size \quad of \quad original \quad image}{Size \quad of \quad compressed \quad image} \tag{2.3}$$

There are many other definitions used to express CR in a different way. Among them the Compression Percentage (CP) is the compression ratio expressed as percentage and Bit Rate (BR) refers to the average number of bit per pixel of the compressed image. As the source entropy is the lower bound on the bit rate that lossless compression can achieve, the efficiency of lossless compression methods can be measured by determining how close its BR from the source entropy[33]. Suppose that the pixel gray values range from 0 to $M\text{-}1$. Let p_i be the probability of the gray value i, the information content of the image is given by its entropy as given in Equation (2.4) [36]. The unit of entropy is bits per pixel.

$$H = -\sum_{i=0}^{M-1} p_i \log p_i \tag{2.4}$$

2.4.2 Computational Speed

Since users expect their images to be transmitted at the minimum time, it is important to that computational speed of the compression algorithm is to be increased. The computational speed of compression algorithm is measured by compression/decompression time (CT/DT). CT/DT in seconds are calculated based on the number of clock ticks spent to execute the coder/decoder, as number of ticks per second is constant for given processor. If the combined time that is taken for compression and decompression is small then we may define compression speed as high. To compute the duration of CT or DT in seconds, the numbers of ticks at the start (START) and at the finish (FINISH) of the process are used as shown in Equation (2.5).

$$\text{Duration (CT or DT)} = \frac{\text{FINISH - START}}{\text{CPU speed (ticks per second)}} \tag{2.5}$$

The duration depends on the complexity of the algorithms and the speed of the processor. Considering compression/decompression times, some compression methods are symmetric, which means equal time for compression and decompression. An asymmetric algorithm takes more time to compress than to decompress.

2.4.3 Distortion Measurements

The introduced distortion into the reconstructed image during lossy compression process can be measured according to different image quality matrices. These metrics can be broadly classified into two categories, subjective and objective. Subjective quality metrics is a method of evaluation of images by the viewers and it emphatically examines fidelity and image intelligibility. In objective measures, some statistical indices are calculated to indicate the reconstructed image quality. The image quality metrics provide some measures of the closeness between two digital images by exploiting the differences in the statistical distribution of pixel values. The most commonly used metrics for comparing compression are Mean Square Error (MSE) and Peak Signal to Noise Ratio (PSNR)[37].

Mean Square Error

Mean Square Error (MSE) is the mean of square distance (difference) between pixels in the original image and their respective values in the reconstructed image. MSE can be expressed as Equation (2.6):

$$MSE = \frac{1}{N \times M} \sum_{i=0}^{N-1} \sum_{j=0}^{M-1} \left(New_{ij} - Original_{ij} \right)^2 \tag{2.6}$$

Where New_{ij} is the pixel intensity of the decompressed image at position *i,j* and $Original_{ij}$ is the original pixel intensity at position i,j, N and M are the dimensions of the image.

Peak Signal to Noise Ratio

PSNR is a measure of the peak error. Because images may have wide dynamic range, PSNR is usually expressed in decibel scale. PSNR (dB) is given by Equation (2.7):

$$PSNR = 10 \log_{10} \left[\frac{MAX^2}{MSE} \right] \tag{2.7}$$

Where MAX is the maximum pixel value of the image and can be found form the number of bits per pixel (B) as follows:

$$MAX = 2^B - 1 \tag{2.8}$$

It is quit clear from Equation 2.7 that the lower MSE value the higher is the PSNR and the better the compression ratio is.

2.5 Medical Image Compression

Due to increased necessity for telemedicine applications, there is desperate demand to store and hold medical images in digital form for transmission and archive in order to efficiently use these two limited resources. The transmission or exchange of medical image is to help deliver healthcare to patients in remote areas (tele-healthcare) and share medical knowledge over distance for better medical services (tele-consultation). Telemedicine is primarily concerned with the transmission of medical data between rural and urban areas. So it is important that the technology takes advantage of existing cost-effective communication infrastructure. The time for image transfer must be minimized in a remote telemedicine consultation. It is not acceptable for medical experts to spend a significant amount of time simply waiting for image data to arrive.

The need for archive grows due to the fact that medical images need long-term storage for future interpretation or research to study and combat certain diseases. The transmission/storage problem of medical images is noticeably increasing due to the fact that such images occupy large amount of storage space. The dimensions of medical image vary from one modality to another while the grey level can reach 12 bits. Table 2.1 shows typical image sizes for some medical image modalities.

For example, a typical mammogram must be digitized at a resolution of about 4000 x 5000 pixels and 12 bits, resulting in approximately 40Mb of digital data. Such high resolution is required in order to detect isolated clusters of micro-calcifications that herald an early stage cancer. In a single medical ultrasound examination there are on the average 10 to 20 still images generated equaling to approximately 24.6 to 49.2Mb of grayscale image data, which means that a large volume of digital image data is generated. Due to the rising numbers of patients and elongated case histories, ultrasound images accumulate rapidly and filling limited storage space available in hospitals.

Table 2.1: Sizes and brightness levels of various medical images[38]

Modality	Spatial resolution(pixels)	Brightness Level(bits)
CT SCAN	512 × 512	8 to 12
MRI	256 × 256	12
Mammogram	4000 × 5000	12
Ultrasound	512 × 512	8
X-ray	2048 × 2048	12

Moreover, the large number of medical images that are produced in moderate hospital escalating the problem by increasing the required storage. This massive amount of data not only makes the storage and transmission expensive, but also affects the speed of communication. Therefore, an effective compression is essential to reduce the file size as much as possible, making storage access and transmission facilities more practical and efficient.

2.6 Survey of Medical Image Compression

2.6.1 Lossless Medical Image Compression

During the last few years there have been many research works on medical image compression. Generally speaking, most of these works are based on the pre-exist image compression methods. However, research on medical image compression concentrates on methods that are used for continuous-tone and grayscale images. As an initial step, the evaluation of compression method on medical images is essential. For example as in [39], Clunie has evaluated a large set of lossless image compression on multiple Modalities. Lossless JPEG[40], JPEG-LS[41], CALIC[42], S+P[43], SZIP[44], PNG , PACKBITS, Unix pack, Unix compress, CREW [45] and GNU gzip [46] are tested on sample set of digital radiography, computed tomography, MRI, mammography, US and NM . But there is no indication of how many images are involved. The work concluded that the JPEG, JPEG-LS, and SZIP codecs were noticeably faster than the others and CALIC was noticeably slower. JPEG-LS, JPEG2000 and CALIC performed equally well and outperformed existing JPEG and dictionary-based schemes which performed poorly. One of the major drawbacks of this study is that the compression methods are evaluated on different type of images despite the variation in the textures. The study used many general-purpose compressions like SZIP, UNIX pack, COMPRESS and GZIP which are preferred for non-image data. Compression method like PackBits is simple compression scheme for run-length encoding of general data.

In another work by Kivijärvi [47], general-purpose and image compression methods have been applied on medical images of various modalities, namely computed radiography, computed tomography, MRI, NM, and US. It was observed that CALIC and JPEG-LS performed well as compared to Lossless JPEG and PNG. This study hadn't the opportunity to examine the performance of latest JPEG2000 scheme. The measurement of compression ratio was taken as the average of the results of all modalities, regardless of the fact that different modalities may have different redundancies.

In another research, Denecker [48] use five image-based compression schemes: lossless JPEG , BTPC[49], FELICS[50], S+P and CALIC and two general-purpose compression schemes GZIP and STAT on computed tomography, MRI, PET, US, X-Ray and angiography images. It is indicated that CALIC performed best and S+P achieved second best performance. The performances of lossless JPEG and GZIP are not up to the mark. In the study the number of tested images was not specified. So it is difficult to interpret their results.

From these studies it can be readily inferred that some compression methods such as Lossless JPEG, JPEG-LS, CALIC, S+P, BTPC, FELICS, PNG and JPEG2000 are performing efficiently and showing some variation on various medical modalities. These methods are always dominating in the research work of many people.

2.6.2 Lossy Medical Image Compression

In lossy compression, Erickson [5] reviews some previous work in medical image compression and suggests that irreversible compression can be used for medical image storage and transmission. However, the irreversible compression must be used carefully without compromising diagnostic quality. He discussed compression of images from a variety of medical imaging modalities, including computed tomography, MRI, chest radiography, and US showing that some types of medical images tolerate much higher levels of compression than others. Compression tolerance is defined as the maximum compression in which the decompressed image is acceptable for interpretation. Chest radiographs are very tolerant of compression (at least 40:1 for SPIHT wavelet), bone x-rays are moderately tolerant (between 20:1 and 40:1), and computed tomography, MRI, and US images exhibit fairly low tolerance to compression (less than 20:1). He found in his study that wavelet compression such as JPEG2000 and SPIHT outperform JPEG due to the blocking artifacts produced by JPEG. In this study all the conclusions are based only on literature survey.

Out of different lossy compression methods JPEG has been used for a long time for medical images especially on DICOM [51]. Wavelet-based lossy image compression in general (JPEG2000 and SPIHT in particular) are introduced recently as efficient methods that give the best tradeoff between compression efficiency and image quality. Robinson in 2003 has shown that lossy mode of BTPC is an efficient method that can generally compete with JPEG in different types of images [49].

Przelaskowski applied four effective lossless coders (Binary context-based Arithmetic Coder (BAC), CALIC, JPEG-LS and JPEG2000) and two wavelet lossy coders JPEG2000 and modified Basic Wavelet Technique (MBWT) on 22 selected mammograms. It is found that BAC and CALIC are giving better bit rate values than JPEG-LS and JPEG2000. This work mainly emphasizes on subjective quality measurements to measure the distortion that is made by lossy methods. The study concluded that the radiologists agreed that wavelet compression up to 1 bit per pixel is safe to be used without loosing the diagnostic accuracy of compressed mammograms[52]. They also reported that lossless compression schemes can only achieve CR less than 2:1.

The same author Przelaskowski [53] has updated his previous work by testing five more lossless compression methods; namely Adaptive Predictive Tree (APT), SPIHT, optimized JPEG2000, JPIG and JB2 on 131 mammograms. It was shown that CALIC, JPEG-LS, and SPIHT have performed well. It can be clearly noticed that there is inconsistency in the results of his two works on lossy compression. His results show that the compression ratio 14:1 is the accepted limit for lossy wavelet compression on mammograms without degrading quality.

In another work by Delgorge [54], six lossless compression techniques (Huffman coding, arithmetic coding, Storer and Szymanski's modified version of Lempel Ziv's algorithms (LZSS), RLE [55] coding and Fano algorithms) are applied on 10 ultrasound images. Later he included JPEG-LS also. The study found that although arithmetic coding gives the best compression rate, the adaptive Huffman method gives the best compromise between compression rate and computing time. Because the arithmetic coding associates with larger coding time and RLE is not suited to ultrasound image images, as its compression rate is the largest. The study also compares adaptive Huffman with the lossless mode of JPEG-LS to conclude that JPEG-LS is the best for lossless compression of ultrasound images. All these techniques are known as entropy coders normally used as a last step in compression algorithms. Any practical comparison should use state of art schemes which combine some preprocessing techniques such as context predictive or transforms prior to those entropy coders. For lossy comparison the author has chosen Near-Lossless mode of JPEG-LS, JPEG and JPEG2000 using MSE, PSNR and compression time as the metrics. Near-Lossless mode of JPEG-LS has been reported as the best method when the compression ratio is less than 5 (closer to lossless) and JPEG2000 becomes the optimal method for higher compression ratio.

2.7 Region-based Image Compression

In recent years, much attention has been paid to region-based coding due to its functionality that suite various applications in which certain parts of an image are more meaningful than the others parts of the image. Thus, these parts can be encoded in such away to preserve image quality; one of these applications is the compression of medical image data for archiving and transmission.

2.7.1 Shape Adaptive DCT

Shape Adaptive DCT (SA-DCT) algorithm was adopted for coding arbitrary shaped image segments in DCT-based compression [56]. The algorithm is to encode only the Region of Interest (ROI) separately from the background employing DCT on 8 x 8 image blocks. The two dimensions DCT of the ROI block is computed in two steps, each involving only one dimension DCT. First, the vertical DCT is computed by transforming each column of foreground pixels. This is followed by the horizontal DCT which transforms each row of coefficients obtained from the vertical DCT. To compute the vertical DCT of a block, each column which may contain different number of ROI pixels is shifted upwards, so that all columns are justified to the top of the block. The horizontal DCT is computed for each row of coefficients obtained from the previous step, as follows. First, each row of different number of coefficients is shifted left, so that all rows are left justified. After transformation, the number of DCT coefficients obtained is the same as the number of pixels that form the ROI. The DC coefficient is located in the upper left corner of the block, as occurs in the block based DCT. SA-DCT algorithm is supported in MPEG-4 standard for its computational efficiency, however, as all DCT-based methods, it suffers blocking artifacts that limits its use for low bit rate coding the foreground.

2.7.2 ROI in JPEG2000

A better alternative which works on wavelet-based image compression is to scale up the wavelet transformed coefficients of ROI so that the bits associated with ROI are more significant than the bits associated with the non-Region of Interest (non-ROI). Then during the embedded coding process, the most significant ROI bit-planes are placed in the bit-stream before any non-ROI bit-planes of the image. Two kinds of this scaling method are defined in JPEG2000 standard: the maximum shift (MAXSHIFT) and the general scaling-based method as shown in Figure 2.5[57]. MAXSHIFT separates the ROI from non-ROI by scaling up the coefficient associated with ROI through a number of bit shift. The scaling value is chosen to be sufficiently large to ensure that all the significant bits associated with ROI will be in higher bitplanes than all the significant bits associated with non-ROI. MAXSHIFT allows arbitrary shaped coding without explicitly transmitting the shape information, as the decoder can separate ROI and the non-ROI coefficient by looking at the coefficient magnitudes. The major limitation of MAXSHIFT is that it doesn't have the flexibility to control the relative quality between ROI and non-ROI. This limitation has been solved in the general scaling based method in which the relative importance of the ROI and non-ROI is controlled by scaling up certain number of bit-shifts.

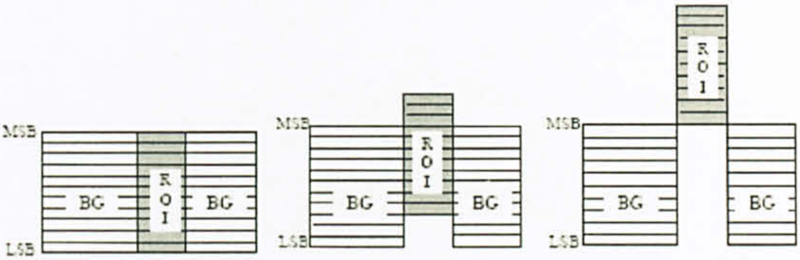

NO ROI Scaling based MAXSHIFT

Figure 2.5: General Scaling and MAXSHIFT ROI method in JPEG2000[57]

2.7.3 Shape Adaptive DWT

Shape Adaptive Discrete Wavelet Transform (SA–DWT) [58] is studied as a new region-based paradigm that decomposes arbitrarily-shaped objects and offers superior rate-distortion performance and better visual quality than the previous techniques. SA–DWT can retain most of the features of conventional DWT while working strictly on the ROI and never computed outside its boundaries. SA-DWT preserves the spatial correlation and self-similarity property of wavelet transforms. The 2-dimension SA-DWT for an arbitrarily shaped visual object can be done through number of steps of 1-dimension wavelet transform. In each row that corresponding to the shape information provided by the mask and with a proper subsampling strategy, a length-adaptive 1-dimension wavelet transform is applied to each segment of consecutive pixels. The lowpass wavelet coefficients are placed into the corresponding row in the lowpass band and the highpass wavelet coefficients are placed into the corresponding row in the highpass band. The above operations are performed for each column of the lowpass and highpass objects. These operations are repeated to the lowpass-lowpass band object until the level of wavelet decomposition is reached.

As the conventional wavelet transform is only performed on rectangular image region and cannot be done on arbitrary shape region, SA-DWT is identical to the conventional wavelet transform when applying it in a rectangular region (Figure 2.6).

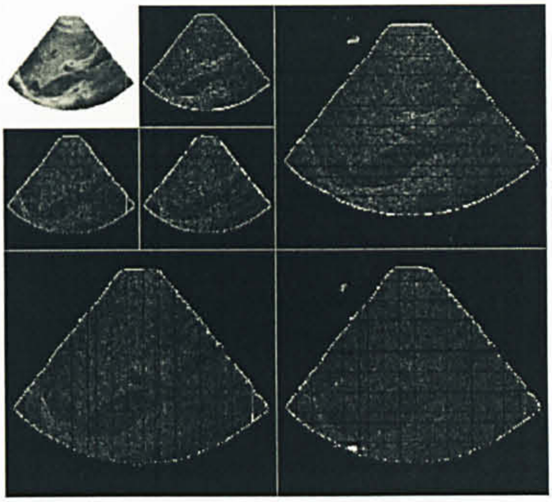

Figure 2.6: Multi-resolution decomposition of ultrasound image scanned area using SA-DWT

2.8 Summary

Various medical imaging modalities are frequently used to acquire interior structures and the functions of the living human body. Mammography and ultrasound imaging are the most common in tele-healthcare for their cost-effective and providing sufficient and reliable diagnostic information. Due to the large size of these images compression is essential. Image compression methods are categorized as lossless and lossy. The former perfectly reconstructs the original image. However, it can achieve low compression ratio. Lossy compression degrades the image to obtain much higher compression ratio than lossless methods. To have a comparison between various images compression schemes, different performance criteria such as compression ratio, compression speed and distortion Measures (i.e. MSE and PSNR) are generally used. In an effort to optimally compress medical images various methods are used, out which lossless compression like LJPEG, JPEG-LS, CALIC, FELICS, BTPC, JPEG2000, S+P and PNG in addition to lossy compression such as JPEG, BTPC, JPEG2000 and SPIHT are used in the literature. Region-based coding such as ROI in JPEG2000, SA-DCT and SA-SWT suites various applications in which certain parts of an image are more important and need to be preserved more than the other parts of the image.

CHAPTER 3

EVALUATION OF IMAGE COMPRESSION SCHEMES

3.1. Introduction

It is noticeable in the literature that mammograms and ultrasound images dominate in tele-consultations among the experts worldwide. Accordingly, the most efficient image compression techniques are needed to be studied in order to choose the best compression which will increase transmission speed and reduce storage space. The first half of this research work is concentrating on evaluation different compression algorithms to decide which ones are more suitable for mammograms and ultrasound images. Importance of mammograms and ultrasound images in tele-healthcare is described. A brief overview of all compression methods that used in this work is presented. It is followed by a review of some software implementation and compression libraries. Finally the methodology of evaluating the compression methods for the above images is described in detail.

3.2. Mammograms and Ultrasound Image Compression

Medical Imaging methods such as mammography and ultrasonography are cost-effective screening tools that provide sufficient and reliable diagnostic information to estimate the degree of complexity in telemedicine applications.

Because of its simplicity, low radiation, portability and low cost, periodical screening by mammography is currently considered as the most effective way to prevent the fatal stage of breast cancer [16].

Ultrasound image of abdominal organs is considered as the most widespread and versatile medical imaging modality for diagnosis of various major diseases[21]. Unlike other medical imaging modalities, ultrasound is the safest imaging modality as the patient is not exposed to any kind of radiation. Furthermore, Ultrasound equipment is relatively small, easy to handle, quickly to perform and more economical.

Using an optimal image compression scheme for mammograms and ultrasound is essential to reduce the storage requirement and transmission facilities more efficient. However, medical image which holds important diagnostic values (i.e. micro-calcifications in mammograms and speckle texture in ultrasound), cannot afford too much degradation. Thus an ideal compression method must be designed in order to give the best compromise between the higher compression ratio and the vital diagnostic quality.

There are numerous image compression techniques (lossless and lossy) proposed and found in the literature. However, In this work, based on the literature survey, eight efficient lossless compression schemes namely Lossless mode of JPEG (LJPEG), JPEG-LS, CALIC, FELICS, BTPC, JPEG200, Reversible Wavelets (S+P) and PNG and four lossy compression methods namely, BTPC, JPEG2000, JPEG and SPIHT are studied to investigate the limitation of lossless and lossy compression schemes and to determine the optimum trade-off between the distortion and compression efficiency for mammograms and ultrasound images.

3.3. Efficient Lossless Image Compression Schemes

Eight efficient lossless image compression methods have selected according to their performance on medical images in general and mammograms and ultrasound images in particular. Out of these eight methods LJPEG, JPEG-LS, CALIC, FELICS and BTPC are predictive-based schemes, JPEG200 and S+P are transform-based methods and PNG represents the dictionary-based scheme.

3.3.1 LJPEG

LJPEG is a commonly used lossless method to compress 8 and 16-bit grayscale images in medical applications. It is a totally independent algorithm from the well known baseline JPEG that uses DCT for lossy compression. LJPEG algorithm employs simple linear prediction followed by Huffman coding. In LJPEG prediction scheme, up to three previously observed neighboring samples I_w , I_{nw} and I_n can be combined to calculate the prediction value $\hat{x}$ of the current sample x among seven possible predictors:

I_w , I_n , I_{nw} , $(I_w + I_n - I_{nw})$, $(I_w + (I_n - I_{nw})/2)$, $(I_n + ((I_w - I_{nw})/2)$, and $((I_w + I_n)/2)$

The user must specify which prediction value should be used for the compression/decompression process. I_a denotes the intensity value at location a with respect to the current sample. Therefore, a generic position a is the different direction from the current sample x (w is left pixel, n is above pixel, nw is upper pixel to the left). The prediction error ($x-\hat{x}$) always has much smaller entropy than the original intensity values, which implies that the prediction process removes a great deal of inter-pixel redundancy. Therefore, these prediction errors are then encoded instead of the actual density values by Huffman coding.

3.3.2 JPEG-LS

JPEG-LS is a standard for lossless compression based on LOCO-I compression algorithm which combines good performance with fast and efficient implementation[25]. JPEG-LS allows a near-lossless mode which refers to a lossy algorithm for which each reconstructed image sample differs from the corresponding original image sample by not more than a pre-specified value which can be controlled by the encoder. The algorithm employs nonlinear simple edge detector predictors on causal neighborhoods, as defined by gradient information. Context modeling is designed to reduce the number of free parameters by defining the coding distributions at each context. For a given context, the encoder adapts to the best encoding method chosen from a fixed set that is matched to single parameter, exponentially decaying distributions. Efficient implementation is achieved through adaptive Golomb-Rice coding or RLE [41].

3.3.3 CALIC

Context-based Adaptive Lossless Image Coding (CALIC) is a compression method that puts heavy emphasis on image data modeling which make it relatively complex especially when arithmetic coding is used. A unique feature of CALIC is the use of a large number of modeling contexts to condition a non-linear predictor and make it adaptive to varying source statistics. In this adaptation process, CALIC only estimates the expectation of prediction errors conditioned on a large number of contexts rather than estimating a large number of conditional error probabilities. CALIC operates in either binary or continuous-tone modes, depending on the context of the current pixel. In the continuous-tone mode, gradient adjusted prediction takes place and is further improved by error feedback, where prediction errors are modeled under different contexts, leading to reduced conditional entropies. The coding step may involve either arithmetic or Huffman coding [42].

3.3.4 FELICS

Fast, Efficient, Lossless Image Compression System (FELICS) is a simple-to-implement method that combines the prediction and error modeling steps by utilizing the two nearest neighbors of a pixel in a raster scan order to estimate the probability distribution of the pixel intensity. Based on a parameter estimation method, the most suitable error model is chosen from a set, and the intensity is encoded using the Rice code of the model. The method uses prefix coding, and codes pixel values relative to the range described by the values in location *w(left pixel)* and *n* (above pixel). A 1-bit code describes if the pixel is in this center range, if not a 1-bit code describes which side (above and below) the value lies. The code for the center range is a function of the number of values lying in the range, and the code for the above and below ranges is symmetrical with respect from the distance to the center range [50].

3.3.5 BTPC

Binary Tree Predictive Coding (BTPC) is multi-resolution general-purpose image compression method which decomposes the image into a binary tree. It is designed to perform both lossless and lossy compression, and to be effective for different types of images. It is well suited for coding multimedia images which combine text, graphics and photographs, and is also appropriate as a general-purpose method when the image type is not known in advance. BTPC uses a binary pyramid, predictive coding and Huffman coding. BTPC is inherently progressive and a straightforward modification of the decoder to write directly to an on-screen picture buffer which allows simple progressive image recovery [49].

3.3.6 JPEG2000

JPEG2000 is an efficient coding standard for lossy and lossless multi-component still images and it is based on the discrete wavelet transform (DWT), scalar quantization, context modeling, arithmetic coding and post-compression rate allocation. The encoding process consists of the following four stages. First, for each component, the pixel data is transformed using reversible filter (for lossless mode) or irreversible filter (for lossy) wavelet transformation and an orientation tree sub-band structure is generated. Secondly in lossy mode, the wavelet transform coefficients are quantized into integer indices. In the third stage, the indices of each sub-band are divided into small code blocks (e.g. 32x32 pixels) and bit-plane coding is performed in each code block independently. The coded data constructs several quality layers. Finally, the code blocks are also grouped into precincts with a nominal size for each subband. The code coming from each precinct layer, resolution level and component will be wrapped into a packet and all the packets are organized to form the final bitstream in a certain progressive order[26].

3.3.7 S+P

The Said-Pearlman (S+P) transform is a reversible wavelet transform that allows for reversible image recovery by truncating the transform coefficients at some steps in the transformation and encoding all of the transform coefficients. The S+P is similar to the Haar wavelet image representation and allows for either progressive fidelity or progressive resolution implementations. The S+P transform utilizes information from both the low and high-resolution bands for prediction and truncates the prediction value to an integer for efficient implementation. This transformation reduces the entropy in the resulting image representation, which is then encoded using either arithmetic or Huffman coding [43].

3.3.8 PNG

The Portable Network Graphics (PNG) is an image file format that is recommended as a web standard by the Word Wide Web Consortium (W3C). Its dictionary-based compression method that uses preprocessing (predictive) to remove data redundancy, that is followed by LZ77 and the deflate algorithm. Huffman coding is used in PNG as entropy coder [32].

3.4. Efficient Lossy Image Compression Schemes

As an outcome of the literature survey, four frequently used lossy schemes namely JPEG2000, BTPC, JPEG and SPIHT are discussed. BTPC and JPEG2000 that are described in the sections 3.3.5 and 3.3.6 under lossless schemes can also operate in lossy mode. In the lossy mode of these compression methods additional quantization step is involved (see section 2.3.3.1).

3.4.1 JPEG

JPEG is an international standard for compression of continuous-tone images developed by Join Photographic Expert Group (JPEG), in a collaboration of three international standard organizations (ISO, CCITT, and IEC).The resulting JPEG standard includes four basic modes: sequential, progressive, hierarchical encoding and lossless. The group of the first three is known as baseline JPEG which is most popular and commonly used lossy compression. In the baseline, the image is divided in 8x8 blocks. Each block is transformed with the DCT. The transformed blocks are quantized with a uniform scalar quantizer, zigzag scanned and entropy coded with Huffman code. The quantization step size for each of the 64 DCT coefficients is specified in a quantization table. The DC coefficients of all blocks are coded separately, using a predictive scheme.

3.4.2 SPIHT

Set Partition in Hierarchical Trees (SPIHT) is an image compression algorithm that exploits the inherent similarities across subbands in a wavelet decomposition of an image. It implies uniform quantization and bit allocation applied after wavelet decomposition. The algorithm codes the most important wavelet transforms coefficients in priority and transmits the bits so that an increasingly refined copy of the original image is obtained. The order in which coefficients are transmitted is recovered on the decoder using some information obtained from sets being examined for significance during the sort. These sets are created using hierarchical tree data structure. One of the advantages with SPIHT is that it produces an optimal embedded bitstream. This means that the bitstream can be truncated at any instant, and is then guaranteed to yield the best possible reconstruction [27].

3.5. Image compression Software Implementations and Libraries

A typical software implementation of image compression consists of two separate components, encoder and decoder (codec) as shown in Figure 3.1. The former compresses the original image into a more compact format suitable for transmission and storage. The decoder decompresses the received image and reconstructs it to the exact or approximate original form. The process of reconstructing the image is always determined by the particular needs of the application.

Figure 3.1: A typical data compression system (codec)

Instead of implementing each algorithm from scratch; there are some optimized reusable compression libraries that can be incorporated in any application that transmits or archives collection of images. In accordance to this, some attention is given to the libraries that incorporate most of the above mention compression algorithms. These libraries are open source packages. Some commonly used compression schemes with their respective programming libraries are presented in Table 3.1. All the source codes of these libraries are in C/C++ language and they are arranged in a way to be used in MS Visual C++. One of the prominent obstacles that face the implementation of these libraries in MS Visual C++ under WINDOWS operation system is that most of them have been developed under Linux-like operation systems which need many changes when adapted to WINDOWS, such as changing some header files. The essential component of any compression software is the library written to provide general implementations of procedures commonly used in coding and compression applications such as entropy coding, scalar quantization, vector quantization and wavelets. These compression libraries are useful in the development of compression systems and in academic research.

Table 3.1: Lossless/Lossy compression schemes with their respective libraries

Lossless	Lossy	Libraries	Descriptions
LJPEG	JPEG	IJG JPEG library	Lossless JPEG
FELICS		Managing Gigabyte(MG)	Fast Efficient Lossless Image compression System
CALIC		X. Wu & N.D. Memon implementation	Context-based Adaptive Lossless Image Coder
JPEG-LS		HP JPEG-LS	Lossless/Near Lossless based on LOCO-I
JPEG2000		JasPer	JPEG2000 wavelet-based standard
BTPC		BTPC 5.0/ ZLIB	Binary Tree Predictive Coding
PNG		LIBPNG/ ZLIB	Portable Network Graphics
S+P	SPIHT	QccPack	Set Partitioning in Hierarchical Tree Reversible Wavelets (S+P)

Any library will provide a set of functions for reading and writing the respective image file format, and supporting conversion to some other popular image file formats and color space conversion. Any application programs may make use of the library routines or easily add support for a new feature or image format by linking the application against the library during compilation without having to modify the library in any way. All the source codes of the programming libraries that are used in this study are highly optimized C/C++ code. Each library function is very general in its implementation in order to be useful in a large variety of applications.

3.6. Experiment

3.6.1 Sample Images Database

The test images that are used in the study of performance evaluation are initially obtained in the form of the conventional mammograms and ultrasound films from local hospitals. These images were collected from different patients and covering a wide verity of abdominal and breast diseases. Sample of these images is shown in Figure 1 and Figure 2 in Appendix A. The dimensions of each image , their sizes and entropy are shown in table 1 and table 2 for mammograms and ultrasound images respectively. The images were digitized by using a high resolution scanner to obtain Portable any Map (PNM) image format where "N" can be one of three forms: Bit, Grey and Pixel. It is a convenient simple method of saving raw image data (with no compression) and easy to use in any applications. These formats are used to store black and white images PBM (Portable BitMap), greyscale images PGM (Portable GreyMap), as well as RGB color images PPM (Portable PixMap). For each of the three formats there is either a binary or an ASCII version. All PNM file format consist of two parts, a header and the image data. The header consists of at least three parts normally delimited by carriage returns and/or linefeeds. The first "line" is a magic PNM identifier: P1, P2, P3, P4, P5 or P6. The first three (P1, P2, P3) are for ASCII version while (P4, P5, P6) are for binary version. Therefore, P1 or P4 are used in PBM, P2 or P5 are used in PGM, and P3 or P6 are used in PPM .The next line consists of the width and height of the image as ASCII numbers. The last part of the header gives the maximum value of the color components for the pixels. This allows the format to describe more than single byte color values. In addition to the above required lines, a comment can be placed anywhere with a "#" character, the comment extends to the end of the line.

3.6.2 System setup

All the compression software's explained above are implemented and the performance measurements are carried in the Telemedicine and Intelligent Imaging Laboratory of PETRONAS University of Technology using the system setup shown in the Table 3.2.

Table 3.2: System setup for the experiment

Computer	Pentium IV 2.8 MHz
Memory	256 Megabytes
Operating System	Microsoft Windows XP
Programming Development Environment	Microsoft Visual C++

The programming language C/C++ is chosen primarily due to the availability of similar development environments for most of today's computing platforms. Besides, all the source codes are reusable and simple to modify.

3.6.3 Evaluation Procedure

After acquiring mammograms and ultrasound films from local hospitals and digitizing them in uncompressed grayscale format (PGM), the entropy of each image is measure as shown in equation 2.4. The performances of the different lossless and lossy schemes are measured. The steps of the procedure are shown in the flow diagram in Figure 3.2. The performance evaluation of lossless is presented to determine the best among the eight compression methods on mammogram and ultrasound images in terms of compression ratio and computational speed. Next the evaluation of lossy compression schemes is carried to determine the optimum trade-off between the distortion and compression efficiency. The results of the above evaluation will be used in our proposed hybrid compression scheme.

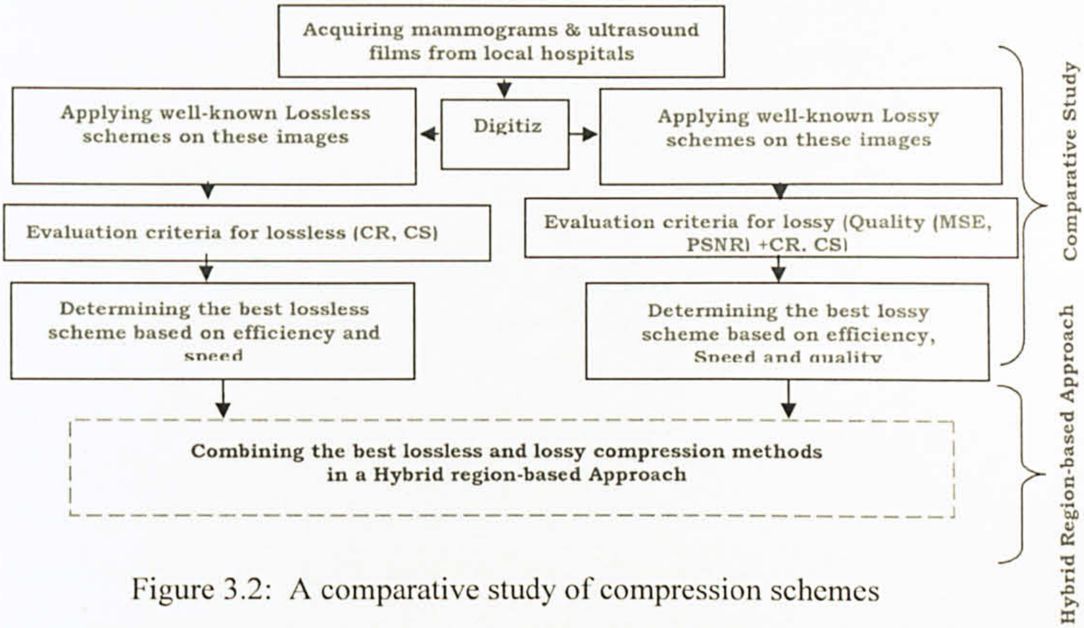

Figure 3.2: A comparative study of compression schemes

3.6.3.1 Evaluation of lossless Compression schemes

To investigate the compression efficiency and the maximum achievable compression ratio for mammograms and ultrasound images, performances of the eight lossless methods have been studied. The major focus of this study is on the compression efficiency and compression/decompression time of each compression scheme. Large number of mammograms and ultrasound images which are different in texture and size are used.

After compressing and decompressing all the sample test images using the above methods, the compression ratios are calculated up to 3 floating points. All the commands that used to call the coders for compressing and decompressing are arranged in batch files to collectively process all the sample images. Example of these batch files are shown in Appendix B. For each image, compression ratio, compression and decompression time are calculated.

3.6.3.2 Evaluation of lossy Compression schemes

The same set of sample images are coded and decoded using the four selected lossy compression algorithms to determine the optimum trade-off between the distortion and compression efficiency. For each test image, nine different compression ratios were selected: 5:1, 15:1, 25:1 35:1, 45:1, 55:1, 65:1, 75:1 and 80:1. Since lossless compression may give a compression ratio less than 5, the lower limit of CR is chosen as 5:1. In order to keep the distortion within the limit the highest value for CR has been chosen 80:1.

The results of average measure of the PSNR and MSE for the four methods at different compression ratios are also calculated.

The best scheme is selected according to one of these distortion metrics (MSE or PSNR) for a given compression ratio. A lower value for MSE means lesser error (better quality), and as seen from the inverse relation between the MSE and PSNR, this translates to a high value of PSNR. Logically, a higher value of PSNR is preferable. Also compression and decompression time is measured. All the related batch file commands are shown in Appendix B.

3.7. Summary

Mammograms and ultrasound images have great significance for diagnostic and therapeutic applications. Compression of these images faces a great challenge to compromise between the higher compression ratio and the relevant diagnostic information. Therefore, selecting a suitable method is critical for medical image coding. There is numerous image compression techniques (lossless and lossy) proposed and found in the literature. In this work, a comprehensive comparative survey is needed to compare different compression techniques. Eight efficient lossless compression methods and four lossy compression methods have been studied. This comparative study uses compression ratio, compression speed and distortion made by lossy compression to pinpoint efficient and well suited compression methods for mammograms and ultrasound images. The source codes of the programming libraries that are used in study are implemented in Visual C++ under Windows XP operating System.

CHAPTER 4

EFFICIENT COMPRESSION SCHEMES FOR MAMMOGRAMS AND ULTRASOUND IMAGES

4.1 Introduction

In the previous chapter, the eight lossless schemes, namely CALIC, JPEG2000, JPEG-LS, FELICS, Lossless mode of JPEG, S+P, PNG and BTPC and the four lossy methods namely JPEG, BTPC, JPEG2000 and SPIHT are discussed. In order to determine the best among the above schemes, large number of mammograms and ultrasound images obtained from local hospitals are processed and analyzed. However, only the results of a set of 21 test images which are of different sizes and texture in each modality have been included.

4.2 Performance of the lossless schemes on mammograms

For each of the sample images, the eight lossless compression methods are applied and the compression ratio and the compression/decompression time are calculated.

4.2.1 Compression Efficiency

The results of compression efficiency obtained for the 21 samples of different entropies mammograms are plotted in Figure 4.1. The numerical values of the entropies are given in Table 1 in Appendix A and the compression ratios are given in Table 1 in Appendix C.

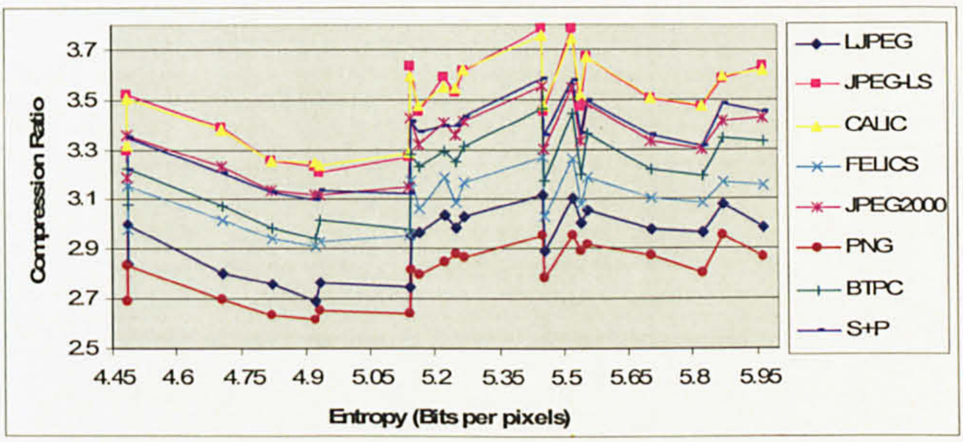

Figure 4.1: Compression efficiency on mammograms

It may be seen from the results that CALIC and JPEG-LS are equally efficient regardless of texture and size of the images. Although the two wavelet-based schemes JPEG2000 and S+P are using different integer wavelet filter and different embedded coding, they are found to perform equally and to be next best to CALIC and JPEG-LS. JPEG2000 uses bi-orthogonal 3/5 and Embedded Block Coding with block Truncation (EBCOT) whereas S+P uses the spatial orientation tree of SPIHT for coding the coefficients. LJPEG and PNG are found to be lagging behind all the other schemes in terms of efficiency even though LJPEG outperforms PNG. To ensure the best of LJPEG performance, all the seven possible prediction values are tried (section 3.3.1), among which the best prediction value that gives higher compression ratio is selected. BTPC and FELICS are found to perform well but slightly lower in efficiency than the wavelet schemes (JPEG200 and S+P).

4.2.2 Compression Speed

Figure 4.2 and Table 2 in Appendix C show the results of the compression and decompression times obtained for the above samples using the eight lossless schemes. CALIC seems to be extremely slow compared to all other methods. FELICS is the fastest algorithm because of its simple prediction with a two-neighboring pixel context (section 3.3.4). LJPEG and JPEG-LS are somewhat much closer to FELICS. It is seen that PNG and BTPC take more time for compression but less time for decompression and they have less compression speed compared to the two wavelet-based algorithms. But S+P is faster than JPEG2000. The compression/decompression time taken by CALIC is estimated to be around 10 times that of JPEG-LS and 3 to 3.5 times that of JPEG2000.

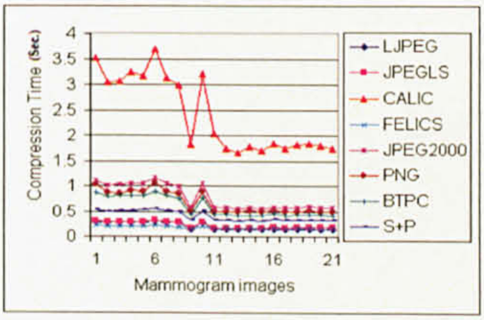

(a) Compression time in seconds

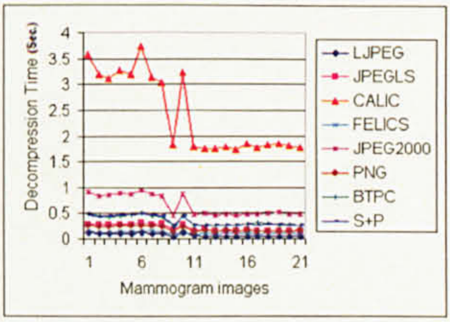

(b) Decompression time in seconds

Figure 4.2: Compression/decompression time in seconds on mammograms

Except CALIC all other methods show closer compression speed. In Figure 4.3 the compression/decompression time of these seven methods are re-plotted after excluding CALIC in order to make the difference clear.

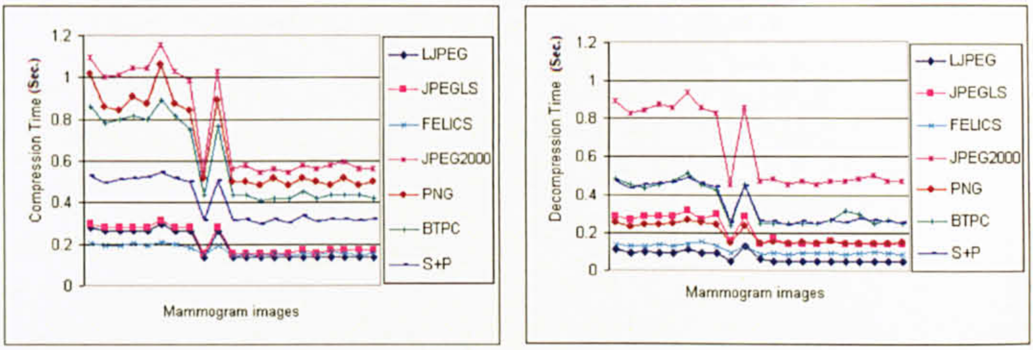

(a) Compression time in seconds (b) Decompression time in seconds

Figure 4.3: Compression/decompression time without CALIC on mammograms

4.3 Performance of the lossless schemes on ultrasound images

4.3.1 Compression Efficiency

The results obtained for compression efficiency on the test samples of 21 ultrasound images of different entropies applying the eight lossless schemes are shown in Figure 4.4. The numerical values of the entropies are given in Table 2 in Appendix A and the compression ratios are given in Table 3 in Appendix C. It is found that CALIC is outperforming JPEG-LS and they are the two best schemes for ultrasound images regardless of texture and size.

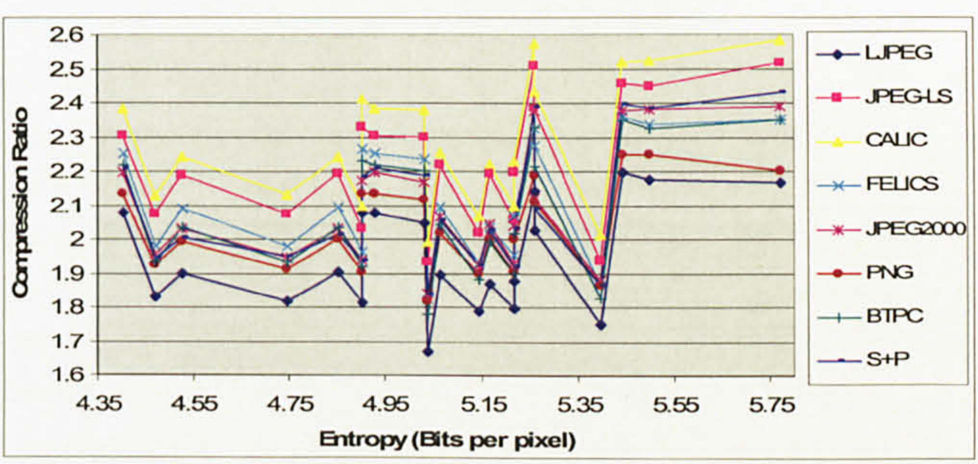

Figure 4.4: Compression efficiency on ultrasound images

LJPEG is found to be lagging behind all the schemes in terms of efficiency. PNG is slightly outperforming LJPEG. FELICS, BTPC, JPEG2000 and S+P are showing close performance and found to lie in the middle range.

4.3.2 Compression Speed

Figure 4.5 (a) and (b) and Table 3 in Appendix C show the compression and decompression times respectively for the above eight lossless schemes. It can be seen that FELICS is the fastest and the CALIC is the slowest. LJPEG and JPEG-LS are somewhat much closer to FELICS. It may be noted that the above four algorithms (FELICS, CALIC, LJPEG and JPEG-LS) are symmetric. PNG and BTPC have less compression speed in comparison to the two wavelet-based algorithms. S+P is faster than JPEG2000.

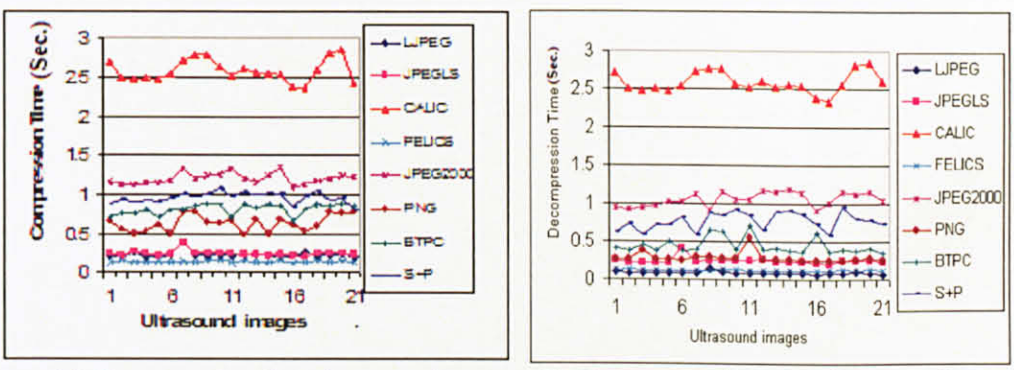

(a) Compression time in seconds (b) Decompression time in seconds

Figure 4.5: Compression/decompression time in seconds on ultrasound images

4.4 Comparison of lossless schemes on both modalities

From the earlier results, it can be clearly stated that CALIC and JPEG-LS give best performance for both modalities. Their performances are very close for mammograms but for ultrasound images CALIC is leading. PNG and LJPEG are lagging behind all the other schemes on both modalities. However, LJPEG outperforms PNG on mammograms whereas PNG performs significantly better than LJPEG on ultrasound images. JPEG200 and S+P are showing close performance on both modalities. Their performances are more close to CALIC and JPEG-LS on mammograms but not so on ultrasound images. FELICS and BTPC are outperformed by JPEG200 and S+P on mammograms. However, all the four methods (FELICS, BTPC, JPEG2000 and S+P) show closer performance on ultrasound images.

The compression/decompression time of the eight lossless compression methods on mammograms show that FELICS is the fastest algorithm followed by JPEG-LS, LJPEG and PNG which are slightly outperform BTPC. Due to the complexity of wavelet transform, both JPEG2000 and S+P. CALIC is extremely slow.

Based on both the compression efficiency and speed, it is found that JPEG-LS is well suited for lossless compression of mammograms and ultrasound images.

4.5 Performance of Lossy schemes on mammograms

For performance evaluation of the four lossy methods (JPEG, JPEG200, BTPC and SPIHT) on mammograms, the quality of the recovered images based on PSNR and MSE and compression/decompression time are measured.

4.5.1 Image Quality

Figures 4.6 and 4.7 and Table 4.1 show the results of average measure of the PSNR and MSE on 21 mammogram for the four lossy methods at different compression ratio (from 5:1, 15:1, 25:1 35:1, 45:1, 55:1, 65:1, 75:1 and 80:1). The highest values of PSNR and the lowest value MSE present the best quality of the test images. It is inferred that quality of the test images drop very fast in JPEG compared to the other schemes when compression ratio is increased. This drop is due to the artifacts resulting from the block-based DCT (section 3.4.1).

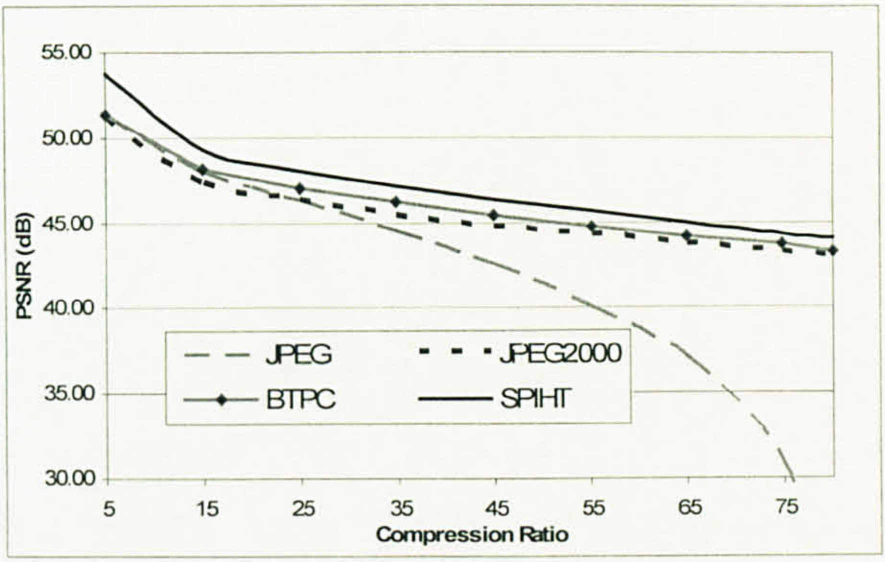

Figure 4.6: Comparison between PSNR and CR on mammograms

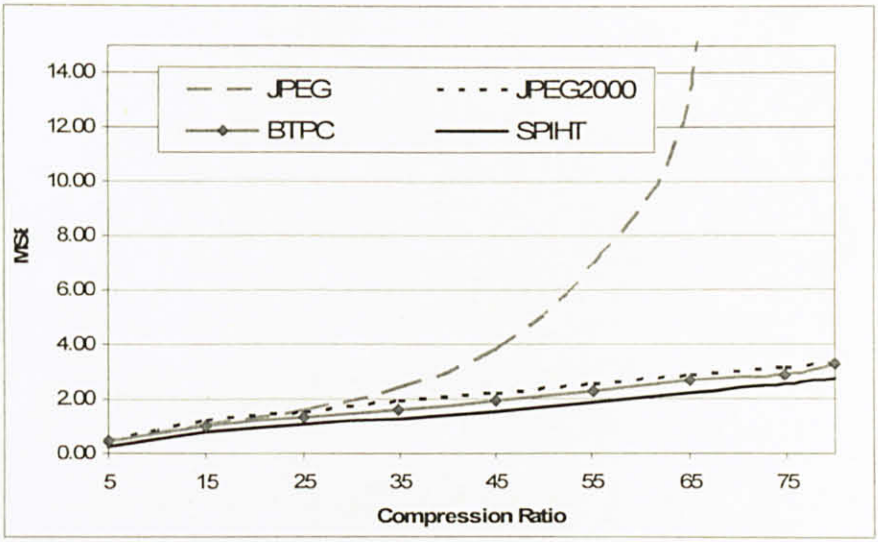

Figure 4.7: Comparison between MSE and CR on mammograms

For both the criteria PSNR and MSE, SPIHT provides better image quality than the other methods for all test images and for all compression ratios. It may be noted that the SPIHT shows slow degradation in quality compared to the others. BTPC exhibit the second best quality after SPIHT. At low compression ratios (less than 15: 1) JPEG shows better performance than JPEG2000. For higher values of CR JPEG2000 is better than JPEG.

Table 4.1: Average distortion measurement (PSNR and MSE) vs. different CR on mammograms

CR	SPIHT		BTPC		JPEG000		JPEG	
	PSNR	MSE	PSNR	MSE	PSNR	MSE	PSNR	MSE
5	53.77	0.28	51.37	0.47	51.21	0.50	51.40	0.48
15	49.32	0.77	48.19	1.02	47.35	1.21	48.00	1.05
25	48.03	1.05	46.97	1.34	46.30	1.54	46.35	1.57
35	47.15	1.29	46.20	1.61	45.39	1.91	44.55	2.42
45	46.35	1.56	45.43	1.93	44.77	2.20	42.59	3.80
55	45.61	1.87	44.71	2.29	44.21	2.51	40.06	6.94
65	44.95	2.19	44.12	2.64	43.69	2.84	37.04	13.36
75	44.32	2.53	43.72	2.88	43.25	3.14	31.06	56.33
80	44.00	2.73	43.22	3.25	43.01	3.32	20.99	536.52

4.5.2 Compression Speed

The average compression/decompression time in seconds are calculated for the above four methods and the results are shown in Figure 4.8 and Table 4.2.

JPEG takes less time but its distortion rate is very high. SPIHT takes more compression/decompression time than JPEG but less distortion. Hence, SPIHT gives the best trade-off between the distortion and compression efficiency.

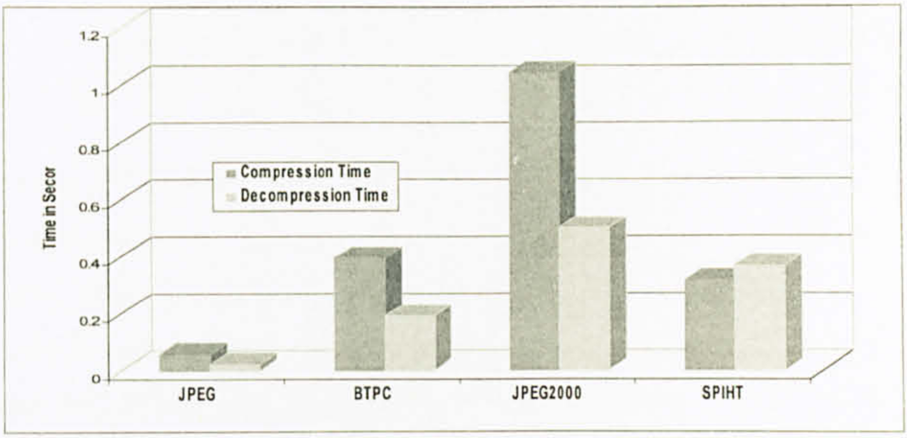

Figure 4.8: Average compression/decompression time in seconds for the four lossy methods on mammograms

Table 4.2: Average of Compression/decompression time for the four lossy methods applied on mammograms

Images	JPEG		BTPC		JPEG2000		SPIHT	
	CT	DT	CT	DT	CT	DT	CT	DT
Mammo1	0.078	0.031	0.421	0.171	1.265	0.609	0.286	0.356
Mammo2	0.078	0.015	0.39	0.125	1.25	0.578	0.357	0.395
Mammo3	0.078	0.031	0.531	0.156	1.328	0.593	0.427	0.359
Mammo4	0.078	0.031	0.406	0.296	1.437	0.578	0.483	0.391
Mammo5	0.078	0.031	0.515	0.14	1.375	0.562	0.482	0.401
Mammo6	0.093	0.031	0.671	0.14	1.593	0.625	0.545	0.414
Mammo7	0.078	0.031	0.671	0.281	1.453	0.578	0.552	0.386
Mammo8	0.015	0.031	0.546	0.14	1.234	0.75	0.634	0.362
Mammo9	0.046	0.015	0.343	0.062	0.765	0.343	0.453	0.248
Mammo10	0.078	0.031	0.64	0.265	1.593	0.593	0.331	0.643
Mammo11	0.046	0.015	0.234	0.281	0.859	0.5	0.158	0.512
Mammo12	0.046	0.015	0.234	0.203	0.625	0.453	0.195	0.235
Mammo13	0.046	0.015	0.203	0.328	0.593	0.5	0.187	0.315
Mammo14	0.046	0.015	0.218	0.203	0.875	0.312	0.189	0.215
Mammo15	0.046	0.015	0.218	0.343	0.796	0.328	0.187	0.23
Mammo16	0.046	0.031	0.234	0.187	0.812	0.328	0.172	0.546
Mammo17	0.046	0.015	0.484	0.078	0.843	0.515	0.189	0.23
Mammo18	0.046	0.015	0.234	0.078	0.656	0.531	0.179	0.238
Mammo19	0.046	0.015	0.25	0.328	0.859	0.328	0.19	0.234
Mammo20	0.046	0.015	0.234	0.093	0.828	0.328	0.196	0.687
Mammo21	0.031	0.015	0.578	0.078	0.859	0.515	0.201	0.251
Average	**0.056714**	**0.02186**	**0.393095238**	**0.1893**	**1.042762**	**0.497476**	**0.31395**	**0.3641905**

4.6 Performance of Lossy schemes on ultrasound images

4.6.1 Image Quality

The 21 test images are coded and decoded using the four lossy compression algorithms. For each test image, nine different compression ratios were selected: 5:1, 15:1, 25:1 35:1, 45:1, 55:1, 65:1, 75:1 and 80:1(section 3.6.3.2).

Figure 4.9 and 4.10 show the results of average measure of PSNR and MSE for the four methods at different compression ratios. Table 4.3 shows the detailed numerical values of the results of PSNR and MSE for nine different compression ratios. It seems that the results on ultrasound images and mammograms are similar for the four methods except that at compression ratios more than 15:1, BTPC showed better quality than JPEG2000 on mammograms and JPEG2000 provided better quality on ultrasound images.

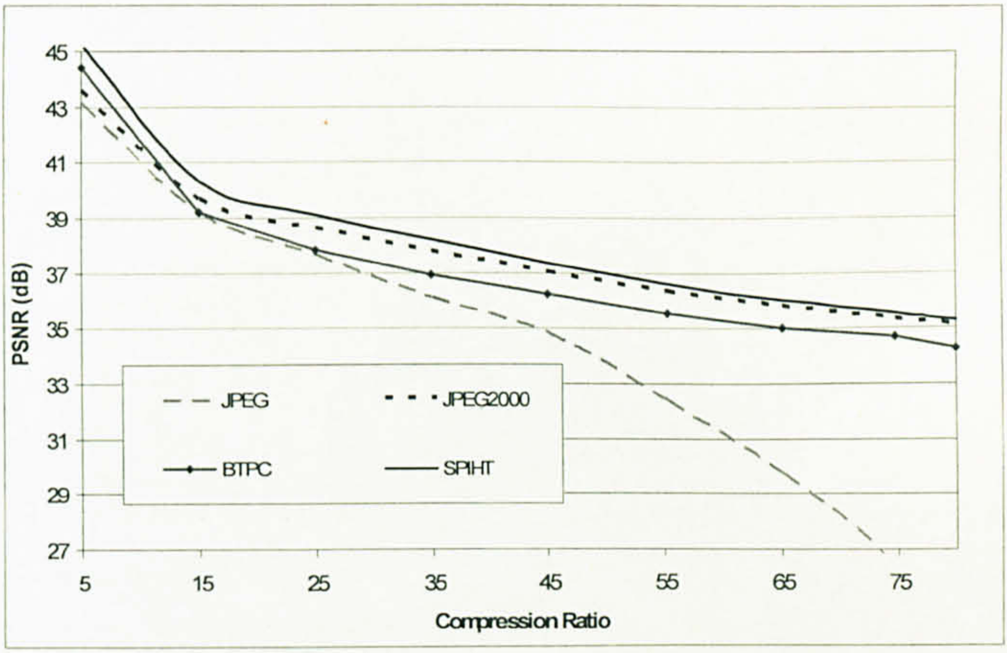

Figure 4.9: Comparison between PSNR and CR on ultrasound images

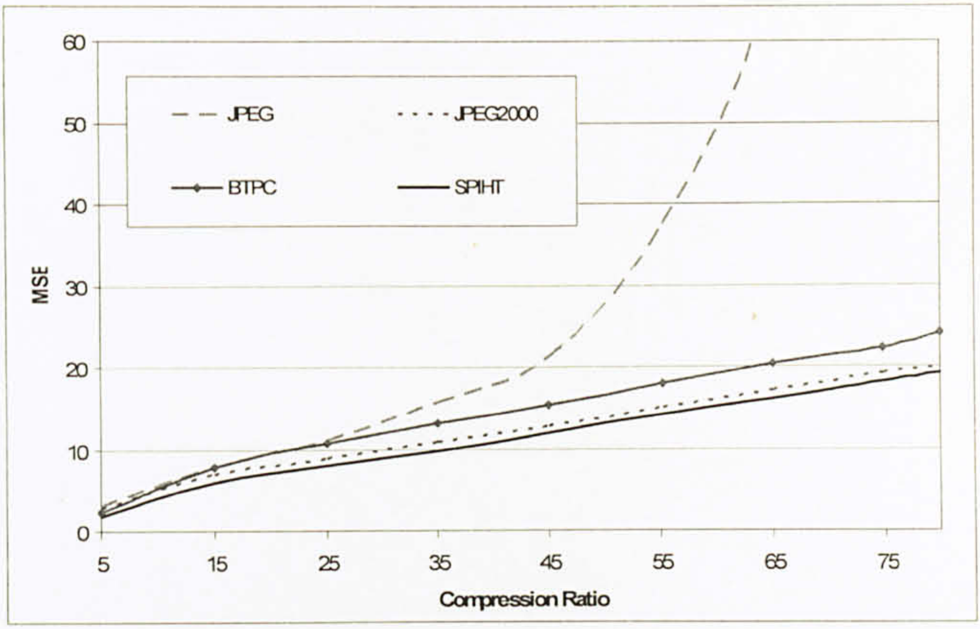

Figure 4.10: Comparison between PSNR and CR on ultrasound images

Table 4.3: Average distortion measurement (PSNR and MSE) vs. different CR on ultrasound images

CR	SPIHT		BTPC		JPEG000		JPEG	
	PSNR	MSE	PSNR	MSE	PSNR	MSE	PSNR	MSE
5	44.80	2.20	44.27	2.41	43.28	3.06	43.18	3.13
15	39.88	6.68	38.85	8.48	39.26	7.718	38.83	8.52
25.	38.77	8.64	37.60	11.31	38.30	9.62	37.52	11.51
35	37.10	10.37	36.73	13.8	37.60	11.31	36.23	15.49
45	37.30	12.23	36.16	15.76	36.94	13.16	34.61	22.51
55	36.60	14.20	35.57	18.03	36.37	14.99	32.78	34.27
65	36.01	15.97	35.03	20.41	35.89	16.74	30.30	60.62
75	35.67	17.61	34.87	21.18	35.47	18.45	26.82	135.18
80	35.44	18.59	34.47	23.25	35.30	19.21	21.57	453.17

4.6.2 Compression Speed

Table 4.4 shows numerical values of CT/DT of 21 ultrasound images using the four lossy methods. The above data is represented as bar chart in Figure 4.11 showing the average values of the compression/decompression times for each method. It can be clearly seen that JPEG is the fastest and JPEG2000 is slowest. SPIHT is the second fastest.

JPEG takes less time but its distortion rate is very high. SPIHT is takes more compression/decompression time than JPEG but less distortion. Hence, SPIHT gives the best trade-off between the distortion and compression efficiency.

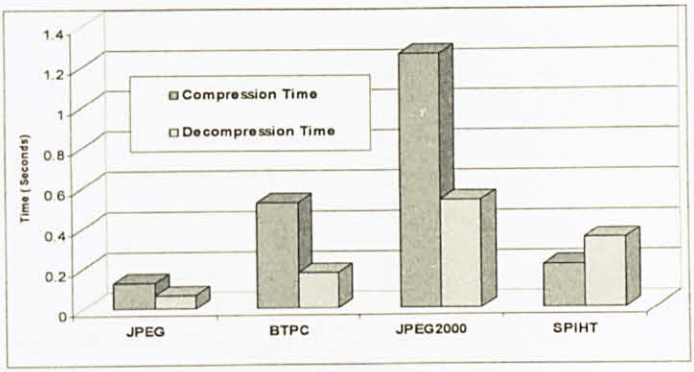

Figure 4.11: Average compression/decompression time in seconds for the four lossy methods on ultrasound images

Table 4.4: Average of Compression/decompression time for the four lossy methods applied on ultrasound images

Images	JPEG		BTPC		JPEG2000		SPIHT	
	CT	DT	CT	DT	CT	DT	CT	DT
Ultrasound1	0.095	0.058	0.376	0.159	1.154	0.482	0.185	0.245
Ultrasound2	0.099	0.06	0.466	0.165	1.242	0.449	0.183	0.313
Ultrasound3	0.097	0.061	0.385	0.166	1.156	0.528	0.218	0.269
Ultrasound4	0.104	0.061	0.389	0.159	1.221	0.561	0.211	0.388
Ultrasound5	0.099	0.061	0.595	0.164	1.228	0.455	0.215	0.252
Ultrasound6	0.102	0.061	0.539	0.167	1.34	0.45	0.215	0.263
Ultrasound7	0.1	0.06	0.383	0.159	1.264	0.641	0.213	0.281
Ultrasound8	0.104	0.061	0.588	0.162	1.273	0.611	0.227	0.617
Ultrasound9	0.101	0.058	0.632	0.153	1.265	0.618	0.247	0.266
Ultrasound10	0.104	0.061	0.64	0.17	1.32	0.612	0.223	0.281
Ultrasound11	0.098	0.062	0.395	0.17	1.222	0.593	0.188	0.26
Ultrasound12	0.1	0.062	0.392	0.416	1.245	0.644	0.182	0.545
Ultrasound13	0.675	0.065	0.404	0.17	1.237	0.45	0.217	0.27
Ultrasound14	0.101	0.063	0.687	0.167	1.382	0.452	0.218	0.271
Ultrasound15	0.099	0.062	0.7	0.17	1.35	0.482	0.215	0.349
Ultrasound16	0.098	0.095	0.658	0.153	1.15	0.555	0.215	0.568
Ultrasound17	0.095	0.058	0.645	0.164	1.199	0.579	0.196	0.283
Ultrasound18	0.096	0.095	0.644	0.164	1.279	0.448	0.218	0.265
Ultrasound19	0.104	0.063	0.375	0.164	1.438	0.487	0.223	0.437
Ultrasound20	0.102	0.095	0.404	0.16	1.347	0.493	0.233	0.526
Ultrasound21	0.096	0.059	0.679	0.149	1.168	0.579	0.22	0.28
Average	**0.127095**	**0.065762**	**0.522666667**	**0.17481**	**1.260952381**	**0.531857**	**0.21247619**	**0.344238**

4.7 Summary

A comparative study of lossless compression schemes applied on large number of mammogram and ultrasound images has been carried out. The results for a set of 21 test cases of different sizes and texture of each modality have been included.

To evaluate the lossless compression methods, three criteria namely, compression ratio, compression time and decompression time were used. JPEG-LS shows high compression ratio through different entropies and much less compression/decompression. Based on these two features, the results of the analysis indicate JPEG-LS is found to be well suited for compressing mammograms and ultrasound images.

The lossy methods are evaluated using MSE and PSNR as criteria to quantify the distortion.

It is found that SPIHT is an efficient method that shows the better compromise between compression ratio and image quality than other lossy schemes with a reasonable compression speed.

CHAPTER 5

HYBRID REGION-BASED IMAGE COMPRESSION SCHEME

5.1 Introduction

In mammograms and ultrasound images there are only small regions of interest (ROI) which are diagnostically relevant while the remaining regions are much less important. The proposed approach is to retain the quality by using efficient lossless compression on ROI and optimal lossy compression on non-regions of interest (non-ROI), thus yielding a high overall compression ratio while still being diagnostically lossless. The approach described in this work is a hybrid technique of applying a modified lossless JPEG-LS algorithm which is found to be the best approach among the eight lossless algorithms on the ROI (sections 4.2 an 4.3) and Shape Adaptive SPIHT algorithm which is found to be best among the four efficient lossy compression methods on non-ROI (sections 4.5 and 4.6). First JPEG-LS with the proposed modification is described. This is followed by detailed description of SPIHT algorithm with shape adaptive approach. The above two algorithms are combined to yield a Hybrid Region-based Image Compression Scheme (HYRICS) which is applied on the selected mammograms and ultrasound images with and without preprocessing.

5.2 JPEG-LS

JPEG-LS is designed to achieve high compression efficiency at very low computational complexity and memory requirement. This method has lossless and near lossless modes. Here only lossless mode is described. For an input image, a prediction scheme is first operated to decide whether the run-length compression mode or the predictive coding mode should be selected to encode the current pixel, depending on the values of previously encoded pixels in a surrounding neighborhood. The prediction scheme and context modeling are the core features of the JPEG-LS modeler as seen in Figure 5.1. The idea of prediction is to guess the current pixel value based on the previous neighboring pixels and to output the difference between the actual and the guessed values. It is expected that the differences are low so that the image can be effectively compressed.

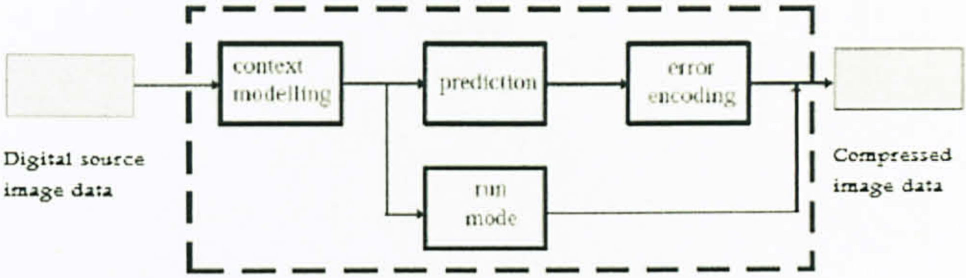

Figure 5.1: JPEG-LS lossless simple coder diagram [41]

The algorithm will scan the image in raster order (from left to right and top to bottom) when estimating the prediction values. Let the values of the pixels at locations W, NW, N and NE shown in Figure 5.2 (a) are X_w, X_{nw}, X_n and X_{ne} respectively with respect to pixel value X_l at the current location L. The initial prediction values $\hat{X}$ are obtained by applying the formula in Figure 5.2(b).

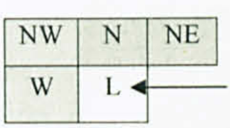

Current pixel location

If $X_{nw} \geq \max(X_w, X_n)$ then

$$\hat{x} = \max(X_w, X_n);$$

else if $X_{nw} \leq \min(X_w, X_n)$ then

$$\hat{x} = \min(X_w, X_n);$$

else

$$\hat{x} = X_w + X_n - X_{nw}.$$

(a) (b)

Figure 5.2: (a) Four neighboring pixels (b) formula to obtain the initial prediction

This formula is based on the idea of taking an average of nearby pixel while taking into account the edge to capture the horizontal, vertical and diagonal edges. If horizontal edge detected, X_w will be taken as prediction value. X_n will be taken for vertical edge otherwise, $X_n + X_w - X_{nw}$ will be taken as a prediction of diagonal edge. The initial prediction is then refined using an average value of the prediction in that particular context. The context in JPEG-LS also reflects the local variation in pixel values. However, they are computed differently from CALIC.

First measure of differences D1, D2 and D3 are computed as followed:

$$\begin{aligned} D1 &= X_{ne} - X_n \\ D2 &= X_n - X_{nw} \\ D3 &= X_{nw} - X_w \end{aligned} \tag{5.1}$$

The values of these differences define a three-component context vector Q. The components of Q (Q1, Q2 and Q3) are defined by the following mapping:

$$\begin{aligned} & D_i \le -T_3 \Rightarrow Q_i = -4 \\ & -T_3 < D_i \le -T_2 \Rightarrow Q_i = -3 \\ & -T_2 < D_i \le -T_1 \Rightarrow Q_i = -2 \\ & -T_1 < D_i \le 0 \Rightarrow Q_i = -1 \\ & D_i = 0 \Rightarrow Q_i = 0 \\ & 0 < D_i \le T_1 \Rightarrow Q_i = 1 \\ & T_1 < D_i \le T_2 \Rightarrow Q_i = 2 \\ & T_2 < D_i \le T_3 \Rightarrow Q_i = 3 \\ & T_3 < D_i \Rightarrow Q_i = 4 \end{aligned} \tag{5.2}$$

In equation 5.2, T1, T_2 and T_3 are positive coefficients that can be specified by the user. However, JPEG-LS define default values calculated from the pixel depth of the original image (i.e. 3, 7, and 21 are optimal values of T1, T2 and T3 respectively for 8 bit grayscale images). Given nine possible values for each component of the context vector, this result in 9x9x9 = 729 possible contexts. In order to simplify the coding process, the number of contexts is reduced by replacing any context vector Q whose first nonzero element is negative by –Q. Whenever this happens, a variable SIGN is also set to -1; otherwise, it is set to +1.this reduce the number of contexts to 365. The vector Q is then mapped into a number between 0 and 364.

The variable SIGN is used in the prediction refinement step[41]. The correction is first multiplied by SIGN and then added to the initial prediction.

The prediction error r_n is mapped into an interval that is the same as the range occupied by the original pixel values M. The mapping used in JPEG-LS is as follows:

$$\begin{aligned} & r_n < \frac{M}{2} \Rightarrow r_n \leftarrow r_n + M \\ & r_n > \frac{M}{2} \Rightarrow r_n \leftarrow r_n - M \end{aligned} \tag{5.3}$$

Finally, the prediction errors are encoded using adaptively selected codes on Golomb codes, which have also been shown to be optimal for sequences with a geometric distribution. Golomb code encodes an integer in two parts: a unary representation and a modified binary representation (using bits if and bits otherwise). Golomb codes are optimal [41] for one-sided geometric distributions of nonnegative integers.

5.2.1 Modification on JPEG-LS

The current JPEG-LS algorithm is not supporting shape adapting coding. So in this work the existing JPEG-LS is modified such that the compression can operate only in a predefined arbitrary area specified by the mask. In this modified prediction scheme the entire region outside ROI regions will be discarded. In this modified JPEG-LS algorithm, when estimating the prediction values, the four previous neighboring pixels that involved as a context for the prediction are dynamically changed for every pixel that is within the ROI area. If the current pixel is in the first row of ROI then both X_{nw} and X_n will be assigned to zeros otherwise if the previous X_{nw} is part of ROI then it will be assigned to X_n otherwise X_n is zero (Equation 5.4).

$$\begin{aligned}
&If\ X_l \in ROI_FIRST_ROW \\
&\quad X_{nw} = 0; \\
&\quad X_n = 0; \\
&else\ if\ \ previous(X_{nw}) \in ROI \\
&\quad X_n = X_{nw}; \\
&else \\
&\quad X_n = 0;
\end{aligned} \tag{5.4}$$

If the current pixel is ROI left edge then X_w will be assigned to zero otherwise X_w is previous ROI pixel X_{l-l} (Equation 5.5).

$$\begin{aligned}
&If\ X_l \in ROI_LEFT_EDGE \\
&\quad X_w = 0; \\
&else \\
&\quad X_w = \text{previous}(X_l);
\end{aligned} \tag{5.5}$$

X_w will be taken as prediction value when horizontal edge is detected. If vertical edge is detected X_n will be taken as a prediction value. Otherwise $(X_n + X_w - X_{nw})$ will be taken as a prediction value for the diagonal edge.

The prediction value is calculated as shown above only if X is within the ROI determined by the mask. When the next related horizontal pixel is processed, the previously encoded pixel will be assigned as X_w and accordingly previous pixel at X_n will be assigned as X_{nw}. X_n and X_{ne} will be given new values according to their respective locations in ROI. If any of X_n or X_{ne} is located in non-ROI it will be assigned to zero.

The same procedure will be followed for other related pixels of the region. The compression process can operate only in a predefined area specified by the mask. In this modification all the region outside ROI will be discarded.

5.3 Characteristics of Wavelet Decomposition in SPIHT

Set Partitioning in Hierarchical Trees (SPIHT) is an improved version of Embedded Zerotree Wavelet (EZW) algorithm [59]to encode the wavelet coefficients. In next subsection some important characteristics of wavelet is described. Then a Detailed description of SPIHT algorithm is presented.

5.3.1 Spatial Orientation Trees

In SPIHT a wavelet transform is performed on the image to reduce the correlation between neighboring pixels. In wavelet transform, subband decomposition is produced by an analysis filter bank followed by downsampling; this constitutes one stage of the two dimension subband decomposition of an image as depicted in Figure 5.3 in which the energy of the original image is concentrated in the lowest frequency band (LL) of the transformed image. In a two channel separable system, the initial high-pass and low pass filters and downsampling are applied horizontally to the rows of an image. The subsequence filters and downsampling are then applied vertically to the resulting columns.

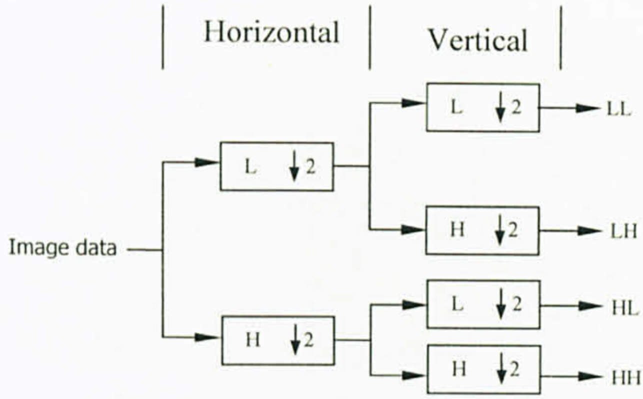

Figure 5.3: Two dimensional subband analysis

Consequently, the image is split into four bands that show a strong self-similarity denoted LH, HH, HL, and LL, according to whether the rows and columns received the low-frequency or high-frequency filtering. Only the low band LL is input once more to analysis filter bank decomposed and downsampling operation, this is referred to octave-band decomposition. The reconstructing operation is an inverse process consists of an upsampling operation followed by a synthesis filter bank. One of the most important characteristics of wavelet transformed is the spatial orientation of the coefficients. A spatial orientation tree is defined as a set of coefficients from different bands that represent the same spatial region in the image. As an example, two-level wavelet decomposition of ultrasound image with spatial orientation tree is shown in Figure 5.4. For simplicity, only two levels of the transform are shown here. The first transform level results in sub-bands LH1, HH1, HL1, and LL1. Only sub-band LL1 is passed on for further wavelet decomposition, generating the next transform level and creating sub-bands LH2, HH2, HL2, and LL2. As it seen, these octave-bands have similarities with each other that represent the same spatial location of the original image and the same orientation, but at different scales. The different scales of the subbands imply that a region in the sub-bands is representing the same region in the original image. SPIHT defines spatial parent-children relationships in the decomposition structure to exploit the self similarities properties of DWT images. To explain the balanced tree structures used in SPIHT, a portion of the parent-child relationships is depicted in Figure 5.4(c). The arrows in the figure identify the parent-children dependencies in a tree. The start of arrow line is parent coefficient, and end of arrow indicates four children coefficients.

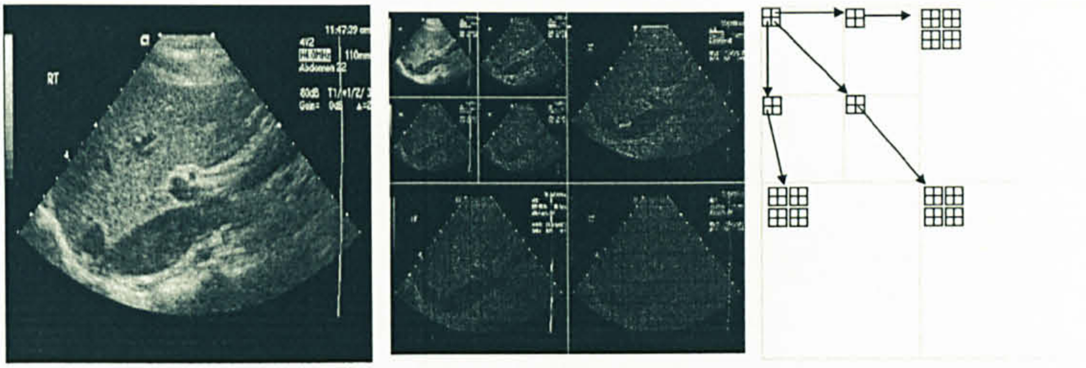

(a) (b) (c)

Figure 5.4: 2-level wavelet decomposition of US image with spatial orientation tree

(a) Original image (b) Transformed image (c) Part of parent-child relationships

In transformed image, each coefficient X_i (except the coefficient in the top-left corner in the lowest band and the three highest bands) is related to exactly four coefficients in the next highest band. Those four coefficients correspond to the same orientation and spatial location as X_i does in the original image. Each of these four is in turn related to four in the next band, and so on. These coefficients are collectively called the descendants of X_i. The spatial self-similarity between the parent and a child pixel suggests that an encoding scheme that moves from the parent to the child will exhibit decreasing coefficient magnitudes. In another words, it is often true of image data that when a coefficient X_i has magnitude less than some threshold T, all of its descendants will also be less than T.

5.3.2 SPIHT Algorithm

The characteristics of wavelets decomposition are exploited by the SPIHT algorithm. It begins at the top of the tree and encodes higher-order bits before lower-order bits decomposing each sub-tree whenever it finds a coefficient in a sub-tree which exceeds the current threshold.

For easy understanding of SPIHT algorithm Khalid Sayood [59] defines the following functions and notation:

- $C_{i,j}$ is the coefficient at location (i, j).
- $O_{i,j}$ is the set of coordinates of the four offspring's of the coefficient at location (i ,j).

$$O_{i,j} = \{C_{2i,2j}, C_{2i+1,2j}, C_{2i,2j+1}, C_{2i+1,2j+1}\} \tag{5.6}$$

- $D_{i,j}$ is the set of descendants of the coefficient at location (i,j).descendants include the offspring's , the offspring's of the offspring's, and so on.
- H is set of all root nodes, essentially all the coefficients on the low frequency band of the octave-band decomposition.
- $L_{i,j}$ this is the set of coordinates of all the descendants of the coefficient at location (i,j) Except for the immediate offspring's of the coefficient at location (i,j).

$$L_{i,j} = D_{i,j} - O_{i,j} \tag{5.7}$$

Any set ($D_{i,j}$ or $L_{i,j}$) is said to be significant if any coefficient in the set has a magnitude greater than the certain threshold. Finally, thresholds used for checking significance are power of 2. So in essence, the algorithm sends the binary representation of the integer value of the coefficients. The bits are numbered with the least significant bit being the zeroth bit, the next bit being the first significant bit, and the *last* bit (k-1) being referred to as most significant bit. The magnitude sorting algorithm in SPIHT achieves embedded coding by using three lists of coefficients: L*ist of Significant Pixels* (LSP), L*ist of Insignificant Pixels* (LIP) and L*ist of Insignificant Sets* (LIS). LSP will contain the coordinates of coefficients that are significant with respect to the current threshold t. opposing LSP, LIP contains coordinates of coefficients that are insignificant with respect to t. LIS contains the coordinates of the roots of insignificant set of type D or L.

The algorithm starts by determining the initial value of the threshold t from equation.

$$t = 2^{\lfloor \log_2 (C_{\max}) \rfloor} \tag{5.8}$$

where C_{max} is the maximum magnitude of the coefficients to be encoded. The initial state of SPIHT algorithm is shown in Figure 5.5. The LSP is initially empty. LIS is initialized with the set H. LIS with elements of H that have descendants are also placed as type D entries.

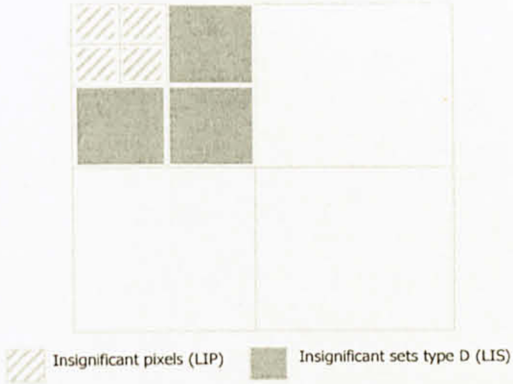

Figure 5.5: Initial state of SPIHT algorithm [60]

All the steps of SPIHT algorithms are shown in the flowchart given in figure 5.6. In each iteration, there are three steps: the sorting pass, the refinement pass, and the updating quantization step. The purpose of the sorting pass is to manipulate the three lists so that they are correct with respect to the current value of the magnitude threshold T. In the sorting pass, the member of LIP is processed first and then the members of LIS. This is essentially the significance map encoding step. The element of LSP in the refinement step is then processed. Each coordinate contained in LIP is then examined. If the coefficient at that coordinate is significant (that is greater than 2^N), transmit a 1 followed by a bit representing the sign of the coefficient (1 for positive, 0 for negative). Then the coefficient will be moved to the LSP list. If the coefficient at that coordinate is not significant, a 0 is transmitted.

After examining each coordinate contained in LIP, the set in LIS will be examined. If the set at coordinate *(i, j)* is not significant, a 0 will be transmitted otherwise a 1 will be transmitted. What comes after that depends on whether the set is of type D or L.

If the set is of type D, each of the off-springs of the coefficient at that coordinate will be checked. In other words, the four coefficients whose coordinates at in *O(ij)* will be checked. For each coefficient that is significant, transmit 1 and the sign of the coefficient. Then move the coefficient to LIP. For the rest, transmit a 0 and then add their coordinates to the LIP. Now that the coordinate of *O (ij)* has been removed from the set, what is left is simply the set *L(ij)*. If this set is not empty, it will be removed to the end of LIS and mark it to be type L. Note that this new entry into the LIS has to be examined during this pass. If the set is empty; the coordinate *(ij)* will be removed from the list.

If the set is of type L, then each coordinate will be added in O(ij) to the end of the LIS as the root of a set of type D. again note that these new entries are the LIS have to be examined during this pass . Then the coordinate (*ij*) will be removed from the LIS.

The refinement pass follows the sorting pass and outputs the bit corresponding to the current magnitude threshold for each of pixels in the LSP which were not added in the immediately previous sorting pass. The quantization for each significant coefficient is refined in a successive manner. A quantization threshold is used in coefficient magnitude test and then successively decreased by a factor of two in each pass of the algorithm. When the bit budget is reached, the algorithm will stop. The algorithm can be halted at any time needed, such as if the compressed data stream has reached the size we desire.

5.3.3 Shape Adaptive SPIHT Encoding

The conventional DWT is not supporting an arbitrary shaped ROI of an image, but it supports only a rectangular shaped regions. The SPIHT algorithm can be made to encode arbitrary shaped objects by incorporating a Shape Adaptive-Discrete Wavelet Transform (SA-DWT) (section 2.7.3). SA-DWT is identical to the conventional wavelet transform when applying it in a rectangular region and preserves the spatial correlation and self-similarity property of wavelet transforms. In a SA-DWT, the number of coefficients is exactly equal to the number of pixels in the object, which is achieved by using a mask that is opaque for object pixels and transparent everywhere else. In Shape Adaptive SPIHT (SA-SPIHT) encoding, each time a coefficient is to be encoded; its position with respect to the mask is taken into consideration. If a coefficient is within the opaque region of the mask, it is encoded. All transparent coefficients are considered to be insignificant at all times, and thus encoding is avoided. Similarly, shape information is also used to determine which coefficients are to be decoded and which are not during the decoding process. The coding algorithm needs to keep track of the locations of wavelet coefficients according to the shape of the object. To obtain the information about object coefficients, a mask image which specifies the object is decomposed by the same SA-DWT used in the wavelet decomposition of the image. In each decomposition stage, each subband of the decomposed mask contains information for specifying the object in that subband. By successively decomposing the approximation coefficients (LL subband) for a number of decomposition levels, information about object coefficients is obtained. Once the object coefficients are identified, SPIHT coding algorithm will be applied on these coefficients to create the embedded bit stream. In order to efficiently code object coefficients by taking advantage of the ROI information in the transform domain, a region-based extension of SPIHT algorithm is used. When the spatial orientation trees are established in the initialization step of SPIHT, the object information obtained from decomposition of the object mask is used to mark the spatial orientation tree. If all coefficients or some coefficients in a spatial orientation tree belong to the object, the corresponding tree is marked as an object tree. If all coefficients in a tree are outside the object, this tree is identified as a background tree. The background tree is skipped at the initialization stage. Also when a node and all its descendants in a spatial orientation tree are outside the object, the tree is pruned from that node. By doing so, no information about coefficients outside the object needs to be coded. Figure 5.7 gives an example of the parent-children relationship after SA-DWT decomposition of an image containing an object. Shaded blocks represent object coefficients, and striped blocks are the background coefficients that have descendants inside the object.

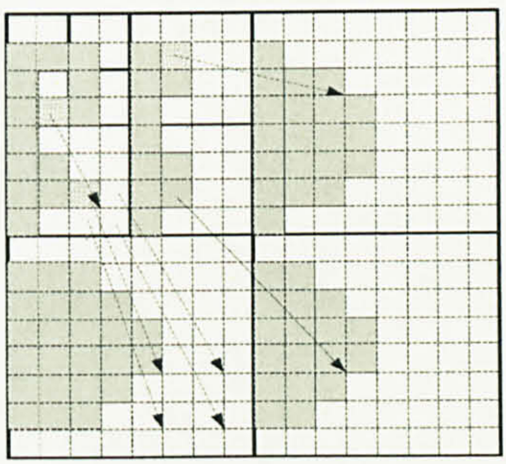

Figure 5.7: Parent-children relationship in SA-DWT subbands [60]

Solid arrows represent the parent-children relationship in the coefficient tree that should be kept. Dashed arrows specify the sub-branches in the coefficient tree that can be pruned.

5.4 Hybrid Region-based Compression Schemes

In the proposed Hybrid Region-based Image Compression Scheme (HYRICS), modified JPEG-LS is applied on ROI to preserve the significant diagnostic quality and SA-SPIHT is used to encode the remaining non-ROI in a lossy manner. Figure 5.8 shows the steps that describe HYRICS. After acquiring mammograms and ultrasound films from local hospitals and digitizing them, the disease affected regions of interest are roughly marked by expert radiologist. Based on these markings an Arbitrary Shaped Mask (ASM) is generated to differentiate the pixels that belong to the ROI and non-ROI. This shape information is needed by compression scheme before starting the real compression process. Figure 1 and 2 in Appendix D shows all the generated masks for all the mammograms and ultrasound images that are used as test cases. Each mask is represented as a binary image, where zeros correspond to ROI and ones correspond to the non-ROI. Figure 5.9 shows an example of mammogram image on which HYRICS is applied. In the figure (a) is the original image; (b) shows the region marked by the expert radiologist; (c) is the resulting generated mask that identifies the ROI.

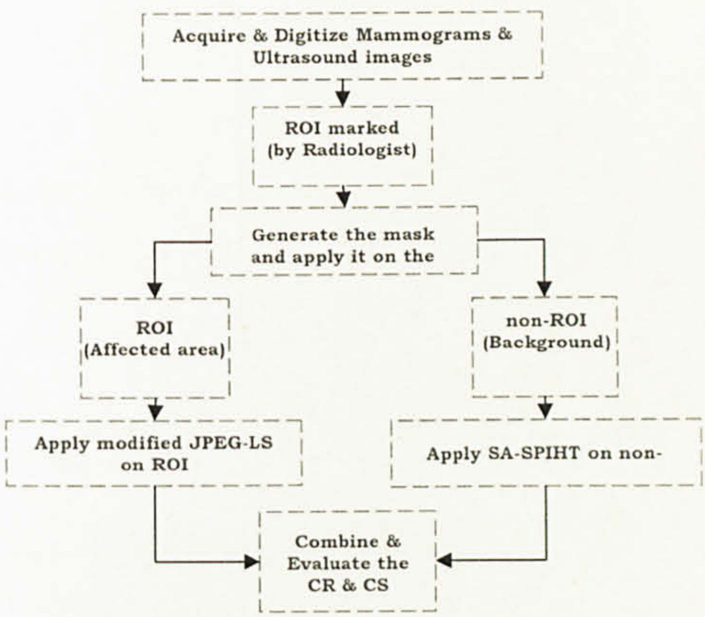

Figure 5.8: HYRICS Steps

(d) shows the decompressed image of ROI by the modified JPEG-LS. (e) shows the reconstructed image of non-ROI by SA-SPIHT. By combining images of (d) and (e) the resultant decompressed image is obtained as in (f).

For evaluating the compression efficiency of HYRICS, the compressed sizes of both ROI and the non-ROI are to be taken into account. The compression ratio achieved by SA-SPIHT is always very high because it is operating on larger area not containing disease affected regions where more degradation in the quality is acceptable. This factor contributes for higher compression efficiency of HYRICS.

Lets S_{orig} be the size of the original image. S_{roi} and S_{nroi} are the sizes of the ROI and non-ROI respectively. C_{roi} and C_{nroi} are the sizes of the compressed ROI and the compressed non-ROI respectively. The compression ratios of JPEG-LS, SPIHT and HYRICS can be calculated as follows:

$$CR_{JPEG-LS} = \frac{S_{roi}}{C_{roi}},\ CR_{SPIHT} = \frac{S_{nori}}{C_{nori}} \ \ and\ CR_{HRICS} = \frac{S_{orig}}{C_{roi} + C_{nroi}} \tag{5.9}$$

From these formulas, a relation between the three compression ratios (CR_{HYRICS}, $CR_{JPEG-LS}$ and CR_{SPIHT}) with respect to the original image size can be given as follows:

$$CR_{HRICS} = \frac{S_{orig}}{\dfrac{S_{roi}}{CR_{JPEG-LS}} + \dfrac{S_{nroi}}{CR_{SPIHT}}} \tag{5.10}$$

The percentage of the ROI region is also affecting the overall compression ratio of HYRICS. The percentage of both ROI and non-ROI can be expressed in the following equations:

$$P_{roi} = \frac{S_{roi}}{S_{orig}} \times 100 \quad ,\ P_{nroi} = \frac{S_{nroi}}{S_{orig}} \times 100 \ \ and\ P_{roi} = 100 - P_{nroi} \tag{5.11}$$

Therefore, CR_{HYRICS} can be denoted on respect to $CR_{JPEG-LS}$, CR_{SPIHT} and P_{roi} as follows:

$$CR_{HRICS} = 100 \Big/ \left(\frac{P_{roi}}{CR_{JPEG-LS}} + \frac{100 - P_{roi}}{CR_{SPIHT}} \right) \tag{5.12}$$

The compression ratio achieved by SA-SPIHT (CR_{SPIHT}) is always very high because it is operating on larger area not containing disease affected regions where more degradation in the quality is acceptable. Therefore, CR_{SPIHT} contributes more for higher compression efficiency of HYRICS.

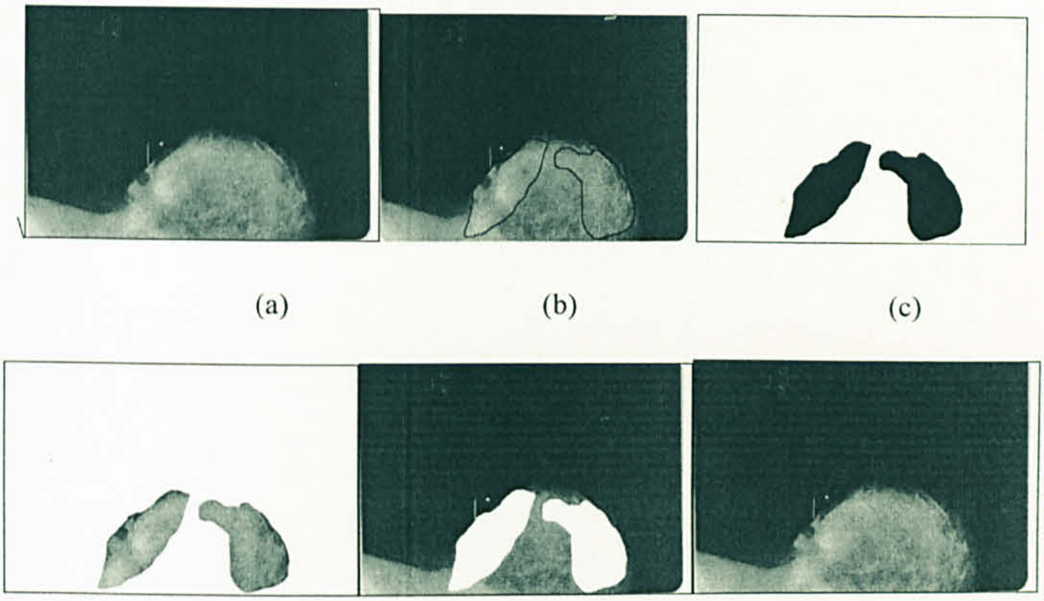

(a) (b) (c)

(d) (e) (f)

Figure 5.9: Sequences of the Hybrid Compression- mammogram 2
(a) Original image; (b) ROI marked by radiologist; (c) Generated Mask for ROI;
(d) Modified JPEG-LS operated ROI; (e) SA-SPIHT operated non-ROI;
(f) Decoded image by combining (d) and (e) by HYRICS

5.5 HYRICS on pre-processed mammograms and ultrasound images

In the example shown in Figure 5.9, HYRICS applied on an image without any pre-processing. The effect on compression efficiency by applying HYRICS on contrast stretched mammograms and ultrasound images have also been studied. One of the benefits of HYRICS besides the high compression efficiency is that itcan be achieved the possibility to contrast stretch only very small area (ROI) for diagnostic proposes and the larger non-ROI will not be processed thus saving a lot of processing time. There are two possibilities for contrast stretching of ROI: (i) contrast stretching before applying compression and (ii) contrast stretching after decompression. Contrast stretching before compression to enhance the diagnostic quality is an irreversible step.

5.6 Summary

JPEG-LS and SPIHT algorithms are reviewed in details. A new modification is introduced to JPEG-LS to allow the algorithm strictly operate on arbitrary shape ROI. SA-DWT is used in SPIHT for coding of non-ROI. All the characteristics of the conventional two dimension wavelet decomposition are well preserved by SA-DWT. Then, the modified approaches are combined in a Hybrid Region-based Image Compression (HYRICS) to be applied on selected mammograms and ultrasound images with and without preprocessing.

CHAPTER 6

RESULTS AND DISCUSSION

6.1 Introduction

The algorithm developed in this work uses the regions of interest that are roughly marked by the expert radiologist to generate appropriate masks. The masked ROI will be compressed using modified JPEG-LS. The remaining non-ROI will be compressed by SA-SPIHT. Then the resultant images after above hybrid compression will be transmitted for tele-consultation. HYRICS was applied on many mammograms and ultrasound images obtained from local hospitals. The results obtained for 21 selected mammograms and 21 selected ultrasound images of different sizes and textures are presented.

6.2 Compression Efficiency

Table 6.1 and Table 6.3 show the results on mammograms and ultrasound images respectively. In each table, column-2 represents the compression ratios obtained by applying normal JPEG-LS on the whole image. Column-3 represents compression ratios obtained using the proposed new modified JPEG-LS applied on ROI. Column-4 shows the compression ratios obtained applying SA-SPIHT on non-ROI. The last column shows the compression ratios obtained by applying the proposed HYRICS. It is noted that the new scheme shows considerable increase in the compression ratio comparing to normal JPEG-LS. For certain mammograms and ultrasound images, it is found that the compression ratios are very high. For certain cases the ratios are found to be low. The reason for such difference is due to the variation in sizes and textures of the sample images and the size of the ROI considered in each sample image.

Table 6.1: Comparison of compression ratios of JPEG-LS and HYRICS on 21 mammograms

Images	JPEG-LS	Modified JPEG-LS	SA-SPIHT	HYRICS
Mammo1	3.340472	2.92304075	79.99842	39.99875
Mammo2	3.571366	2.67827694	79.99541	8.505339
Mammo3	3.446099	2.6068174	79.99698	11.38211
Mammo4	3.295752	2.8735243	79.99622	9.226224
Mammo5	3.286945	2.66980104	79.99543	8.245254
Mammo6	3.272122	2.78747544	79.9986	9.285734
Mammo7	3.326101	2.73854452	79.99904	10.68953
Mammo8	3.697268	2.81259095	79.99448	9.268267
Mammo9	3.514702	2.98663139	79.99797	34.48077
Mammo10	3.677672	2.75819969	79.99935	9.645393
Mammo11	3.57951	2.74638145	80.00012	27.33239
Mammo12	3.666685	3.07486003	79.99792	45.02136
Mammo13	3.868008	2.81857985	80.00151	13.61226
Mammo14	3.502873	2.90763692	79.99727	7.049566
Mammo15	3.83271	2.77706811	79.99597	14.86792
Mammo16	3.512044	2.87775927	79.99279	7.521334
Mammo17	3.719228	2.83601867	79.99541	19.46018
Mammo18	3.549872	3.13787159	79.99873	37.85266
Mammo19	3.515244	2.85179189	79.993	8.289259
Mammo20	3.629403	2.5211459	79.99786	56.85634
Mammo21	3.676769	2.33864254	79.99419	62.13938

It may be seen from Table 6.1 the compression ratios obtained by applying JPEG-LS only on the whole image range from 3.2 to 3.8. However, when HYRICS is applied, the compression ratios vary from 7 to 62. It is noted that the lowest compression ratio for HYRICS is observed on mammo14 where the ROI area is very large (39% of the image). The highest compression ratio is observed on mammo21 where ROI is very small (0.87 %). The effect of the size of ROI on compression ratios can be clearly seen for the 21 images in Table 6.2. Figure 6.1 shows the plot of the compression ratio obtained by HYRICS on mammograms arranged in descending order of percentage of ROI areas. It can be clearly seen that HYRICS gives higher compression efficiency and for low areas of ROI high compression ratios are obtained.

Table 6.2: Effect of ROI area on compression ratio of HYRICS for mammograms

Images	ROI area %	Non-ROI area %	Compression ratio
Mammo1	3.79	96.21	39.99875
Mammo2	29.12	70.88	8.505339
Mammo3	20.31	79.69	11.38211
Mammo4	28.58	71.42	9.226224
Mammo5	30.05	69.95	8.245254
Mammo6	27.49	72.51	9.285734
Mammo7	22.98	77.02	10.68953
Mammo8	27.81	72.19	9.268267
Mammo9	5.12	94.88	34.6
Mammo10	26.05	73.95	9.645393
Mammo11	6.85	93.15	27.33239
Mammo12	3.11	96.89	45.02136
Mammo13	17.81	82.19	13.61226
Mammo14	39.03	60.97	7.049566
Mammo15	15.75	84.25	14.86792
Mammo16	35.96	64.04	7.521334
Mammo17	11.43	88.57	19.46018
Mammo18	4.55	95.45	37.85266
Mammo19	31.98	68.02	8.289259
Mammo20	1.32	98.68	56.85634
Mammo21	0.87	99.13	62.13938

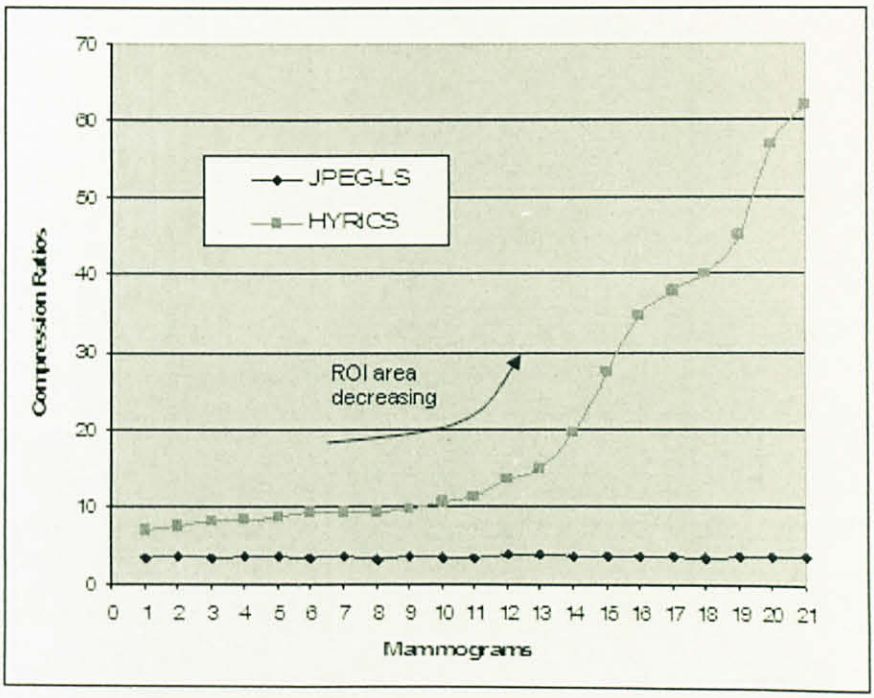

Figure 6.1: Plot of Compression ratios on mammograms arranged in a descending order according to the size of ROI areas

It may be seen from Table 6.3, the compression ratios obtained by applying JPEG-LS only on the whole image range from 1.9 to 2.5 for the 21 ultrasound images. When using HYRICS the ratios vary from 6.3 to 41.9. The lowest compression ratio for HYRICS is observed on ultrasound13 where the ROI area is very large (31.85%). The highest compression ratio is observed on ultrasound7 where ROI is very small (2.77 %).

Table 6.4 shows the effect of ROI area and non-ROI area on compression ratios obtained by HYRICS on ultrasound images. Figure 6.2 shows the plot of percentage of ROI area and the compression ratio obtained by HYRICS on ultrasound images. It can be clearly seen that for low areas of ROI high compression ratios are obtained.

Table 6.3: Compression ratio of the JPEG-LS and the proposed method on 21 ultrasound images

Images	JPEG-LS	ROI-JPEG-LS	SA-SPIHT	HYRICS
Ultrasound1	2.302702	2.34030752	79.99669	23.93241
Ultrasound2	2.071661	2.20804442	79.99748	23.40062
Ultrasound3	2.191392	2.14484384	79.99702	22.34103
Ultrasound4	2.064791	2.12415376	79.9977	10.12332
Ultrasound5	2.191715	2.14142581	79.99895	20.61741
Ultrasound6	2.025028	2.20947476	79.99155	6.686664
Ultrasound7	2.332065	2.36544768	79.99838	41.91202
Ultrasound8	2.302778	2.39102729	79.9965	21.04574
Ultrasound9	2.302341	2.34930521	79.99752	31.5881
Ultrasound10	1.912019	1.97913031	79.9955	32.25395
Ultrasound11	2.206399	2.22219878	79.99999	8.461627
Ultrasound12	2.010044	2.1418692	79.99679	8.459908
Ultrasound13	2.177968	2.14480995	79.99671	6.369004
Ultrasound14	2.043088	2.14776341	79.99571	8.622432
Ultrasound15	2.181235	2.17774518	79.99647	8.725956
Ultrasound16	2.499123	2.40108917	79.99154	9.170192
Ultrasound17	2.381912	3.46763123	79.99806	13.85824
Ultrasound18	1.931095	1.89464654	80.00008	12.03507
Ultrasound19	2.447848	2.35337307	79.99921	29.84179
Ultrasound20	2.444333	2.43562814	79.99563	23.67005
Ultrasound21	2.505162	2.2887515	79.9983	13.49546

Table 6.4: Effect of ROI area on compression ratio of the proposed method for ultrasound images

Images	ROI area %	Non-ROI area %	Compression ratio
Ultrasound1	7.06	92.94	23.93241
Ultrasound2	6.87	93.13	23.40062
Ultrasound3	7.11	92.89	22.34103
Ultrasound4	18.83	81.17	10.12332
Ultrasound5	7.92	92.08	20.61741
Ultrasound6	31.14	68.86	6.686664
Ultrasound7	2.77	97.23	41.91202
Ultrasound8	8.63	91.37	21.04574
Ultrasound9	4.64	95.36	31.5881
Ultrasound10	3.75	96.25	32.25395
Ultrasound11	24.16	75.84	8.461627
Ultrasound12	23.26	76.74	8.459908
Ultrasound13	31.85	68.15	6.369004
Ultrasound14	22.84	77.16	8.622432
Ultrasound15	22.86	77.14	8.725956
Ultrasound16	23.90	76.10	9.170192
Ultrasound17	21.62	78.38	13.85824
Ultrasound18	13.70	86.30	12.03507
Ultrasound19	5.09	94.91	29.84179
Ultrasound20	7.47	92.53	23.67005
Ultrasound21	14.51	85.49	13.49546

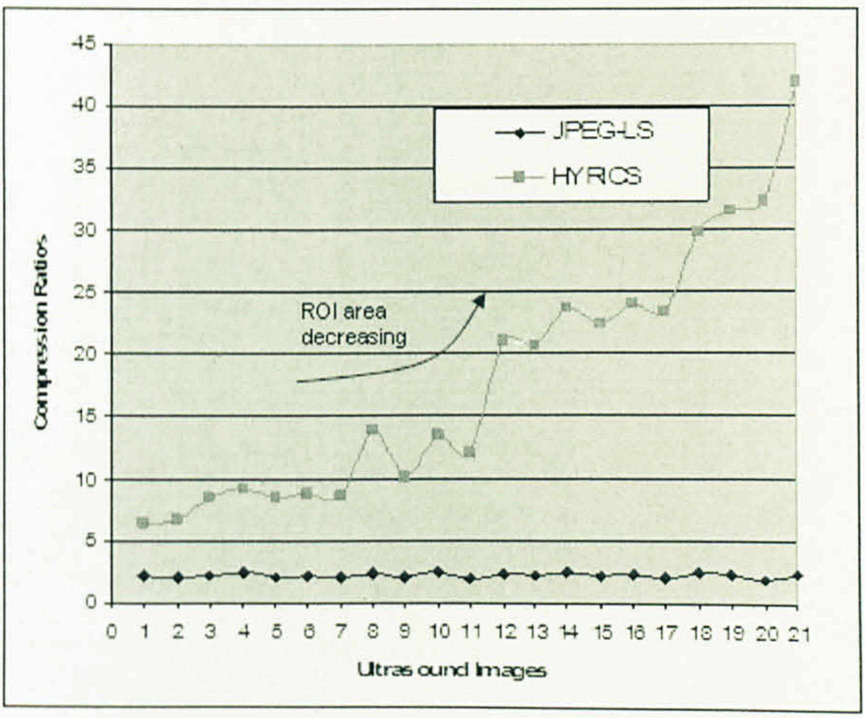

Figure 6.2: Plot of Compression ratios on ultrasound images arranged in a descending order according to the size of ROI areas

6.3 Computational time

Table 6.5 and Table 6.6 show compression/decompression time of JPEG-LS, modified JPEG-LS, SA-SPIHT and HYRICS on mammograms and ultrasound images respectively. For both modalities, computational time (CT + DT) of SA-SPIHT is slightly greater than that of SPIHT. This is mainly because DWT is applied twice on both the original image and the mask. On other hand computational time of modified JPEGL-LS is less than that of JPEG-LS. This shows that HYRICS is fast enough even if the ROI area is larger if the time that spent to mark the ROI is excluded.

Table 6.5: Compression/ Decompression time for JPEG-LS, ROI-JPEG-LS, SA-SPIHT and HYRICS on mammograms

Images	JPEG-LS		ROI-JPEG-LS		SA-SPIHT		HYRICS	
	CT	DT	CT	DT	CT	DT	CT	DT
Mammo1	0.359	0.328	0.046	0.046	3.295	2.279	3.341	2.325
Mammo2	0.296	0.281	0.109	0.125	3.047	2.168	3.156	2.293
Mammo3	0.296	0.297	0.078	0.125	3.12	2.191	3.198	2.316
Mammo4	0.296	0.282	0.109	0.125	2.957	2.299	3.066	2.424
Mammo5	0.296	0.297	0.109	0.125	2.935	2.389	3.044	2.514
Mammo6	0.296	0.328	0.125	0.125	3.559	2.436	3.684	2.561
Mammo7	0.328	0.297	0.094	0.094	3.103	2.296	3.197	2.39
Mammo8	0.296	0.266	0.11	0.11	2.929	2.468	3.039	2.578
Mammo9	0.375	0.156	0.016	0.062	1.805	1.196	1.821	1.258
Mammo10	0.312	0.344	0.109	0.109	3.166	2.643	3.275	2.752
Mammo11	0.171	0.156	0.015	0.015	1.79	1.289	1.805	1.304
Mammo12	0.375	0.281	0.031	0.031	1.817	1.406	1.848	1.437
Mammo13	0.171	0.157	0.047	0.047	1.8	1.236	1.847	1.283
Mammo14	0.171	0.344	0.078	0.078	1.505	1.169	1.583	1.247
Mammo15	0.156	0.172	0.047	0.047	1.902	1.5	1.949	1.547
Mammo16	0.296	0.282	0.078	0.078	1.508	1.232	1.586	1.31
Mammo17	0.171	0.172	0.031	0.032	1.795	1.275	1.826	1.307
Mammo18	0.171	0.188	0.031	0.031	1.756	1.335	1.787	1.366
Mammo19	0.171	0.172	0.063	0.063	1.625	1.165	1.688	1.228
Mammo20	0.171	0.172	0.015	0.031	1.826	1.207	1.841	1.238
Mammo21	0.171	0.172	0.016	0.016	1.705	1.223	1.721	1.239

Table 6.6: Compression/ Decompression time for JPEG-LS, ROI-JPEG-LS, SA-SPIHT and HYRICS on ultrasound images

Images	JPEG-LS		ROI-JPEG-LS		SA-SPIHT		HYRICS	
	CT	DT	CT	DT	CT	DT	CT	DT
Ultrasound1	0.234	0.234	0.031	0.031	2.081	1.365	2.112	1.396
Ultrasound2	0.203	0.203	0.031	0.031	1.786	1.316	1.817	1.347
Ultrasound3	0.187	0.187	0.031	0.046	1.838	1.418	1.869	1.464
Ultrasound4	0.203	0.344	0.062	0.078	1.688	1.347	1.75	1.425
Ultrasound5	0.203	0.25	0.031	0.032	1.856	1.478	1.887	1.51
Ultrasound6	0.296	0.203	0.078	0.094	1.61	1.378	1.688	1.472
Ultrasound7	0.203	0.203	0.016	0.031	2.171	1.621	2.187	1.652
Ultrasound8	0.218	0.219	0.032	0.078	2.101	1.48	2.133	1.558
Ultrasound9	0.218	0.219	0.031	0.031	2.233	1.744	2.264	1.775
Ultrasound10	0.421	0.218	0.031	0.031	1.89	1.636	1.921	1.667
Ultrasound11	0.203	0.485	0.062	0.063	1.674	1.382	1.736	1.445
Ultrasound12	0.203	0.203	0.062	0.063	1.694	1.527	1.756	1.59
Ultrasound13	0.421	0.672	0.125	0.14	1.587	1.384	1.712	1.524
Ultrasound14	0.203	0.219	0.063	0.063	1.656	1.583	1.719	1.646
Ultrasound15	0.203	0.219	0.062	0.063	1.679	1.393	1.741	1.456
Ultrasound16	0.421	0.453	0.062	0.109	1.651	1.587	1.713	1.696
Ultrasound17	0.171	0.203	0.046	0.046	1.645	1.415	1.691	1.461
Ultrasound18	0.203	0.218	0.093	0.093	1.815	1.625	1.908	1.718
Ultrasound19	0.484	0.219	0.031	0.0471	2.129	1.718	2.16	1.7651
Ultrasound20	0.218	0.703	0.046	0.046	2.109	1.494	2.155	1.54
Ultrasound21	0.203	0.203	0.047	0.062	1.878	1.601	1.925	1.663

6.4 HYRICS on preprocessed images

An additional study has also been carried out to find out the effect of the preprocessing (contrast stretching) of only ROI before applying modified JPEG-LS. Contrast stretching enhances the diagnostic value of medical image; however the resulting image is no longer reversible. The results of compression efficiency by applying modified JPEG-LS on contrast stretched mammograms and ultrasound images are shown in Table 6.7 and Table 6.8 respectively. It is quit clear that preprocessing the image before compression improves compression ratios in mammograms only.

For ultrasound images, preprocessing before applying the modified JPEG-LS on ROI decreases the compression ratios on most of the images. However, in few images there are slight improvements in compression ratios due to the speckle texture.

Table 6.7: Compression ratio applying modified JPEG-LS once after contrast stretch compare when preprocessing the mammogram before compression

Images	ROI-JPEG-LS (raw)		ROI-JPEG-LS (Preprocessing)	
	Size	CR	Size	CR
Mammo1	16156	2.92304075	14736	3.2047127
Mammo2	128244	2.67827694	85896	3.99870714
Mammo3	91890	2.6068174	87398	2.74080014
Mammo4	117328	2.8735243	56811	5.93449965
Mammo5	132756	2.66980104	80708	4.39153624
Mammo6	129276	2.78747544	82130	4.38760106
Mammo7	99000	2.73854452	47529	5.70422073
Mammo8	116634	2.81259095	90708	3.61648071
Mammo9	11234	2.98663139	3857	8.69894141
Mammo10	117587	2.75819969	72166	4.49419986
Mammo11	16347	2.74638145	3215	13.9642605
Mammo12	6619	3.07486003	6093	3.34030831
Mammo13	41413	2.81857985	5555	21.0127538
Mammo14	87972	2.90763692	41556	6.15532378
Mammo15	37178	2.77706811	4309	23.9605102
Mammo16	81889	2.87775927	7104	33.172414
Mammo17	26422	2.83601867	5983	12.5243666
Mammo18	9494	3.13787159	5471	5.44524819
Mammo19	73491	2.85179189	28905	7.25068459
Mammo20	3443	2.5211459	1957	4.43551627
Mammo21	2425	2.33864254	1580	3.58937225

Table 6.8: Compression ratio applying the modified JPEG-LS once after contrast stretch compare when preprocessing the ultrasound image before compression

Images	ROI-JPEG-LS (Raw)		ROI-JPEG-LS (Preprocessing)	
	Size	CR	Size	CR
Ultrasound1	25207	2.34030752	35285	1.67187563
Ultrasound2	24452	2.20804442	21752	2.48212129
Ultrasound3	26070	2.14484884	25046	2.2325405
Ultrasound4	69707	2.12415376	73462	2.01557793
Ultrasound5	29093	2.14142581	28568	2.18077924
Ultrasound6	110845	2.20947476	123060	1.99016114
Ultrasound7	9781	2.36544768	8518	2.71618264
Ultrasound8	30160	2.39102729	41868	1.72239856
Ultrasound9	16492	2.34930521	20289	1.90964274
Ultrasound10	14921	1.97913031	18831	1.56819093
Ultrasound11	85487	2.22219878	114890	1.65348688
Ultrasound12	85418	2.1418692	110450	1.65644349
Ultrasound13	116781	2.14480995	146809	1.7061151
Ultrasound14	83624	2.14776341	76575	2.34547264
Ultrasound15	82544	2.17774518	94991	1.89238768
Ultrasound16	78280	2.40108917	73715	2.54978309
Ultrasound17	49045	3.46763123	52855	3.21767049
Ultrasound18	56863	1.89464654	57370	1.87790284
Ultrasound19	18088	2.35337307	24547	1.73413501
Ultrasound20	25637	2.43562814	37075	1.68421305
Ultrasound21	49871	2.2887515	54720	2.08593432

6.5 Case studies on sample Mammograms

6.5.1 Sample mammogram 1

Figure 6.3 and figure 6.4 show an example of right breast image on which the proposed hybrid method is applied. The original image, the arbitrary shaped region that is marked by the radiologist and the resulting generated mask are shown in Figure 6.3. The decompressed image of ROI by the modified JPEG-LS, SA-SPIHT operated reconstructed image of non-ROI and the combining image are shown in figure 6.4. In this sample image, the micro-calcification region is very small compare to the entire image 3.79%. When JPEG-LS is applied only compression ratio 3.340472 can be achieved. However, HYRICS is achieving compression ratio of 39.99875. This high compression is achieved by degrading the quality in non-ROI with compression ratio of 80. It can be seen in Figure 6.4, the micro-calcification in the recovered image is well preserved.

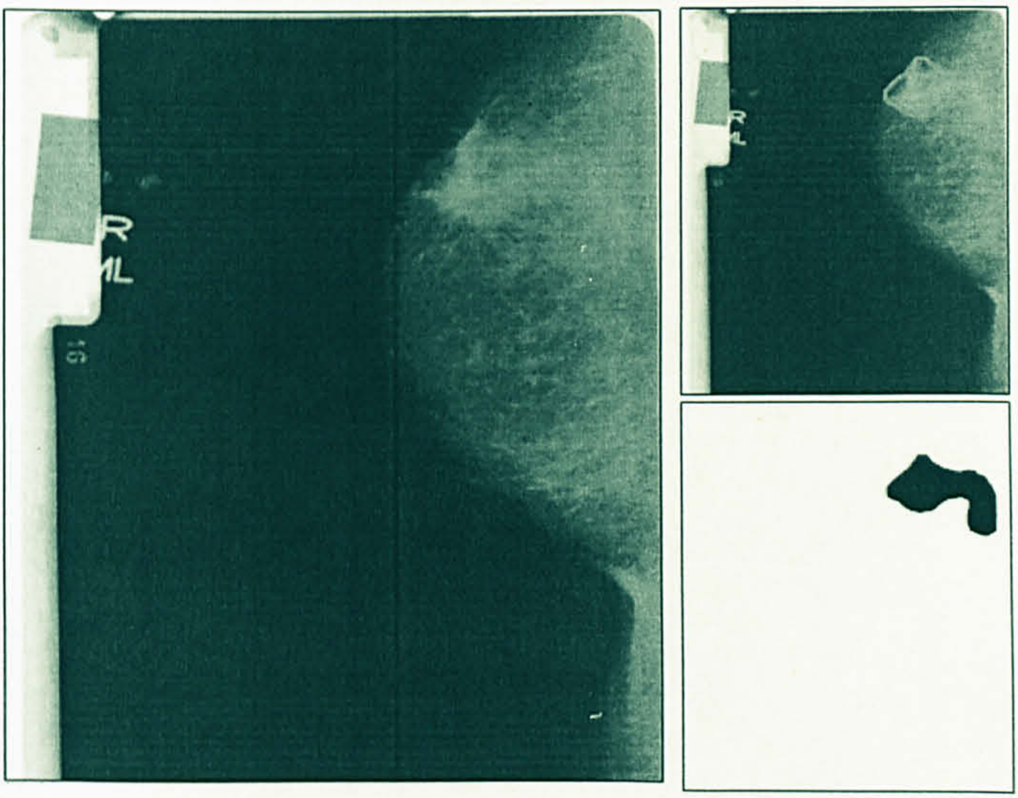

Figure 6.3: Sample mammogram 1
Left is the Original images; Top right is the ROI marked by radiologist; Bottom right is the generated Mask

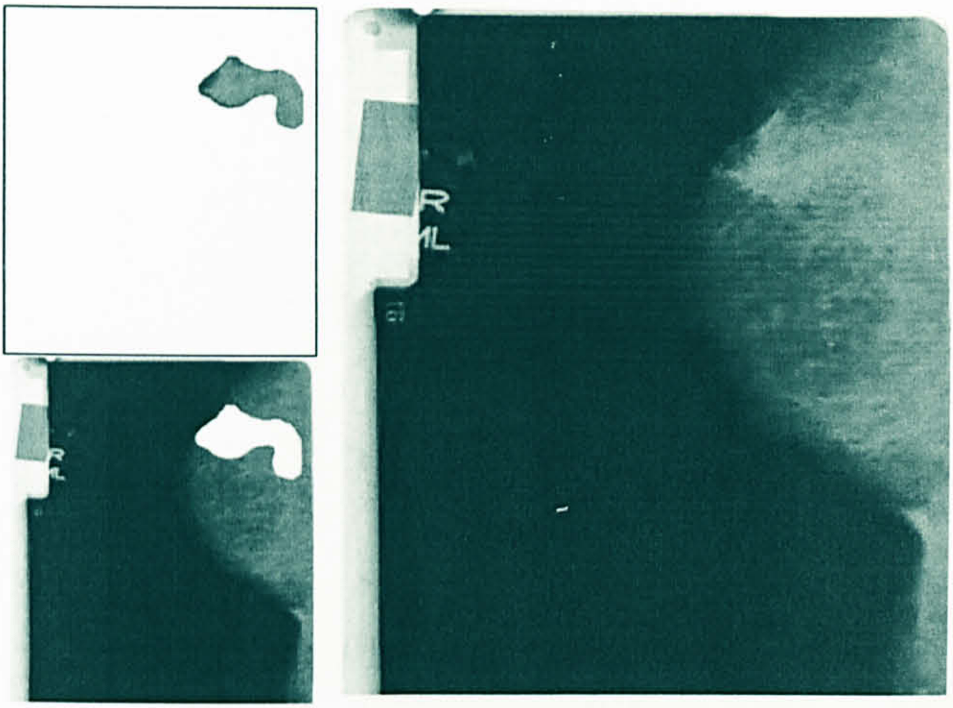

Figure 6.4: HYRICS on sample mammogram 1
Top left is modified JPEG-LS operated ROI;
Bottom left is SA-SPIHT operated non-ROI; Right is Recovered image after combining the above two images

6.5.2 Sample mammogram 2

As it is shown in Figure 6.5 and figure 6.6, the steps of applying the proposed hybrid method in a breast image is presented. In this sample image, JPEG-LS on the entire image is achieving compression ratio of 3.446099. However, as the disease affected region is bigger than the previous sample 20.31%, HYRICS is achieving comparatively less compression ratio 11.38211 but yet far better than JPEG-LS. The quality degradation in non-ROI is remaining the same as the previous sample but a larger area is preserved.

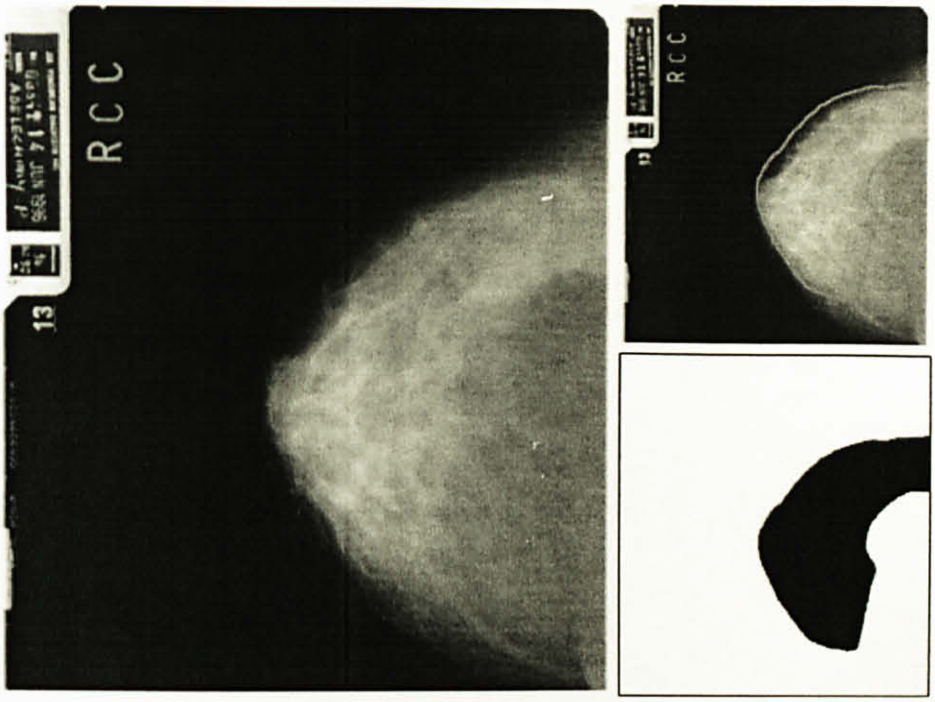

Figure 6.5: Sample mammogram 2
Left is the Original images; Top right is the ROI marked by radiologist;
Bottom right is the generated Mask

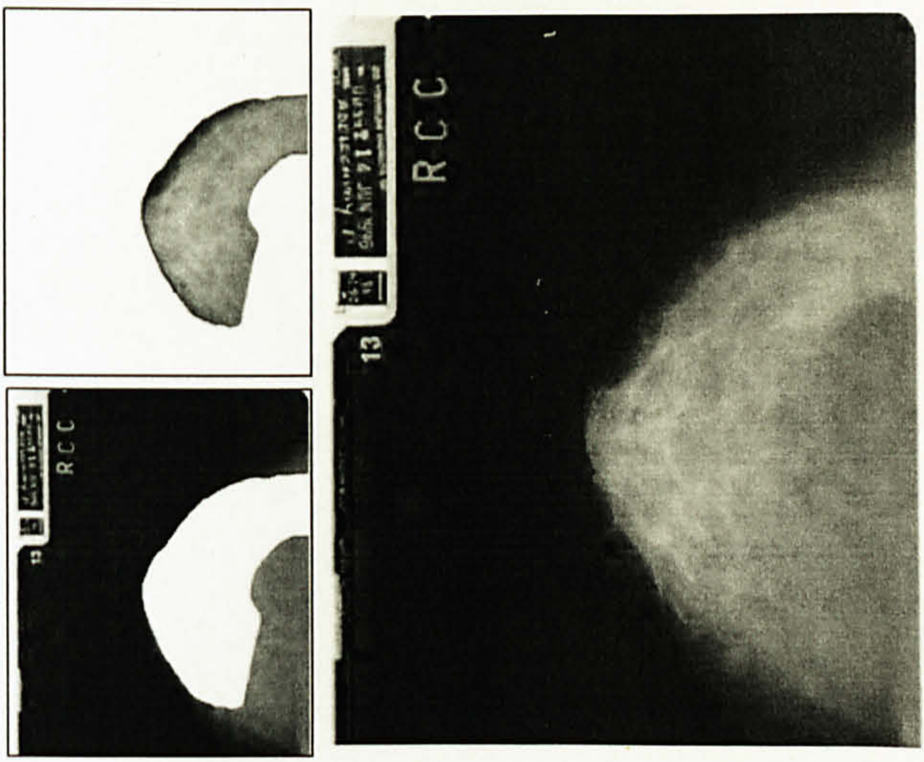

Figure 6.6: HYRICS on sample mammogram 2
Top left is modified JPEG-LS operated ROI;
Bottom left is SA-SPIHT operated non-ROI; Right is recovered image after combining the above two images

6.5.3 Sample mammogram 3

In sample 3 the arbitrary shaped region that is marked by the radiologist is including the entire breast area and equivalent to 30.05% of the image size. JPEG-LS achieving compression ratio 3.286945. Figure 6.7 and figure 6.8 show HYRICS performance on this large ROI sample mammogram in which HYRICS is achieving compression ratio of 8.245254.

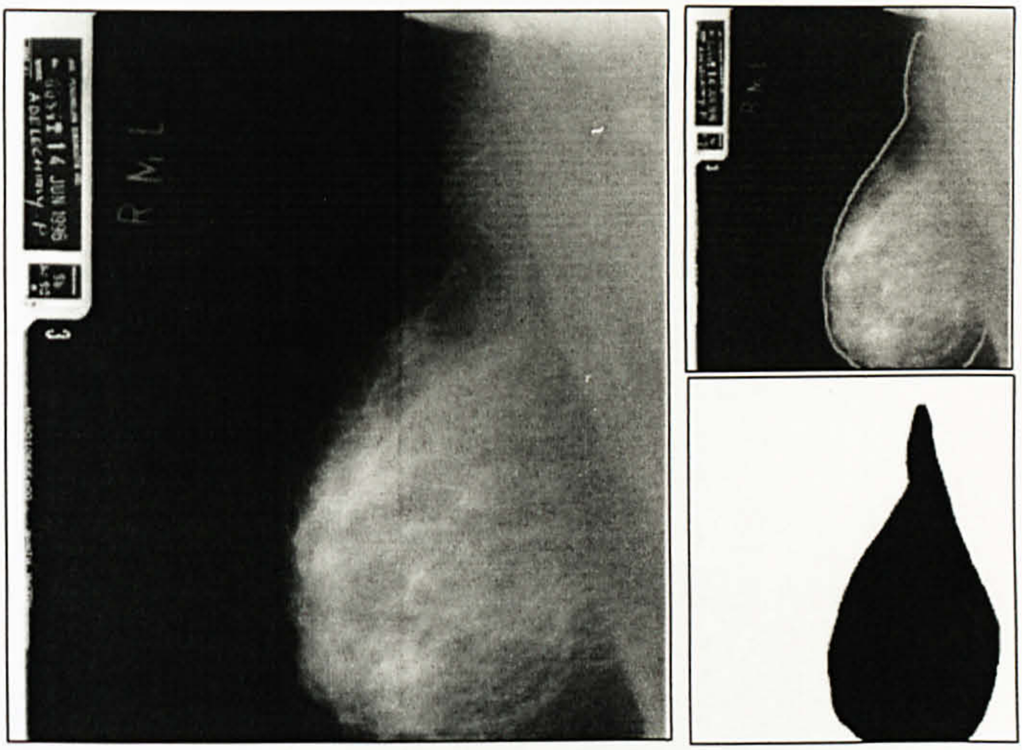

Figure 6.7: Sample mammogram 3
Left is the Original images; Top right is the ROI marked by radiologist;
Bottom right is the generated Mask

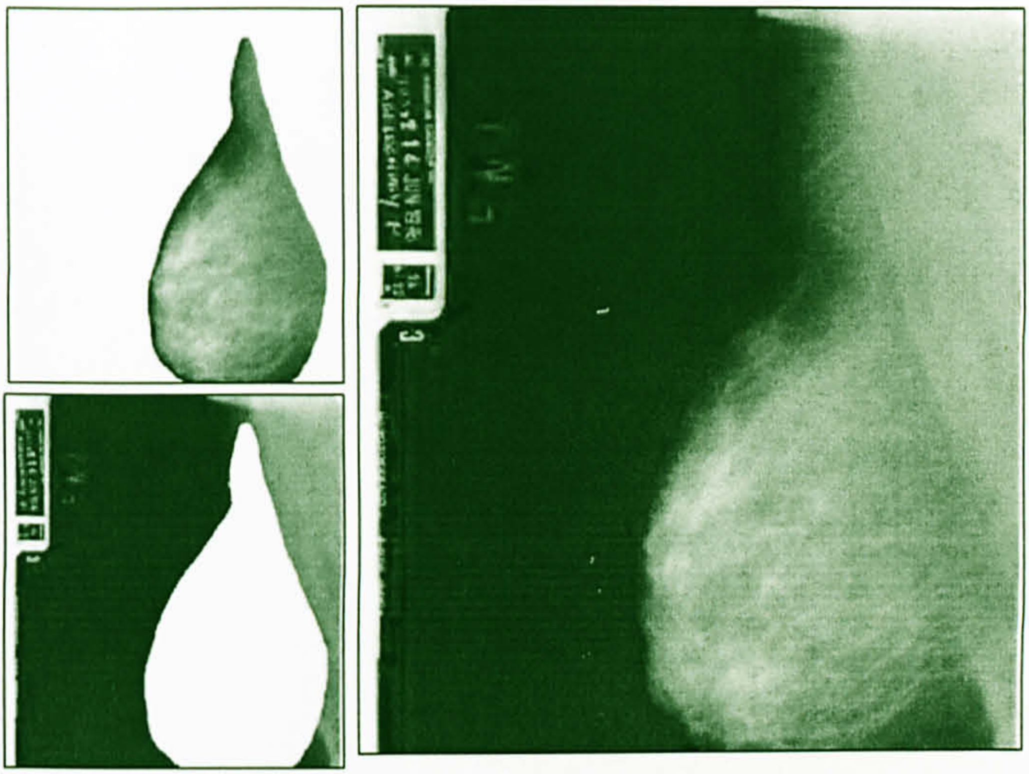

Figure 6.8: HYRICS on sample mammogram 3
Top left is modified JPEG-LS operated ROI;
Bottom left is SA-SPIHT operated non-ROI; Right is recovered image after combining the left two images

6.6 Case studies on sample ultrasound images

6.6.1 Sample ultrasound 1

An example of ultrasound scan of kidney in which the proposed hybrid method is operated is shown in Figure 6.9 and figure 6.10. In this sample, the kidney region is very small 5.09% compare to the entire image. JPEG-LS is achieved 2.45 compression ratio on the entire image. By degrading the quality in non-ROI with compression ratio of 80, HYRICS is achieving compression ratio of 29.84 while reserving the kidney part in the recovered image.

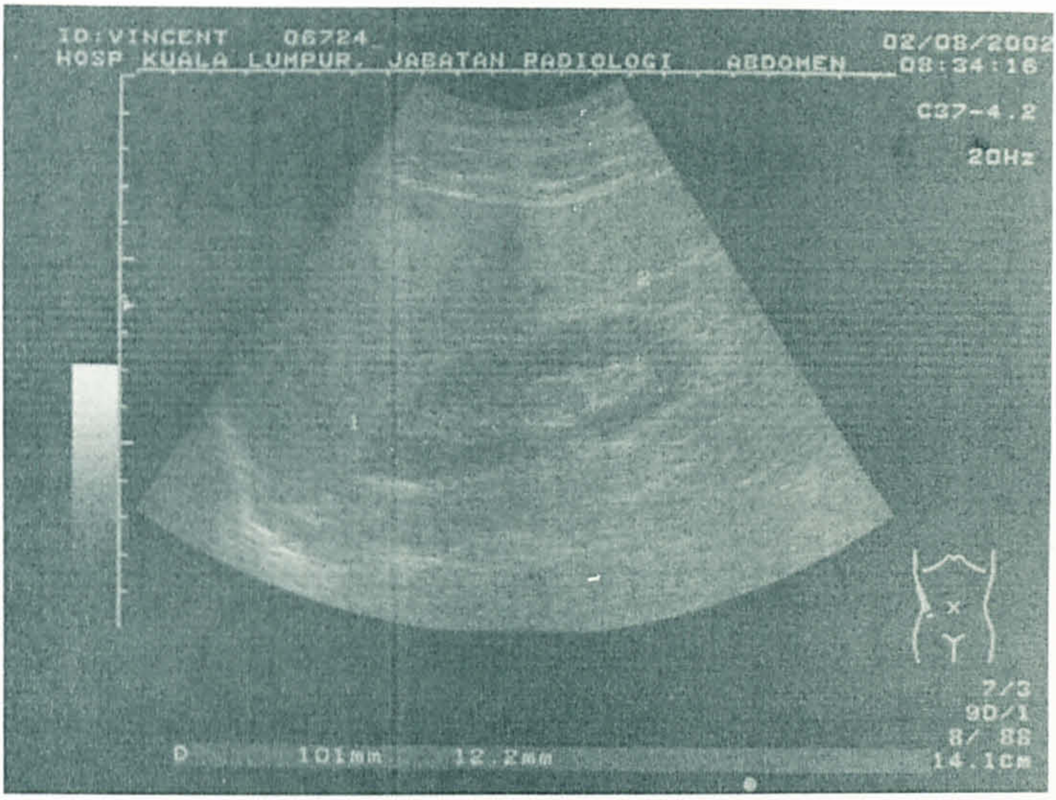

(a)

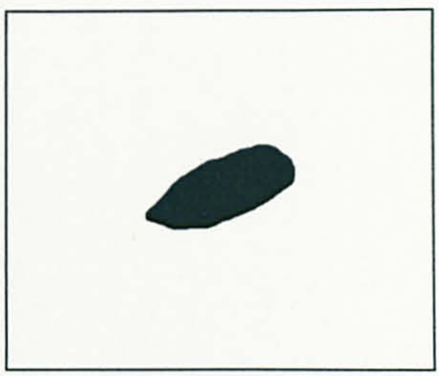

(b) **(c)**

Figure 6.9: Sample ultrasound 1
(a) Original image; (b) ROI marked by radiologist;
(c) Generated Mask

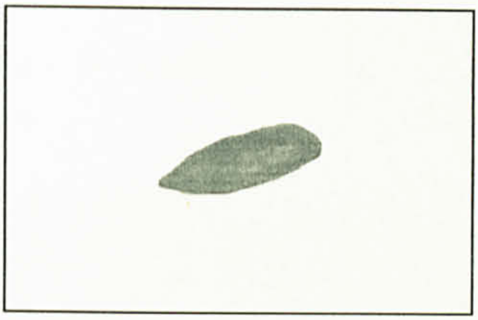

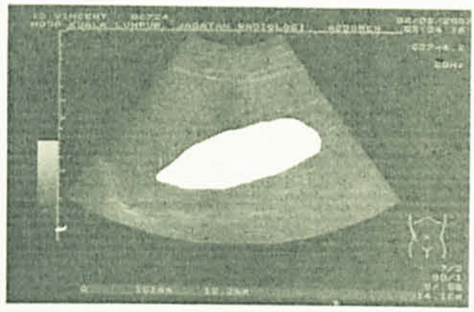

(a) **(b)**

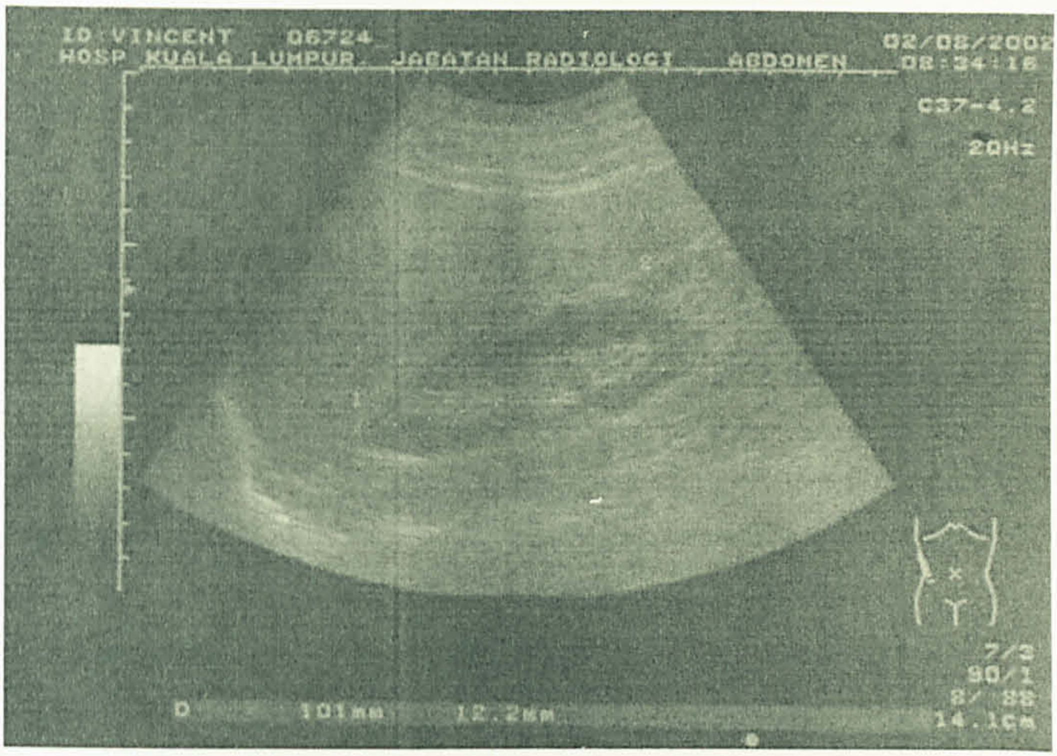

(c)

Figure 6.10: HYRICS on sample ultrasound 1
(a) Modified JPEG-LS operated ROI;
(b) SA-SPIHT operated non-ROI; (c) Recovered image after combining the two images in (a) and (b)

6.6.2 Sample ultrasound 2

As it is shown in Figure 6.11 and figure 6.12, the steps of applying the proposed hybrid method in a breast image is presented. In this sample image, there is two scan areas for two different abdominal organs (spleen and liver). JPEG-LS on the entire image is achieving compression ratio of 2.181235. However, as the disease affected region is relatively large 22.86%, HYRICS is achieving comparatively less compression ratio 8.725956 but yet far better than JPEG-LS. The quality degradation in non-ROI is remaining the same as the previous sample but a larger area is preserved.

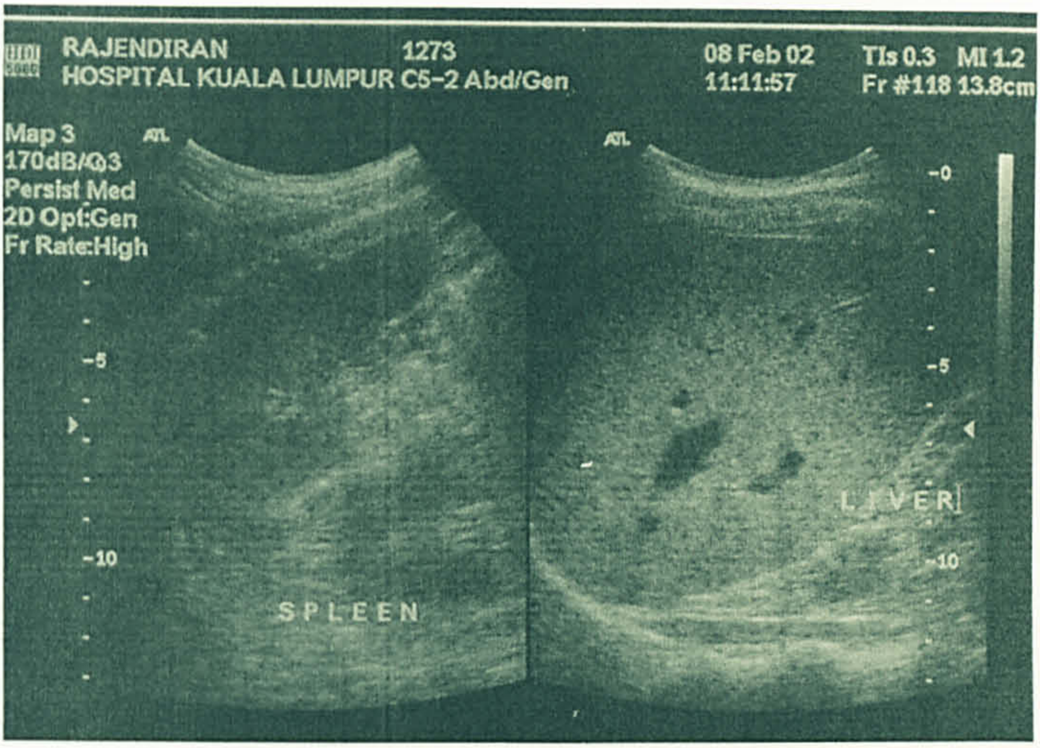

(a)

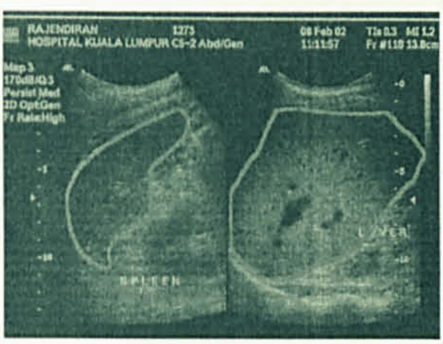

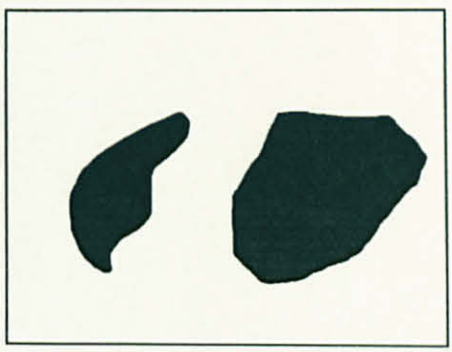

(b) (c)

Figure 6.11: Sample ultrasound 2

(a) Original image; (b) ROI marked by radiologist;

(c) Generated Mask

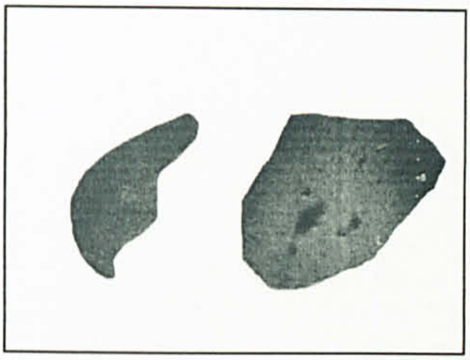

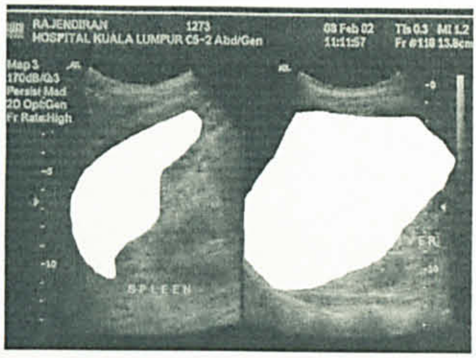

(a) (b)

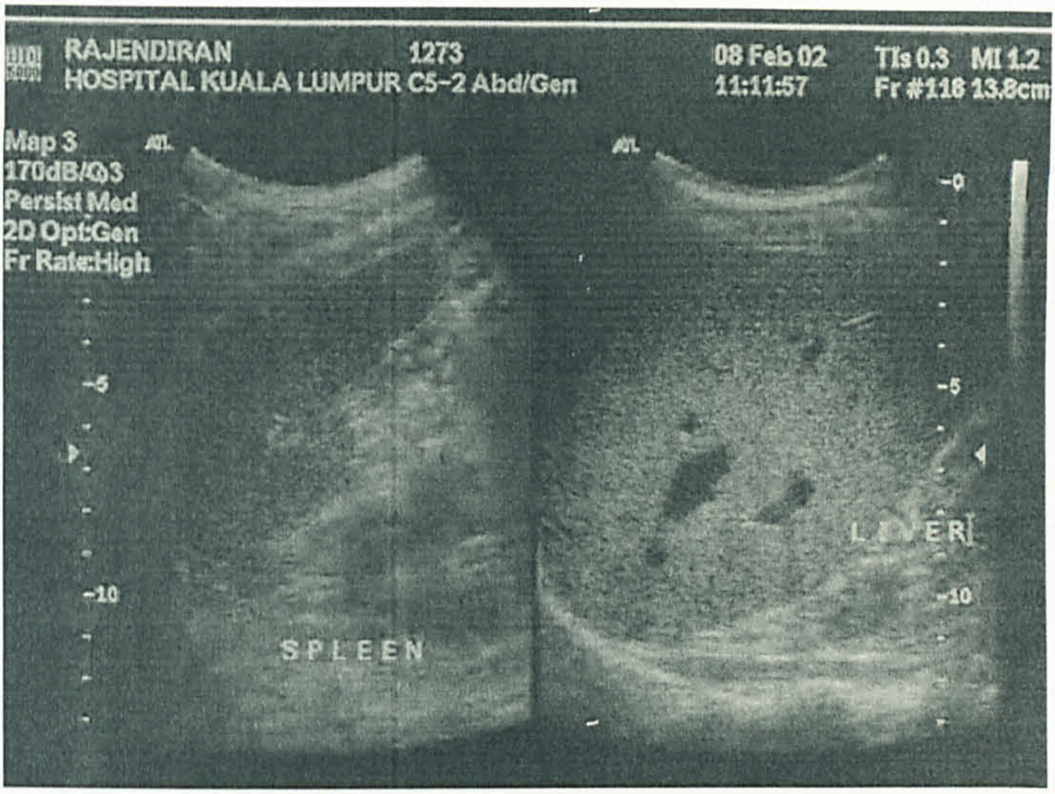

(a)

Figure 6.12: HYRICS on sample ultrasound 2
(a) Modified JPEG-LS operated ROI;
(b) SA-SPIHT operated non-ROI; (c) Recovered image after combining the two images in (a) and (b)

6.6.3 Sample ultrasound 3

In sample 3 the arbitrary shaped region that is marked by the radiologist is including two scan areas for kidney equivalent to 18.83% of the image size. JPEG-LS achieving compression ratio 2.064791. Figure 6.13 and figure 6.14 show HYRICS performance on this relatively large ROI ultrasound in which HYRICS is achieving compression ratio of 10.12332.

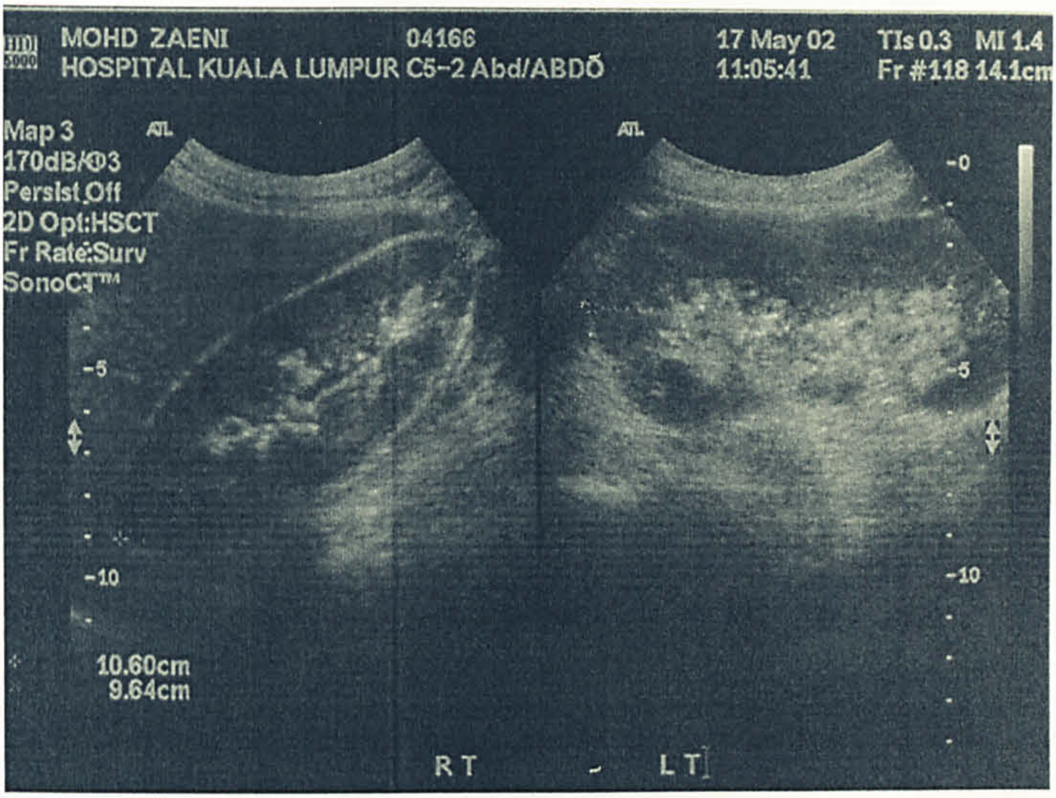

(a)

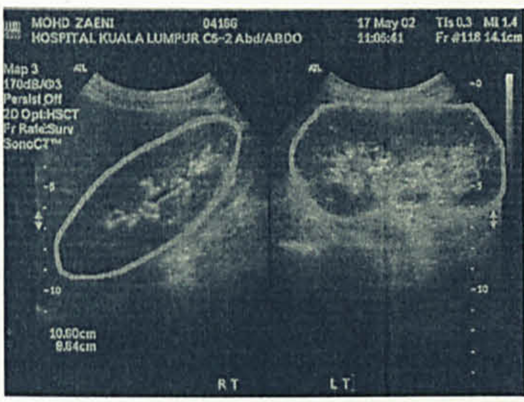

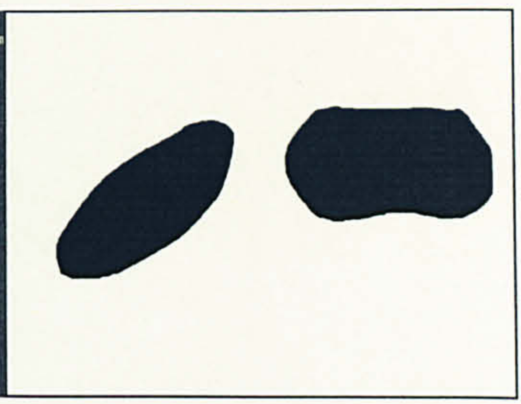

(b) **(c)**

Figure 6.13: Sample ultrasound 3
(a) Original image; (b) ROI marked by radiologist;
(c) Generated Mask

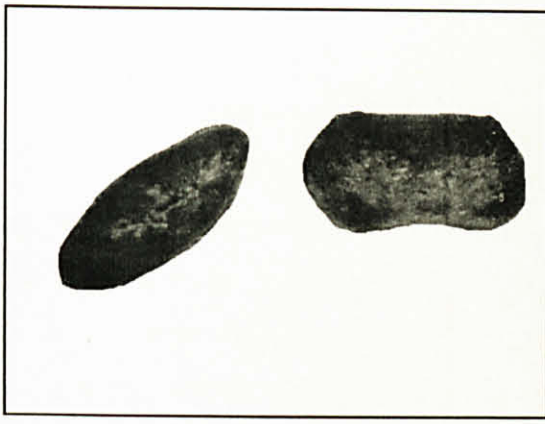

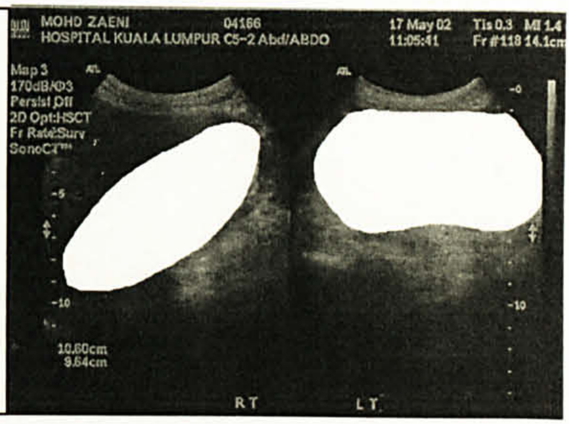

(a) **(b)**

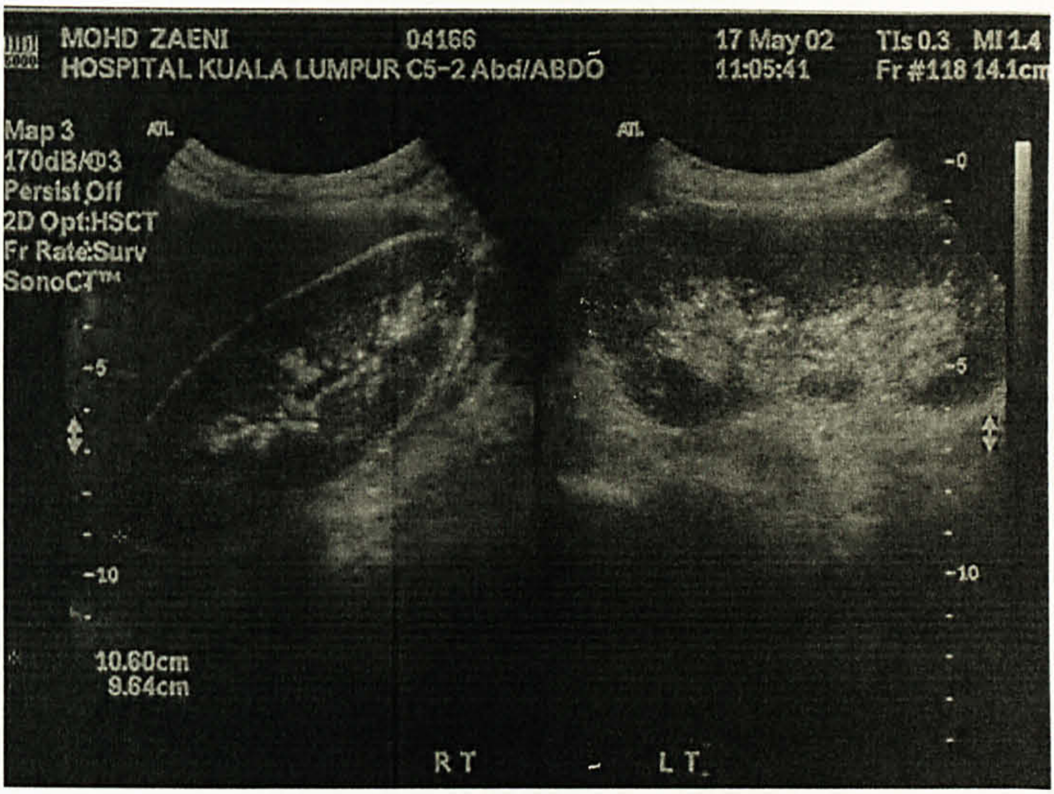

(c)

Figure 6.14: HYRICS on sample ultrasound 3
(a) Modified JPEG-LS operated ROI;
(b) SA-SPIHT operated non-ROI; (c) Recovered image after combining the two images in (a) and (b)

6.7 Summary

The scheme developed in this work is tested on sample set of 21 selected mammograms and 21 selected ultrasound images of different sizes and textures. The relevant diagnostic regions are roughly marked by the expert radiologist and appropriate masks are generated. The results obtained show that the proposed hybrid scheme yields high compression ratios. The compression ratios obtained reach maximum of 41.9 and 62.1 under certain constraints such as size of ROI, specified quality, etc.

It is noticed that the compression/decompression time of the hybrid technique is also depends upon the relative sizes of ROI.

The results of compression efficiency by applying modified JPEG-LS on preprocessed (contrast stretched) images show an increase in compression ratios on mammograms and decline on some of the ultrasound images due to the speckle texture.

CHAPTER 7

CONCLUSION AND RECOMMENDATIONS

7.1 Conclusion

A new approach called Hybrid Region-based Image Compression Scheme (HYRICS) has been proposed for efficient coding of mammograms and ultrasound images for tele-healthcare applications. The proposed method could achieve higher compression ratio possible without compromising the diagnostic quality on the disease affected regions.

In an effort to optimally compress medical images, various techniques have been studied. Out of which frequently used lossless compression schemes like LJPEG, JPEG-LS, CALIC, FELICS, BTPC, JPEG2000, S+P and PNG and lossy compression methods such as JPEG, BTPC, JPEG2000 and SPIHT have been analyzed to highlight their efficiency and suitability for compressing number of mammograms and ultrasound images of different sizes and texture the denoted by their respective entropies.

Three criteria namely, compression ratio, compression time and decompression time are used to evaluate the above eight lossless methods. JPEG-LS is found to give high compression ratio and much less compression/decompression time.

The four lossy methods are evaluated using MSE and PSNR as criteria to quantify the distortion on a range of compression ratios. It is found that SPIHT is the efficient method that shows the better compromise between compression ratio and image quality than other lossy schemes with a reasonable compression speed.

The efficient performances of lossless JPEG-LS and lossy SPIHT are advantageously utilized in HYRICS by applying JPEG-LS on the disease concentrated regions and SPIHT algorithm on the remaining area of the images. A new modification has been introduced for JPEG-LS. The modified JPEG-LS is applied on disease affected arbitrary regions marked by the expert radiologist on the raw images discarding the remaining area on which SA-SPIHT is used.

The results obtained show that the proposed hybrid scheme yields considerable increase in compression ratios. The compression ratios obtained reach maximum of 41.9 and 62.1 for the selected mammograms and ultrasound images respectively under certain constraints such as size of ROI, specified quality, etc.

It is noticed that the compression/decompression time of the hybrid technique is also improved and this improvement depends upon the relative sizes of ROI.

The results of compression efficiency by applying modified JPEG-LS on preprocessed (contrast stretched) images show an increase in compression ratios on mammograms and decline on some of the ultrasound images.

The outcome of the research is that there will be an appreciable increase in compression efficiency for speedy transmission and reduce storage requirement without affecting the diagnostic quality.

7.2 Recommendations

Some segmentation algorithm like region growing technique can be incorporated to automatically select the ROI area that need to be preserved as an alternative to the manual one.

The capability of encoding arbitrary shaped objects by the modified JPEG-LS can be added as an additional feature to the current standard to encode other medical image modalities. For instance, the proposed technique can be used to encode efficiently the brain area in both MRI and CT scan.

HYRICS coders can be optimized more to be faster and memory efficient. For example the modified JPEG-LS and SA-SPIHT can operate concurrently instead of operating sequentially on the two areas.

REFERENCES

1. Wahid, M.I. *Breast Cancer*. Common Cancers 2007 [cited 2007; Available from: http://www.malaysiaoncology.org/article.php.

2. Belizan, J. *Routine ultrasound in early pregnancy*. 1998 [cited 2006; RHL commentary]. Available from: http://www.rhlibrary.com/Commentaries/htm/Jbcom.htm.

3. Russell, S. *Early Detection is the key : Mammography*. 2000 [cited; Available from: http://www.centerforwomen.com/MainFrames/mammography.htm.

4. Chiu, E., *Lossy Compression of Medical Ultrasound Images using Space-Frequency Segmentation*, in *School of Engineering Science*. July 1999, Simon Fraser University.

5. Erickson, B.J., *Irreversible Compression of Medical Images*. 2000, Mayo Foundation, Rochester,MN: Great Falls VA,USA. p. 1-13.

6. Seeram, E. *Using irreversible compression in digital radiology: a preliminary study of the opinions of radiologists*. in *Medical Imaging 2006: PACS and Imaging Informatics*. 2006: SPIE.

7. Sprawls, P., *The Physical Principles of Medical Imaging*. The web-based 2nd ed. 1995: Medical Physics Publishing, Madison, Wisconsin.

8. Bushberg J. T. , J.A.S., E. M. Leidholdt and J. M. Boone, *The essentials of Medical Imaging*. 1994, Philadelphia, USA: Williams & Wilkins.

9. Hornak, J.P., *The basics of MRI*. 1996-2007: Rochester Institute of Technology.

10. Claudio Cipolat, M.G., *The History of Telemedicine*, in *Telemedicine and Teledermatology*. 2003, Curr Probl Dermatol: Basel, Karger. p. 11.

11. Baldwin, F.D. *How Technology is Being Used to Enhance the Delivery of Health Care Services.* 2006 [cited; Available from: http://www.arc.gov/index.do?nodeId=2043.

12. Field, M.J., *Telemedicine: A Guide to Assessing Telecommunications for HealthCare*. 1996, Washington, D.C: National Academy Press.

13. Mikael Jensen , J.E.W. *X-ray imaging: Fundamentals and planar imaging.* 2006 [cited; Available from: http://server.oersted.dtu.dk/personal/jw/webbook/X-ray/Planar/main.pdf.

14. J. H. Hubbell , S.M.S. *Tables of X-Ray Mass Attenuation Coefficients and Mass Energy-Absorption Coefficients.* 1993 [cited; Available from: http://physics.nist.gov/PhysRefData/XrayMassCoef/cover.html.

15. Radiology, C.o. *Glossary of Terms.* 2003 [cited; Available from: http://www.radiologymalaysia.org/Archive/RITHB/glossary.html.

16. *DDSM: Digital Database for Screening Mammography.* 2000 [cited; Available from: http://marathon.csee.usf.edu/Mammography/Database.html.

17. Haacke, E.M., R. W. Brown, M. R. Thompson, R. Venkatesan, *Magnetic Resonance Imaging: Physical Principles and Sequence Design*. 1999, New York: John Wiley & Sons, Inc.

18. Lonsdale, M.N., *Nuclear Magnetic Resonance Imaging lecture notes*. 2004, Department of Clinical Physiology and Nuclear Medicine: Bispebjerg,Copenhagen, NV.

19. Radiological Society of North America, I.R. *Positron Emission Tomography (PET Imaging).* 2005 [cited; Available from: http://www.radiologyinfo.org/en/info.cfm?PG=pet&bhcp=1.

20. (MIRG), M.I.R.G. *Introduction to SPECT.* 2001 [cited; Available from: http://www.physics.ubc.ca/~mirg/.

21. Rumack, C., *Diagnostic ultrasound.* 2nd ed. Vol. 1. 1998, New York: Mosby.

22. R.F. Wagner, M.F.I.a.D.G.B., *Unified Approach to the Detection and Classification of Speckle Texture in Diagnostic Ultrasound.* 1986: Optical Engineering.

23. Ed Chiu, J.V., M. Stella Atkins. *Compression of ultrasound images using wavelet based space-frequency Partitions.* in *Medical Imaging 2000: Image Display and Visualization.* 2000. Seong K. Mun.

24. Bruno Carpentieri, M.J.W., Gadiel Seroussi. *Lossless Compression of Continuous-Tone Images.* in *IEEE.* 2000: Hewlett-Paclard.

25. Marcelo J. Weinberger, G.S., Guillermo Sapiro. *LOCO-I: A Low Complexity, Context-Based, Lossless Image Compression Algorithm* in *Data Compression Conference.* 1996. Snowbird, Utah.

26. A. N. Skodras, C.A.C.a.T.E. *JPEG2000: The Upcoming Still Image Compression Standard.* in *11th Portuguese Conference on Pattern Recognition (RECPA00D).* 2002. Porto, Portugal.

27. Amir Said , W.A.P. *A New Fast and Efficient Image Codec Based on Set Partitioning in Hierarchical Trees.* in *IEEE Transactions on Circuits and Systems for Video Technology.* 1996.

28. Taubman, D. *High performance scalable image compression with EBCOT.* in *IEEE Trans. in Image Processing.* 2000.

29. Huffman, D.A. *A method for the construction of minimum redundancy codes.* in *IRE.* 1952.

30. A. Moffat, R.N., I. H. Witten. *Arithmetic coding revisited.* in *Fifth IEEE Data Compression Conference.* 1995. Los Alamitos, California.

31. Gailly, M.N.a.J.-l., *The Data Compression Book.* 2nd ed. 1995, New York, NY: M&T Books.

32. Randers-Pehrson, G. *PNG (Portable Network Graphics) specification version 1.1.* 1999 [cited; Available from: http://citeseer.ist.psu.edu/randers-pehrson99png.html.

33. Shannon CE, W.W., *The mathematical theory of communication.* 1949: University of Illinois Press, Urbana IL.

34. N.M. Nasrabadi, R.A.K. *Image coding using vector quantization: A review*. in *IEEE Transactions on Communications*. 1980.

35. A. Gersho, R.G., *Vector Quantization and Signal Compression.* 1992, Dordrecht, Netherlands: Kluwer Academic Publishers.

36. Majid Rabbani , P.W.J., *Digital image compression techniques.* 1991, Bellingham, Washington: SPIE-International Society for Optical Engine.

37. Zhang, S.Y.X. *Performance of Lossy Compression Algorithms from Statistical and Perceptual metrics.* in *Proceedings of 12th IEEE Symposium on Computer-Based Medical Systems*. 1999.

38. Wu TC, L.S., Peng CH, Wen CH, Huang SK., *An Economical, Personal Computer-based Picture Archiving and Communication System.* Radiographics, 1999.

39. Clunie, D.A. *Lossless Compression of Grayscale Medical images: Effective of Traditional and State of the Art approaches*. in *SPIE Medical Imaging* 2000.

40. William B. Pennebaker and Joan L. Mitchell, *JPEG, Still Image Data Compression Standard.* 1992, New York: Van Nostrand Reinhold,.

41. M. J. Weinberger, G.S., and G. Sapiro. *The LOCOI lossless image compression algorithm: Principles and standardization into JPEG-LS.* in *Trans. Image Processing*. 2000: Hewlett-Packard Laboratories.

42. Memon, X.W.a.N.D. *Context-based adaptive lossless image coding*. in *IEEE transactions on Communications*. 1997.

43. Pearlman, A.S.a.W. *Reversible image compression via multiresolution representation and predictive coding*. in *SPIE Symposium on Visual Communications and Image Processing,*. 1993.

44. Schindler, M. *szip* 1999 [cited; Available from: http://www.compressconsult.com/szip/.

45. A. Zandi, J.D.A., E.L. Schwartz, and M. Boliek. *CREW: Compression with reversible embedded wavelets*. in *Data Compression Conference*. 1995. Snowbird, Utah: IEEE Computer Society Press.

46. Deutsch P, G.J. *ZLIB Compressed data format specification version 3.3*. 1996 [cited; Available from: ftp://ds.internic.net/rfc/rfc1950.txt.

47. Kivijarvi J, O.T., Kaukoranta T, Kuba A, Nyul L, Nevalainen O. *A comparison of lossless compression methods for medical images*. in *Computerized Medical Imaging and Graphics*. 1998.

48. Koen Denecker, J.v.O., Ignace Lemahieut. *An experimental comparison of several. lossless image coders for medical images*. in *IEEE Data Compression Conference*. 1997. Los Alamitos CA: IEEE Computer Society.

49. Robinson, J.A. *Efficient general-purpose image compression with binary tree predictive coding*. in *IEEE Transactions on Image Processing*. 1997.

50. Vitter, P.H.a.J. *Fast progressive lossless image compression*. in *IST/SPIE International Symposium on Electronic Imaging Science and Technology*. 1994. San Jose, CA, USA.

51. (NEMA), T.A.C.o.R.A.a.t.N.E.M.A. *Digital Imaging and Communications in Medicine (DICOM) Part 5: Data Structures and Encoding*. 1999 [cited; Available from: http://medical.nema.org/dicom/1999/draft/99_05dr.pdf.

52. Przelaskowski, P.S., Anna Kukuła. *Compression of mammograms for medical practice*. in *ACM symposium on Applied Computing*. 2004. Nicosia, Cyprus: ACM Press.

53. Przelaskowski, P.S., Anna Kukuła *Evaluation of mammogram compression efficiency.* Polish Journal of Radiology, 2005.

54. Cécile DELGORGE, C.R., Pierre VIEYRES, Gérard POISSON. *JPEG 2000, an adapted compression method for ultrasound images ? A comparative study.* in *6th World Multiconference on Systemic, Cybernetics and Informatics (SCI 2002).* 2002. Orlando, FL, USA.

55. Golomb, S.W., *Run-length encodings* IEEE Trans Info Theory, 1966. **12(3):399**.

56. Sikora, T. *Low Complexity Shape-Adaptive DCT for Coding of Arbitrarily Shaped Image Segments.* in *Signal Processing: Image Communication (SP:IC).* 1995.

57. A. N. Skodrasa, C.A.C.a.T.E. *Efficient Methods For Encoding Regions Of Interest in the Upcoming JPEG2000 Still Image Coding Standard.* in *IEEE Int. Conf. on Image Processing (ICIP-2000).* 2000. Vancouver, Canada.

58. Li, S.L.W. *Shape-adaptive discrete wavelet transforms for arbitrarily shaped visual object coding.* in *IEEE Transaction on Circuits and System for Video Technology.* 2000.

59. Sayood, K., *Introduction to Data Compression.* 2000: Morgan Kaufmann Series in Multimedia.

60. Wang, K., *Region-Based Three-Dimensional Wavelet Transform Coding.* 2005, Institute for Electrical and Computer Engineering,Department of Systems and Computer Engineering, Carleton University: Ottawa-Carleton.

PUBLICATIONS

[1] Boshara M. Arshin, P.A Venkatachalam and Ahmad Fadzil Mohd. Hani, (2006), "*Evaluation of Ultrasound image Compression*". Proceedings of 9th International Conference in Quality in Research (QIR) 2006, Indonesia.

[2] Boshara M. Arshin, P.A Venkatachalam and Ahmad Fadzil Mohd. Hani.(2006), "*Evaluation of Lossless Ultrasound image Compression*". Proceedings of International Conference on Man Machine Systems ICoMMS 2006, Malaysia.

[3] Boshara. M. Arshin, P. A. Venkatachalam, M.H. Ahmad Fadzil, (2006), "*Lossless Image Compression of Digital Mammograms*," Proceedings of the ICAIET 2006, Sabah, Malaysia

APPENDIX A

The Sample Images

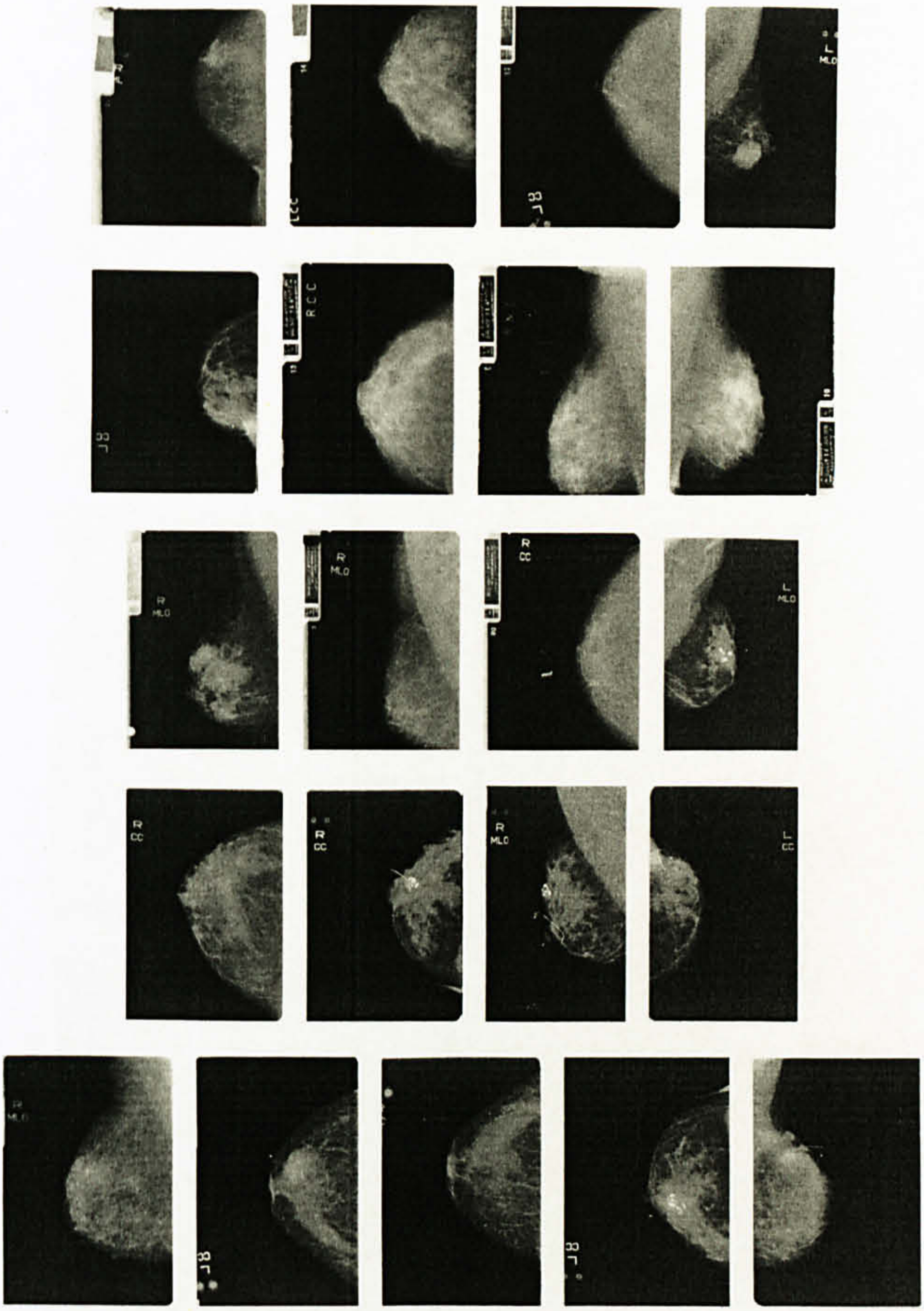

Figure 1 : Sample mammograms that used in the study

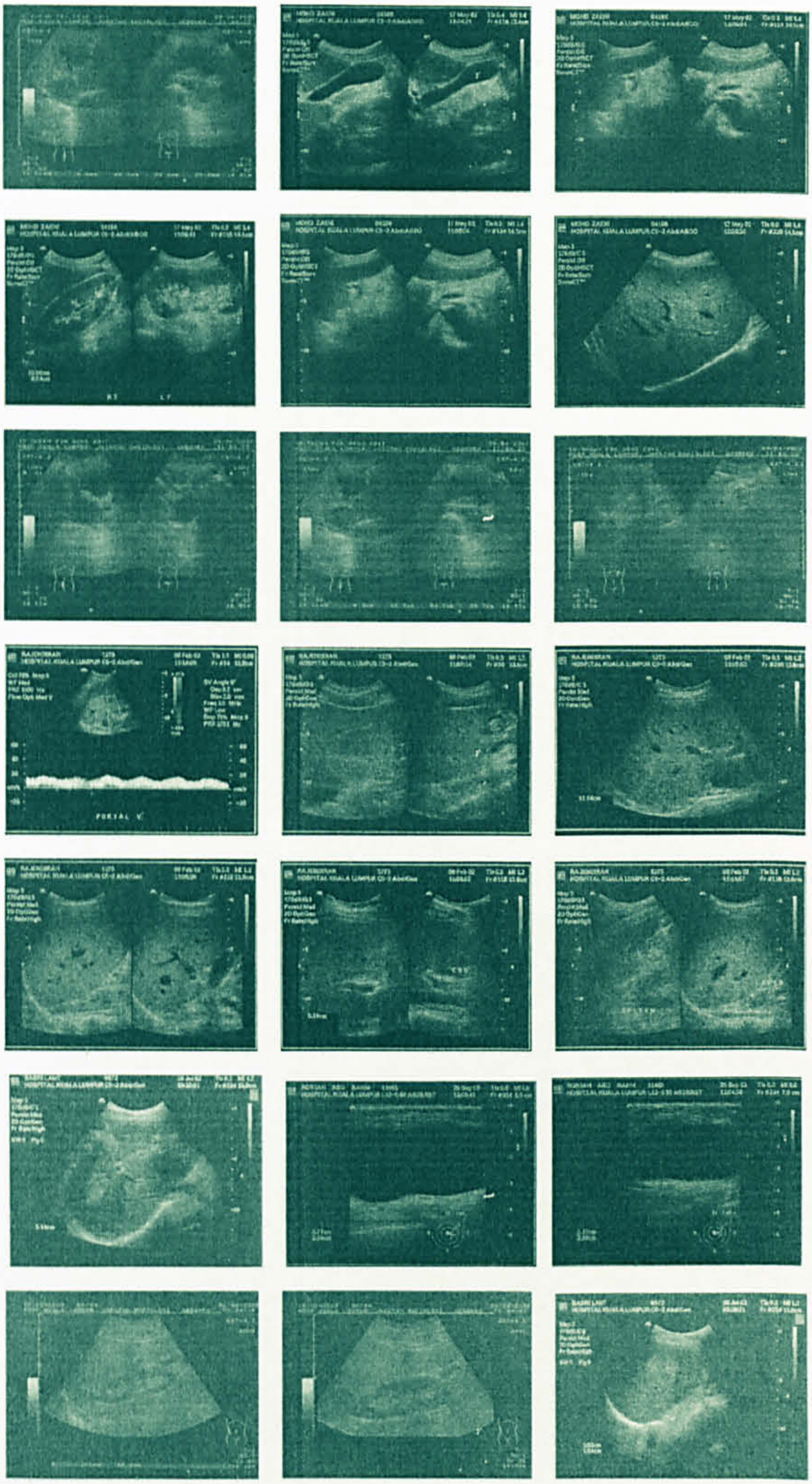

Figure 2: Sample ultrasound images that used in the study

Table 1: Mammograms spatial resolution and sizes

FILE NAME	WIDTH	HIGHT	HEADER	TOTAL SIZE (Bytes)	Entropy (bpp)
mammo1	1000	1222	17	1222017	5.226669
mammo2	1000	1157	17	1157017	5.146805
mammo3	1000	1157	17	1157017	5.452936
mammo4	1000	1171	17	1171017	5.874880
mammo5	1000	1160	17	1160017	5.965056
mammo6	1000	1272	17	1272017	5.558123
mammo7	1000	1156	17	1156017	5.824625
mammo8	1000	1160	17	1160017	4.821750
mammo9	1000	637	16	637016	5.521531
mammo10	1000	1204	17	1204017	4.705745
mammo11	1000	645	16	645016	5.456376
mammo12	1000	647	16	647016	5.164129
mammo13	1000	635	16	635016	4.487730
mammo14	1000	640	16	640016	5.542088
mammo15	1000	643	16	643016	4.487462
mammo16	1000	661	16	661016	5.704017
mammo17	1000	645	16	645016	5.144111
mammo18	1000	659	16	659016	5.269176
mammo19	1000	658	16	658016	5.249721
mammo20	1000	657	16	657016	4.923096
mammo21	1000	648	16	648016	4.932889

Table 2: ultrasound organs, spatial resolution and size

FILE NAME	Organ	WIDTH	HIGHT	HEADER	TOTAL SIZE (Bytes)	Entropy (bpp)
Obdmen1	Urinary/Bladder	1112	822	16	914080	4.902170
Obdmen2	Gallbladder	1050	790	16	829516	5.397674
Obdmen3	Spleen/Pancreas	1060	786	16	833176	5.168990
Obdmen4	Kidney	1054	782	16	824244	5.259995
Obdmen5	Spleen/Pancreas	1058	796	16	842184	5.143429
Obdmen6	Liver	1054	790	16	832676	4.929101
Obdmen7	Urinary/Bladder	1108	822	16	910792	4.745320
Obdmen8	Urinary/Bladder	1112	822	16	914080	4.902170
Obdmen9	Spleen/Pancreas	1112	830	16	922976	4.469665
Obdmen10	Liver/Portal vein	1050	794	16	833716	5.030231
Obdmen11	Lobe of Liver	1054	794	16	836892	5.444924
Obdmen12	Lobe of Liver	1036	816	16	845392	5.217798
Obdmen13	Lobe of Liver	1048	798	16	836320	5.773829
Obdmen14	Vein in Liver	1050	794	16	833716	5.262360
Obdmen15	Spleen/Liver	1048	800	16	838416	5.501622
Obdmen16	Mass in Liver	1048	776	16	813264	5.064322
Obdmen17	Cyst in Breast	1058	786	16	831604	4.402898
Obdmen18	Cyst in Breast	1044	788	16	822688	4.525226
Obdmen19	Kidney	1110	826	16	916876	5.038101
Obdmen20	Kidney	1108	834	16	924088	5.217100
Obdmen21	Liver	1056	784	16	827920	4.851647

APPENDIX B

Batch Files

1. Lossless Methods

CALIC

encode -in ..\Images\mammogram\PGM\mammogram1.pgm -out ..\Compressed\mammogram\CALIC\mammogram1.clc

decode -in ..\Compressed\mammo\CALIC\mammo1.clc -out ..\Recovered\mammo\CALIC\mammo1.pgm

JPEG-LS

cjpegls ..\Images\mammogram\PGM\mammogram1.pgm -o..\Compressed\mammogram\JPEGLS\mammogram1.jls

djpegls ..\Compressed\mammo\JPEGLS\mammo1.jls -o..\Recovered\mammo\JPEGLS\mammo1.pgm

Lossless JPEG

cjpeg -lossless 7 -outfile ..\Compressed\mammogram\LJPEG\mammogram1.ljg ..\Images\mammogram\PGM\mammogram1.pgm

djpeg -pnm ..\Compressed\mammo\LJPEG\mammo1.ljg ..\Recovered\mammo\LJPEG\mammo1.pgm

FELICS

felics -e ..\Images\mammogram\PGM\mammogram1.pgm ..\Compressed\mammogram\FELICS\mammogram1.flc

felics -d ..\Compressed\mammo\FELICS\mammo1.flc ..\Recovered\mammo\FELICS\mammo1.pgm

BTPC

cBTPC ..\Images\mammogram\PGM\mammogram1.pgm ..\Compressed\mammogram\BTPC\mammogram1.btp 100

dBTPC ..\Compressed\mammo\BTPC\mammo1.btp ..\Recovered\mammo\BTPC\mammo1.pgm

PNG

pnm2png ..\Images\mammogram\PGM\mammogram1.pgm ..\Compressed\mammogram\PNG\mammogram1.png

png2pnm ..\Compressed\mammo\PNG\mammo1.png ..\Recovered\mammo\PNG\mammo1.pgm

JPEG2000

jasper -f ..\Images\mammogram\PGM\mammogram1.pgm -F ..\Compressed\mammogram\JPEG2000\mammogram1.jp2 -t pnm -T jp2

jasper -f ..\Compressed\mammo\JPEG2000\mammo1.jp2 -F ..\Recovered\mammo\JPEG2000\mammo1.pgm -t jp2 -T pnm

S+P

PROGCODE ..\Images\mammo\PGM\mammo1.pgm ..\Compressed\mammo\SPIHT\mammo1.SP 1222 1000 1 0

PROGDECD -s ..\Compressed\mammo\SPIHT\mammo1.SP ..\Recovered\mammo\SPIHT\mammo1.pgm 0

2. Lossy Methods

JPEG

cjpeg -quality %2 -outfile ..\Compressed\Obdmen\LJPEG\Obdmen%1.ljg ..\Images\Obdmen\PGM\Obdmen%1.pgm

djpeg -pnm ..\Compressed\Obdmen\LJPEG\Obdmen%1.ljg ..\Recovered\Obdmen\LJPEG\Obdmen%1.pgm

imgcmp -f ..\Images\Obdmen\PGM\Obdmen%1.pgm -F ..\Recovered\Obdmen\LJPEG\Obdmen%1.pgm -m psnr

BTPC

cbtpc ..\Images\Obdmen\PGM\Obdmen%1.pgm ..\Compressed\Obdmen\BTPC\Obdmen%1.btp %2

dBTPC ..\Compressed\Obdmen\BTPC\Obdmen%1.btp ..\Recovered\Obdmen\BTPC\Obdmen%1.pgm

imgcmp -f ..\Images\Obdmen\PGM\Obdmen%1.pgm -F ..\Recovered\Obdmen\BTPC\Obdmen%1.pgm -m psnr

JPEG2000

jasper -f ..\Images\Obdmen\PGM\Obdmen%1.pgm -F ..\Compressed\Obdmen\JPEG2000\Obdmen%1.jpc -t pnm -T jpc -O rate=%2

jasper -f ..\Compressed\Obdmen\JPEG2000\Obdmen%1.jpc -F ..\Recovered\Obdmen\JPEG2000\Obdmen%1.pgm -t jpc -T pnm

imgcmp -f ..\Images\Obdmen\PGM\Obdmen%1.pgm -F ..\Recovered\Obdmen\JPEG2000\Obdmen%1.pgm -m psnr

SPIHT

CODETREE ..\Images\Obdmen\PGM\Obdmen1.pgm ..\Compressed\Obdmen\SPIHT\Obdmen1.sp 822 1112 1 4.6

DECDTREE

y

..\Compressed\ Obdmen\SPIHT\ Obdmen1.sp

y

..\Images\ Obdmen\PGM\ Obdmen1.pgm

1.6

n

n

3. ROI

JPEG-LS

```
@ECHO OFF

IF "%2" == "c" GOTO COMPRESSED

IF "%2" == "d" GOTO DECOMPRESSED

GOTO END

:COMPRESSED

_encoder -i../abdmen/PGM/abdmen%1.pgm -o../abdmen/Compressed/JPEG-LS/Non_SA/abdmen%1.jls

ECHO -------------------------------------------------------------------------------------------

GOTO END

:DECOMPRESSED
```

```
_decoder -i../abdmen/Compressed/JPEG-LS/Non_SA/abdmen%1.jls -o../abdmen/Recovered/JPEG-LS/Non_SA/abdmen%1.pgm

ECHO ------------------------------------------------------------------------------------------

GOTO END

:END
```

Modified JPEG-LS

```
@ECHO OFF

IF "%2" == "c" GOTO COMPRESSED

IF "%2" == "d" GOTO DECOMPRESSED

GOTO END

:COMPRESSED

sa_encoder -i../abdmen/PGM/abdmen%1.pgm -o../abdmen/Compressed/JPEG-LS/Shape_Adaptive/abdmen%1.jls -k../abdmen/MASK/mask%1.pgm

ECHO ------------------------------------------------------------------------------------------

GOTO END

:DECOMPRESSED

sa_decoder -i../abdmen/Compressed/JPEG-LS/Shape_Adaptive/abdmen%1.jls -o../abdmen/Recovered/JPEG-LS/Shape_Adaptive/abdmen%1.pgm

ECHO ------------------------------------------------------------------------------------------

GOTO END

:END
```

SPIHT

```
@ECHO OFF

IF "%2" == "c" GOTO COMPRESSED

IF "%2" == "d" GOTO DECOMPRESSED

GOTO END

:COMPRESSED

ptime spihtencode -w ../filters/CohenDaubechiesFeauveau.5-3.lft 0.1
../abdmen/PGM/abdmen%1.pgm
../abdmen/Compressed/SPIHT/Non_SA/abdmen%1.sp

DIR ..\abdmen\Compressed\SPIHT\Non_SA\abdmen%1.sp

ECHO -------------------------------------------------------------------------------------------

GOTO END

:DECOMPRESSED

ptime spihtdecode -w ../filters/CohenDaubechiesFeauveau.5-3.lft -r 0.1
../abdmen/Compressed/SPIHT/Non_SA/abdmen%1.sp
../abdmen/Recovered/SPIHT/Non_SA/abdmen%1.pgm

ECHO -------------------------------------------------------------------------------------------

GOTO END

:END
```

SA- SPIHT

```
@ECHO OFF

IF "%2" == "c" GOTO COMPRESSED
```

IF "%2" == "d" GOTO DECOMPRESSED

GOTO END

:COMPRESSED

ptime spihtencode -w ../filters/CohenDaubechiesFeauveau.5-3.lft -m ../abdmen/MASK/mask%1.pgm 0.1 ../abdmen/PGM/abdmen%1.pgm ../abdmen/Compressed/SPIHT/Shape_Adaptive/abdmen%1.sp

DIR ..\abdmen\Compressed\SPIHT\Shape_Adaptive\abdmen%1.sp

ECHO ---

GOTO END

:DECOMPRESSED

ptime spihtdecode -w ../filters/CohenDaubechiesFeauveau.5-3.lft -m ../abdmen/MASK/mask%1.pgm -r 0.1 ../abdmen/Compressed/SPIHT/Shape_Adaptive/abdmen%1.sp ../abdmen/Recovered/SPIHT/Shape_Adaptive/abdmen%1.pgm

ECHO ---

GOTO END

:END

Loop all sample images in batch file

FOR %f IN (1 2 3 4 5 6 7 8 9 10 11 12 13 14 15 16 17 18 19 20 21) DO Non-SA-JPEGLS-Mammo %f c

FOR %f IN (1 2 3 4 5 6 7 8 9 10 11 12 13 14 15 16 17 18 19 20 21) DO Non-SA-JPEGLS-Abdomen %f d

FOR %F IN (1 2 3 4 5 6 7 8 9 10 11 12 13 14 15 16 17 18 19 20 21) DO SA-JPEGLS- Mammo %F c

FOR %F IN (1 2 3 4 5 6 7 8 9 10 11 12 13 14 15 16 17 18 19 20 21) DO SA-JPEGLS-Abdomen %F c

FOR %f IN (1 2 3 4 5 6 7 8 9 10 11 12 13 14 15 16 17 18 19 20 21) DO Non-SA-SPIHT- Mammo %f c

FOR %f IN (1 2 3 4 5 6 7 8 9 10 11 12 13 14 15 16 17 18 19 20 21) DO Non-SA-SPIHT-Abdomen %f d

FOR %f IN (1 2 3 4 5 6 7 8 9 10 11 12 13 14 15 16 17 18 19 20 21) DO SA-SPIHT-Mammo %f c

FOR %f IN (1 2 3 4 5 6 7 8 9 10 11 12 13 14 15 16 17 18 19 20 21) DO SA-SPIHT-Abdomen %f d

APPENDIX C (Comparative Study detailed Results)

Table 1: Compression ratio for 21 mammogram images

Compression Scheme	Mammogram images																				
	M1	M2	M3	M4	M5	M6	M7	M8	M9	M10	M11	M12	M13	M14	M15	M16	M17	M18	M19	M20	M21
LJPEG	2.84	3	2.8	2.76	2.69	2.76	2.74	2.95	2.97	3.04	2.98	3.03	3.12	2.89	3.1	3	3.05	2.98	2.96	3.08	2.99
JPEG-LS	3.29	3.52	3.39	3.25	3.23	3.2	3.27	3.63	3.45	3.59	3.52	3.61	3.78	3.45	3.78	3.46	3.67	3.5	3.47	3.58	3.63
CALIC	3.31	3.5	3.38	3.25	3.25	3.23	3.29	3.59	3.48	3.55	3.54	3.62	3.75	3.47	3.75	3.52	3.67	3.5	3.47	3.59	3.61
FELICS	2.98	3.15	3.01	2.94	2.91	2.92	2.95	3.17	3.06	3.19	3.08	3.16	3.27	3.03	3.26	3.08	3.18	3.1	3.09	3.17	3.15
JPEG2000	3.19	3.35	3.23	3.13	3.11	3.12	3.15	3.42	3.32	3.4	3.35	3.41	3.55	3.3	3.54	3.33	3.48	3.33	3.3	3.41	3.43
PNG	2.69	2.83	2.69	2.63	2.61	2.65	2.64	2.82	2.8	2.85	2.88	2.86	2.95	2.78	2.95	2.89	2.91	2.87	2.8	2.95	2.86
BTPC	3.08	3.22	3.07	2.98	2.94	3.01	2.98	3.28	3.23	3.29	3.25	3.31	3.46	3.17	3.44	3.2	3.36	3.22	3.19	3.34	3.33
S+P	3.22	3.35	3.2	3.13	3.1	3.14	3.12	3.41	3.37	3.39	3.39	3.43	3.58	3.35	3.57	3.36	3.49	3.36	3.31	3.48	3.45

Table 2: Compression/Decompression time on 21 mammograms

Compression Scheme	time	Mammogram images																				
		M1	M2	M3	M4	M5	M6	M7	M8	M9	M10	M11	M12	M13	M14	M15	M16	M17	M18	M19	M20	M21
LJPEG	CT	0.281	0.265	0.265	0.265	0.265	0.296	0.265	0.265	0.14	0.265	0.14	0.14	0.14	0.14	0.14	0.14	0.14	0.14	0.14	0.14	0.14
	DT	0.281	0.265	0.281	0.281	0.281	0.312	0.265	0.296	0.156	0.281	0.14	0.171	0.14	0.141	0.14	0.156	0.14	0.14	0.14	0.14	0.14
JPEG-LS	CT	0.296	0.281	0.281	0.281	0.281	0.312	0.281	0.281	0.156	0.281	0.156	0.156	0.156	0.156	0.156	0.171	0.156	0.171	0.171	0.171	0.171
	DT	0.281	0.265	0.281	0.281	0.281	0.312	0.265	0.296	0.156	0.281	0.14	0.171	0.14	0.141	0.14	0.156	0.14	0.14	0.14	0.14	0.14
CALIC	CT	3.515	3.046	3.062	3.234	3.156	3.687	3.109	2.984	1.796	3.187	2.015	1.734	1.656	1.765	1.687	1.828	1.718	1.796	1.828	1.781	1.734
	DT	3.578	3.171	3.093	3.265	3.171	3.718	3.125	3.015	1.812	3.218	1.781	1.734	1.734	1.781	1.718	1.843	1.75	1.812	1.828	1.796	1.75
FELICS	CT	0.206	0.191	0.194	0.202	0.193	0.209	0.199	0.183	0.147	0.195	0.142	0.151	0.141	0.152	0.144	0.155	0.147	0.157	0.152	0.146	0.155
	DT	0.134	0.124	0.126	0.13	0.129	0.139	0.149	0.124	0.088	0.126	0.087	0.088	0.085	0.088	0.092	0.088	0.086	0.089	0.099	0.088	0.087
JPEG2000	CT	1.093	1	1.015	1.046	1.046	1.156	1.031	0.984	0.562	1.031	0.562	0.578	0.546	0.562	0.546	0.578	0.562	0.578	0.593	0.562	0.562
	DT	0.89	0.828	0.843	0.875	0.859	0.937	0.859	0.828	0.453	0.859	0.468	0.484	0.453	0.468	0.453	0.468	0.468	0.484	0.5	0.468	0.468
PNG	CT	1.016	0.86	0.844	0.906	0.875	1.063	0.875	0.844	0.516	0.891	0.5	0.5	0.485	0.516	0.485	0.516	0.5	0.485	0.516	0.485	0.5
	DT	0.254	0.227	0.243	0.244	0.25	0.263	0.254	0.242	0.144	0.238	0.143	0.149	0.143	0.151	0.143	0.158	0.146	0.144	0.145	0.143	0.149
BTPC	CT	0.859	0.484	0.796	0.812	0.796	0.89	0.812	0.75	0.437	0.765	0.437	0.437	0.406	0.421	0.421	0.453	0.421	0.437	0.437	0.437	0.421
	DT	0.781	0.453	0.437	0.453	0.468	0.515	0.453	0.421	0.234	0.453	0.25	0.25	0.25	0.25	0.25	0.265	0.312	0.296	0.25	0.265	0.25
S+P	CT	0.528	0.494	0.511	0.516	0.524	0.545	0.519	0.5	0.313	0.508	0.314	0.32	0.297	0.322	0.302	0.334	0.307	0.32	0.321	0.312	0.318
	DT	0.471	0.435	0.452	0.46	0.463	0.489	0.46	0.441	0.253	0.444	0.258	0.258	0.244	0.258	0.249	0.266	0.252	0.27	0.265	0.258	0.255

Table 3: Compression ratios, compression/decompression time on 21 ultrasound image

Images		LJPEG		JPEG-LS		JPEG2000		CALIC		FELICS		PNG		BTPC		S+P	
Ultrasound1	CR	2.078		2.302		2.194		2.381		2.250		2.133		2.216128805		2.208	
	CT / DT	0.203	0.094	0.234	0.235	1.156	0.937	2.703	2.703	0.127	0.113	0.64	0.263	0.718	0.406	0.858	0.612
Ultrasound2	CR	1.828		2.074		1.952		2.128		1.980		1.923		1.930		1.945	
	CT / DT	0.188	0.078	0.203	0.203	1.125	0.921	2.5	2.5	0.141	0.122	0.546	0.256	0.75	0.375	0.936	0.723
Ultrasound3	CR	1.897		2.188		2.028		2.242		2.087		1.992		2.033		2.005	
	CT / DT	0.25	0.078	0.265	0.203	1.109	0.937	2.468	2.468	0.126	0.109	0.5	0.371	0.75	0.453	0.889	0.583
Ultrasound4	CR	1.816		2.072		1.946		2.133		1.978		1.912		1.932		1.950	
	CT / DT	0.187	0.078	0.234	0.203	1.14	0.968	2.5	2.5	0.127	0.112	0.515	0.252	0.796	0.375	0.917	0.706
Ultrasound5	CR	1.904		2.190		2.028		2.244		2.093		1.999		2.033		2.0127	
	CT / DT	0.187	0.078	0.203	0.203	1.14	1.015	2.484	2.468	0.126	0.111	0.609	0.253	0.703	0.5	0.91	0.711
Ultrasound6	CR	1.815		2.032		1.934		2.100		1.964		1.904		1.918		1.938	
	CT / DT	0.203	0.078	0.218	0.406	1.171	1.015	2.531	2.531	0.13	0.116	0.5	0.25	0.796	0.375	0.945	0.801
Ultrasound7	CR	2.075		2.326		2.172		2.412		2.263		2.133		2.230		2.183	
	CT / DT	0.375	0.078	0.375	0.219	1.312	1.109	2.718	2.718	0.128	0.12	0.765	0.294	0.812	0.39	0.999	0.584
Ultrasound8	CR	2.078		2.302		2.194		2.381		2.250		2.133		2.216		2.208	
	CT / DT	0.203	0.14	0.234	0.235	1.187	0.906	2.781	2.765	0.127	0.116	0.765	0.287	0.843	0.64	0.962	0.864
Ultrasound9	CR	2.045		2.297		2.166		2.380		2.234		2.113		2.198		2.185	
	CT / DT	0.203	0.093	0.234	0.235	1.234	1.14	2.775	2.765	0.139	0.127	0.625	0.27	0.875	0.625	1.002	0.84
Ultrasound10	CR	1.670		1.931		1.840		1.991		1.821		1.816		1.780		1.838	
	CT / DT	0.203	0.078	0.235	0.235	1.25	1.046	2.625	2.562	0.147	0.121	0.625	0.274	0.859	0.39	1.074	0.917
Ultrasound11	CR	1.893		2.217		2.063		2.254		2.094		2.016		2.042		2.057	
	CT / DT	0.203	0.078	0.234	0.235	1.312	1.046	2.515	2.515	0.124	0.114	0.656	0.553	0.703	0.703	0.972	0.836
Ultrasound12	CR	1.788		2.015		1.924		2.069		1.927		1.898		1.879		1.922	
	CT / DT	0.203	0.078	0.219	0.265	1.187	1.156	2.609	2.593	0.136	0.117	0.484	0.252	0.859	0.39	1.034	0.65
Ultrasound13	CR	1.867		2.193		2.043		2.223		2.034		2.000		1.993		2.026	
	CT / DT	0.203	0.078	0.218	0.218	1.156	1.14	2.562	2.515	0.124	0.111	0.671	0.253	0.828	0.406	0.99	0.885
Ultrasound14	CR	1.794		2.054		1.929		2.096		1.952		1.902		1.900		1.919	
	CT / DT	0.203	0.078	0.203	0.219	1.234	1.171	2.546	2.546	0.127	0.116	0.5	0.251	0.859	0.375	1.01	0.904
Ultrasound15	CR	1.879		2.195		2.039		2.232		2.070		2.002		2.019		2.032	
	CT / DT	0.187	0.078	0.218	0.219	1.328	1.125	2.531	2.531	0.143	0.113	0.671	0.25	0.843	0.359	0.997	0.849
Ultrasound16	CR	2.139		2.507		2.375		2.575		2.324		2.188		2.326		2.390	
	CT / DT	0.187	0.063	0.203	0.203	1.078	0.906	2.375	2.375	0.116	0.106	0.609	0.244	0.656	0.609	0.836	0.721
Ultrasound17	CR	2.024		2.382		2.117		2.433		2.274		2.120		2.213		2.0886	
	CT / DT	0.25	0.078	0.187	0.187	1.125	1	2.359	2.328	0.119	0.106	0.515	0.25	0.812	0.359	0.976	0.574
Ultrasound18	CR	1.748		1.937		1.877		2.012		1.864		1.865		1.824		1.866	
	CT / DT	0.203	0.078	0.234	0.234	1.171	1.14	2.593	2.546	0.133	0.122	0.593	0.248	0.859	0.39	1.037	0.954
Ultrasound19	CR	2.197		2.455		2.374		2.519		2.359		2.247		2.349		2.397	
	CT / DT	0.203	0.093	0.234	0.25	1.187	1.109	2.812	2.812	0.128	0.115	0.765	0.266	0.843	0.375	0.917	0.79
Ultrasound20	CR	2.175		2.447		2.377		2.525		2.336		2.248		2.325		2.383	
	CT / DT	0.218	0.078	0.234	0.234	1.234	1.14	2.843	2.843	0.133	0.125	0.75	0.267	0.875	0.406	0.942	0.778
Ultrasound21	CR	2.167		2.516		2.389		2.582		2.349		2.201		2.348		2.429	
	CT / DT	0.187	0.062	0.219	0.219	1.203	1.031	2.421	2.593	0.118	0.109	0.765	0.243	0.843	0.343	0.801	0.73

APPENDIX D

Generated Masks

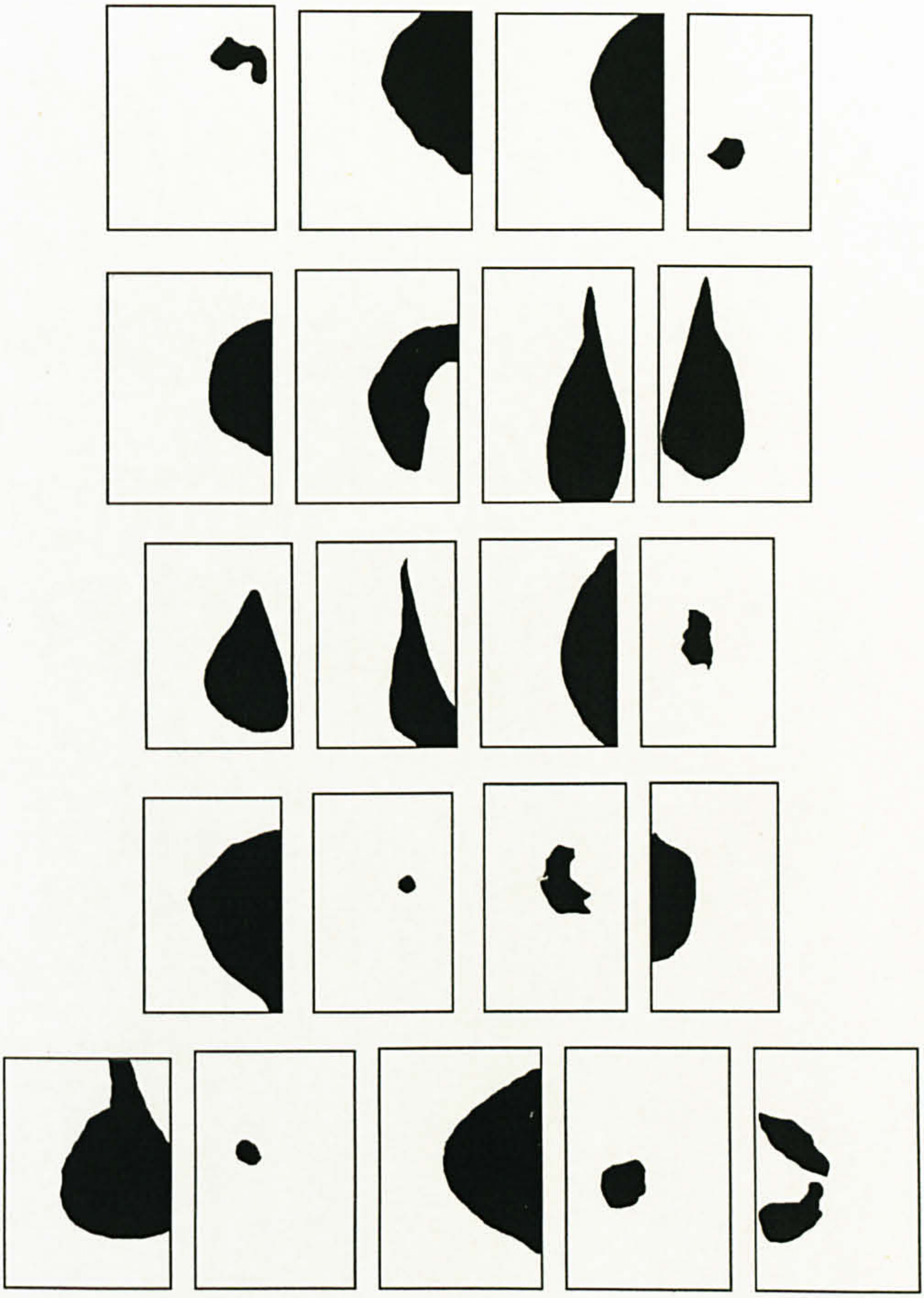

Figure 1: Generated masks for mammograms in Fig.1(Appendix A)

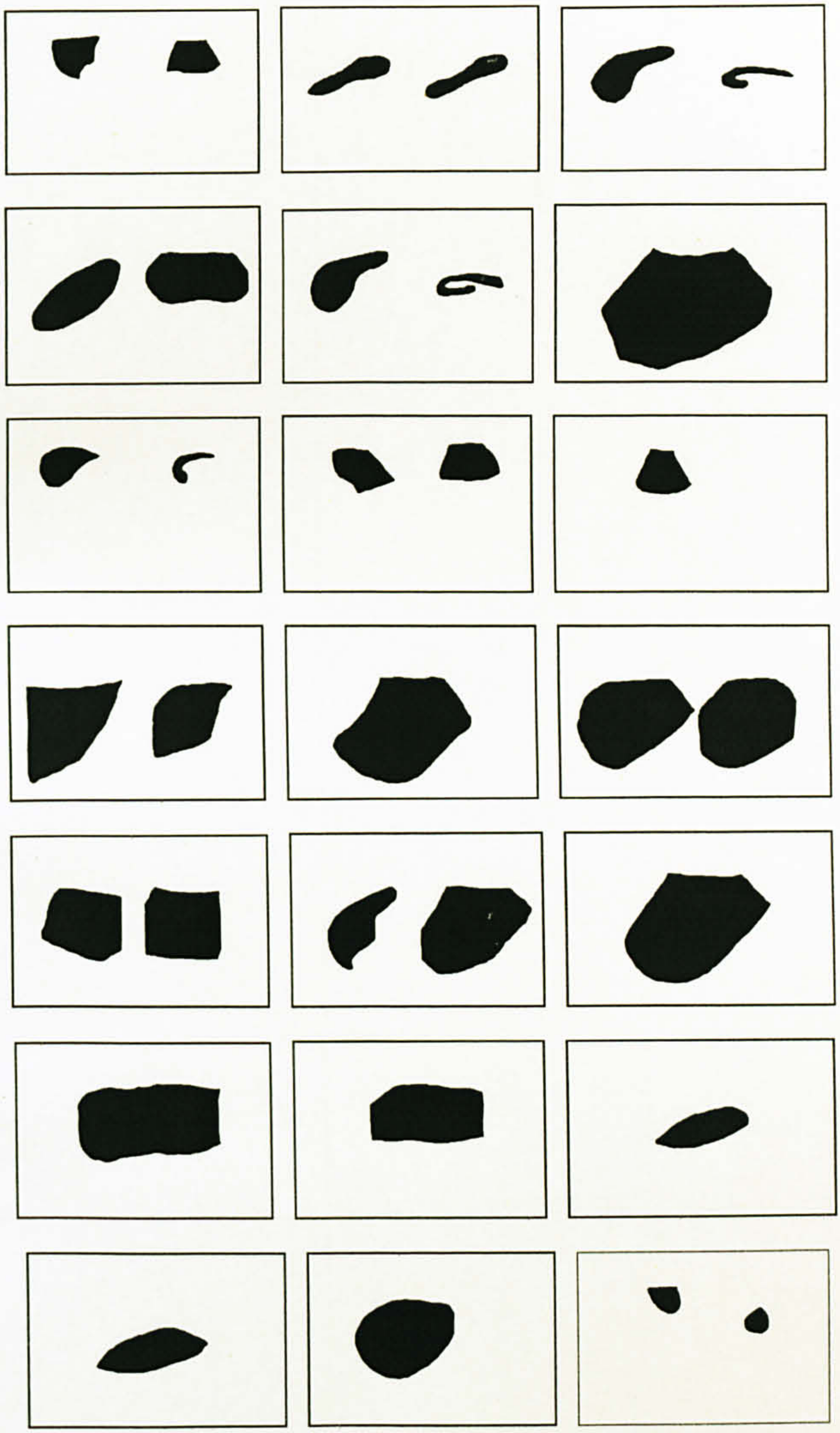

Figure 2: Generated masks for Ultrasound images in Fig. 2 (Appendix A)